STUDYING SURFACE URBAN HEAT ISLAND PHENOMENON USING REMOTE SENSING IN THREE METROPOLITAN AREAS OF TEXAS, USA

by

Chunhong Zhao

A dissertation submitted to the Graduate Council of
Texas State University in partial fulfillment
of the requirements for the degree of
Doctor of Philosophy
with a Major in Geographic Information Science
August 2018

Committee Members:

Jennifer Jensen, Chair

Nathan Currit

Russell Weaver

Qihao Weng

FAIR USE AND AUTHOR'S PERMISSION STATEMENT

Fair Use

Duplication Permission

ACKNOWLEDGEMENTS

I would like to express my sincere gratitude to my advisor, Dr. Jennifer Jensen, for your outstanding guidance, patience, and tremendous support throughout my entire life at Texas State University. I thank your inspiration for me to overcome difficulties, face and solve problems to conduct research in professional way. I admire your success on both of your career and family. You have been serving as a role model as an excellent female professor, researcher, and mentor. Your action and efforts have indeed triggered my thought, gradually helped me, and will also continue to build the value and attitude of my academic life. I will always remember the conversation on the first time I met you, which inspired of the further meaning of having a Ph.D. degree as a female student. Dr. Jensen, I just cannot thank you enough.

My next appreciation goes to my outstanding dissertation committee: Dr. Nathan Currit, who provided essential feedback and suggestions that significantly improved my dissertation; Dr. Russell Weaver, who helped me frame the statistical analysis of the dissertation with insights, expert knowledge with sustained encouragement, and Dr. Qihao Weng, for his thoughtful insights, research advice, suggestions and constructive comments throughout my dissertation and publication. I could not have done it without the unflinching support from all of you in the last years.

A special thank you goes to the assistant from the Texas Natural Resources Information System (TNRIS), who shared the Lidar point data in an efficient way. I am grateful to the amazing family of Geography Department at Texas State University, especially Dr. Alberto Giordano, Dr. Ronald Hagelman, Dr. Benjamin Zhan, Dr. Lawrence E. Estaville, Dr. Yihong Yuan. I thank the graduate staff advisor Ms. Allison Glass-Smith for her professional assistance to guide me through my Ph.D. study, office manager Ms. Angelika Wahl, administrative assistant Ms. Pat Hell-Jones and lab coordinator Mr. Charles Robinson for their priceless support offered me during my entire doctoral program.

My profound gratitude goes to my classmates: Yunuen Reygadas, Shadae Dixon, Hala Odeh, Zahra Ghaffari, David Szpakowski, Francesco Zignol, Saeideh Gharehchahi, Nathaniel Dede-Bamfo, Graciela Sandoval, Niaz Morshed, Ugochukwu Francis Umeokafor, Brendan Lavy, and Peng Fu. I am grateful for your time, accompany, support, and spiritual conversations.

I would like to thank my grandparents Mr. Hongrang Zhao and Ms. Yuzhen Wei, Mr. Shiwei Du and Ms. Zufang Lv. You are my original motivation for pursuit of education. I am grateful to my parents Mr. Junqiao Zhao and Ms. Chengqin Du, my brother Guanchen Zhao for the full love and patience. I love you and miss you so much.

Further thanks go to the support from my master thesis advisor Dr. Xiangzheng Deng and other colleagues. Thank you also goes to Ms. Honghui Song and her family, to my friend Liguang Jiang, Steven Lee, Xueqin Zhang, Fei Xie, Lianfei Jiang, Norton Li for their comfort and morale support. Finally, I would like to give thanks to all the nice people I met during the time studying at Texas State University, their kindness gives me the entire aspiration to be a nice person to the society.

TABLE OF CONTENTS

Page

LIST OF TABLES

Table **Page**

LIST OF FIGURES

Figure **Page**

ABSTRACT

The goal of this dissertation was to investigate the SUHI phenomenon for three metropolitan areas of Texas, USA with remote sensing techniques. A GIS-based Local Climate Zones (LCZs) classification scheme was developed with the aid of airborne Lidar datasets and other freely available GIS data, to map and compare the LCZs for the three metropolitan areas: Dallas-Fort Worth (DFW), Austin, and San Antonio. A decision-making algorithm was built for LCZs mapping, and LCZs datasets were established.

By linking remotely sensed land surface temperature (LST) with LCZs, the study investigated the ability of LCZs for studying SUHI phenomenon and analyzes how different LCZs affect the SUHI in three major metropolitan areas. Landsat 8 image data was acquired for July 20, 2015 and used to calculate LST as SUHI measurement. Results indicated that large LST variations were first demonstrated among LCZs characterized by different land cover, and then urban morphological information. The close association between LCZs and LST demonstrated that the LCZs mapping was useful for comparing and investigating the SUHI.

The geographically weighted regression (GWR) efficiently and accurately explained the underlying factors that contributed to the SUHI based on spatial variation and thus demonstrates improved utility for characterizing SUHI compared to global regression.

1 INTRODUCTION

Urban Heat Island (UHI) refers to a city or urban area that is warmer than the surrounding rural area. UHIs are continuously drawing attention since they were first described in the 1810s (Howard 1818; Oke 1976; Imhoff et al. 2010; Mirzaei 2015). Currently, more than half the world's population lives in cities and this proportion is expected to reach 66 percent by the year 2050 (United Nations 2014). In the urban expansion process, natural landscapes are replaced by built-up land and impervious surfaces, which changes 1) energy absorption, storage, emittance due lower sky view factor, higher heat capacity, and lower albedo; 2) wind turbulence intensity due to building configuration, 3) humidity due to lower evapotranspiration due to reduced vegetation cover, and 4) anthropogenic energy release, etc. (Bowler et al. 2010; Mirzaei and Haghighat 2010; Hart and Sailor 2008). Therefore, the UHI phenomenon has become a well-researched topic due to a series of adverse effects on vegetation phenology (Zhou, Zhao, et al. 2016), air pollution (Sarrat et al. 2006), logical meteorology (Taha 1997), climatic warming (Huang and Lu 2015), energy consumption, and health risks for urban residents (Harlan et al. 2007).

UHI is a multi-scale phenomenon, varying from small scale anthropogenic heat release such as from vehicles, to meso-scale atmospheric interactions (Mirzaei and Haghighat 2010). Hence, UHI has been defined for different layers of the atmosphere and terrestrial surface to integrate these aspects simultaneously with different measurement techniques. Basically, there are two types of UHI studies: atmospheric UHI (AUHI) and surface UHI (SUHI) (Figure 1.1). After the first AUHI case study in London in 1818 (Howard 1818), AUHI magnitude in cities has been reported around the world and AUHI has been further subdivided by observation scope: urban boundary layer (UBL) (Barlow 2014) and urban canopy layer (UCL) (Oke 1995). UCL refers to atmosphere between urban surface and building roof, while UBL extends above UCL and it is a mesoscale concept as a portion of planetary boundary layer (Oke 1976). Voogt and Oke (2003) proposed the term SUHI to refer to UHI study that is measured with land surface temperature (LST), which is measured from airborne or satellite-borne sensors.

1.1 Limitation of traditional UHI investigation

Traditional UHI investigation has focused on AUHI, where the air temperature pattern in an urban area is generally compared to rural areas based on field measurements at isolated fixed or mobile stations. Several limitations exist for UHI studies by field measurements to quantify AUHI. First, it is time-consuming and expensive to develop and maintain monitoring stations and devices. Although some modern devices can capture additional parameters like velocity, turbulence, and even pollution concentration, limited and isolated stationary networks are not capable of capturing heterogeneous thermal characteristics caused by land use and land cover (LULC) (Hu and Brunsell 2015; Shen et al. 2016). Also, generalization and estimation for inaccessible areas as well as considerable observation time periods are needed to accurately describe the AUHI phenomenon. Additionally, there are no systematic criteria for experimental design and communication for AUHI observation. According to a systematic review of methodological quality of 190 AUHI studies published between 1950-2007, half of the sample studies fail to sufficiently control confounding effects of weather, topography, or time, and three quarters fail to communicate basic metadata such as instrumentation and site characteristics (Stewart 2011).

In addition, discrete categorization and definitions of urban and rural land adds uncertainty to traditional UHI measurement and comparison. Moreover, each city is exposed to diverse local and synoptic factors, which makes UHI study complex and specific to localities, and therefore difficult for comparison (Ng 2015). The diversity of size, shape, height, composition, and spatial arrangement of urban canopy components makes it even harder to define a surface datum for AUHI measurements and urban gradients still cannot sufficiently describe the site topography and local environment. To address this issue, the "local climate zone" (LCZ) classification scheme was designed in 2012 to describe landscapes (urban and natural) that exhibit distinct thermal climate characteristic owing to their surface properties. The LCZ classification standardizes the worldwide exchange of urban temperature observations and has been used extensively in both AUHI and SUHI studies (Stewart and Oke 2012).

1.2 Application of remote sensing to UHI studies

1.2.1 Remote sensing platforms for SUHI measurement

In contrast to the direct AUHI measurement, SUHI is an indirect measurement and the intervening atmosphere and the surface radiative properties need to be considered for LST generation. Foremost, LST data is time-synchronized and grid-based for a considerable areal extent (Nichol 1996). So far, various remote sensing sensors have been used to estimate LST with thermal infrared band/bands from coarse to fine spatial resolution (Table 1.1).

Table 1.1 Different remote sensing sensors for urban thermal studies.

Sensor	Spatial resolution of thermal band(s)	Temporal resolution	Sensor operator	Case studies
Advanced Very High Resolution Radiometer (AVHRR)	1.1 km	Twice daily	National Oceanic and Atmospheric Administration (NOAA)	(Streutker 2003; Stathopoulou and Cartalis 2009)
MODerate resolution Imaging Spectroradiometer (MODIS)	Approximately 1 km	Twice daily	Aqua/Terra sensors, Earth Observing System (EOS) of National Aeronautics and Space Administration (NASA)	(Zhang et al. 2010; Zhou, Zhang, et al. 2016; Connors, Galletti, and Chow 2013)
Advanced Along Track Scanning Radiometer (AATSR)	1 km	35 days	European Space Agency (ESA)	(Fabrizi, Bonafoni, and Biondi 2010)
Advanced Space borne Thermal Emission and Reflection Radiometer (ASTER)	90 m	16 days	Terra (NASA)	(Buyantuyev and Wu 2009; Zheng, Myint, and Fan 2014)
Thematic Mapper (TM), Enhanced Thematic Mapper Plus (ETM+)	30 m after resampling	16 days	NASA Landsat 5 and Landsat 7, separately	(Weng, Lu, and Schubring 2004; Rajasekar and Weng 2009a)
Thermal Infrared Sensor (TIRS)	30 m after resampling	16 days	NASA Landsat 8	(Guo et al. 2015; Peng et al. 2016)

1.2.2 Modeling SUHI with remote sensing data

UHIs demonstrate temporal characteristics, from daily to annual, and even decadal variation. How to make use of remotely sensed thermal data from different sources to generate a consistent and long term LST is of importance to understanding the environmental and ecological process for a specific urban area. Several studies have successfully conducted spatial sharpening (e.g., image merging, image/data fusion, downscaling, and disaggregation) (Weng 2009), by using statistical downscaling with the aid of shorter wavelength data (Deng and Wu 2013), or physical downscaling (Guo and Moore 1998). The Spatial and Temporal Adaptive Reflectance Fusion Method (STARFM) was originally proposed to predict daily surface reflectance and vegetation index values by combining MODIS and Landsat (Gao et al. 2006). It has been used to assess the seasonal variation of vegetation (Hilker, Wulder, Coops, Seitz, et al. 2009) and land use changes (Hansen et al. 2008).

Based on that, some improvements have been made with more applications. For instance, Spatial Temporal Adaptive Algorithm for mapping Reflectance Change (STAARCH) was utilized for detecting disturbance related changes in forests (Hilker, Wulder, Coops, Linke, et al. 2009). Based on STARFM, Huang et al. (2013) established a new weight function, assuming that the bilateral filtering is determined by spatial distance as well as photometric similarity, to account for effect of neighboring pixels. STARFM has been applied in urban thermal studies and its performance has been proved (Liu et al. 2016; Liu and Weng 2012). Weng, Fu, and Gao (2014) modified STARFM by considering annual temperature cycles (ATC) as well as landscape heterogeneity. The modified algorithm, Spatio-temporal Adaptive Data Fusion Algorithm for Temperature (SADFAT), was implemented in Los Angeles, California with promising results. Based on the improvements of spatial sharpening algorithms, some recent studies have contributed to SUHI evaluation analysis with high spatio-temporal LST datasets (Shen et al. 2016; Liu et al. 2016).

In addition, the complete spatial coverage of LST makes SUHI morphological modeling possible. Changes in the UHI shape and structure can be recorded over time to provide a qualitative UHI description (e.g., UHI evolution). For example, Streutker (2003) modeled and quantified SUHI evolution of Houston, Texas, by applying a Gaussian surface to fit AVHRR image data on a planar rural background to measure the magnitude, spatial extent, orientation, and central location of the SUHI. SUHI evolution also been studied in eight Asian mega cities (Tran et al. 2006), Indianapolis (Rajasekar and Weng 2009b), Beijing (Zhou et al. 2011; Quan et al. 2014), Milan (Anniballe, Bonafoni, and Pichierri 2014), and Wuhan, China (Wang, Zhan, and Guo 2015).

Instead of measuring SUHI intensity for an entire city in terms of the SUHI shape features, some researchers have focused on identifying SUHI hotspots by focusing on LST heterogeneity and variation (Bottyán and Unger 2003; Zhang and Wang 2008; Lu and Weng 2006). Spatial association has been widely used to quantify spatial patterns, particularly to derive LST hotspots or clusters. Whereas global autocorrelation analysis yields only one statistical result to summarize the entire area (Wong et al. 2016), some recent studies have adopted Local Indicators of Spatial Autocorrelations (LISA) statistics (e.g., Local Moran's I, Getis G) to detect LST clusters. As opposed to a global measurement of spatial autocorrelation, local Moran's I indicates an attribute value of a location in relation to values of its neighbors and can be helpful to identify hotspots with high influencing effects on adjacent areas (Guo et al. 2015; Xie, Fu, and Wang 2011; Das Majumdar and Biswas 2016) and quantify spatial patterns (Chen, Jiang, and Xiang 2015).

Another direction focuses on time series LST generation and trend analysis from a considerable amount of imagery. Along this line, the magnitude, spatial extent, and maximum of thermal patterns have been identified (Keramitsoglou et al. 2011). Mean annual surface temperature, yearly amplitude of surface temperature, and phase shift parameters have also been investigated (Bechtel 2012).

1.2.3 SUHI and AUHI formation studies

As mentioned in the beginning, UHI is due to various factors including urbanization and climatic factors. Remote sensing provides considerable data support to empirically study SUHI and related surface characteristics (Table 1.2). First, physical land properties influence LST and the SUHI phenomenon (Zhou, Huang, and Cadenasso 2011; Zheng, Myint, and Fan 2014; Li et al. 2012; Peng et al. 2016; Myint et al. 2015). Also, SUHI is strongly related to the urban morphology and building environment characteristics (e.g., Chun et al. 2014). Furthermore, associative studies of UHI (especially SUHI) and socioeconomic conditions have been increasing with a considerable amount of case studies (Table 1.2). Remote sensing technology has provided a unique way to study urban thermal character, such as temperature-vegetation index (TVX) approach (Das Majumdar and Biswas 2016).

Table 1.2 Summary of literature on empirical relationships between SUHI and various factors.

Factors	Methods	Empirical case studies
Land cover and landscape architecture		
Vegetation abundance, NDVI, etc.	• Pearson correlation • Ordinary least squares (OLS) regression • Regression tree • Spatial Auto-Regression (SAR) • Geographically weighted regression (GWR) • Analysis of variance (ANOVA)	• Beijing (Li et al. 2012; Kuang et al. 2014) • Shanghai (Yue et al. 2007) • Guangzhou (Guo et al. 2015) • Wuhan (Wu et al. 2014) • Chongqing (Luo and Peng 2016) • Milan (Italy), Tampa Bay (Florida), and Las Vegas (Nevada) (Xian and Crane 2006) • Indianapolis (Indiana) (Weng, Lu, and Schubring 2004) • Phoenix (Myint et al. 2013) • Columbus (Chun and Guldmann 2014) • Baltimore (Levy 2016)) • Toronto (Rinner and Hussain 2011) • More than 3000 global settlements (Zhang et al. 2010) • Tehran, Iran (Amiri et al. 2009) • 419 Global Big Cities (Peng et al. 2012)
Built-up land intensity or impervious surface percentage, etc.	• Adjusted stratified stepwise regression • OLS regression • GWR	• Shanghai (Zhu et al. 2013) • Guangzhou (Guo et al. 2015) • Chongqing (Luo and Peng 2016) • Phoenix (Myint et al. 2013) • Tampa Bay (Florida), and LasVegas (Nevada) (Xian and Crane 2006) • Shanghai, Guangzhou, Beijing, Changsha, Lanzhou and Fuzhou (Tang and Xu 2016) • Top 38 most populated urban areas in U.S. (Imhoff et al. 2010)

Table 1.2-Continued

Landscape component and configuration, etc.	• OLS regression • Nonlinear regression • Regression tree • ANOVA • SAR • Multilevel regression • Longitudinal OLS • GWR • Longitudinal GWR • Pearson correlation	• Beijing (Peng et al. 2016; Song et al. 2014) • Shanghai (Zhang et al. 2013; Li et al. 2014; Li et al. 2011) • Guangzhou (Guo et al. 2015) • Shenzhen (Li et al. 2010) • Zhuhai (Du, Xiong, et al. 2016) • Wuhan (Wu et al. 2014) • Brisbane (Australia) (Deilami, Kamruzzaman, and Hayes 2016) • Phoenix (Li et al. 2016; Buyantuyev and Wu 2009) • Phoenix and Las Vegas (Myint et al. 2015) • Baltimore (Levy 2016) • Gwynns Falls watershed, Baltimore (Huang and Cadenasso 2016; Zhou, Huang, and Cadenasso 2011) • Austin (Kim et al. 2016b)
Urban morphology		
Topography, etc.	• Correlation • OLS regression • GWR	• Beijing (Kuang et al. 2014) • Shenzhen (Li et al. 2010) • Taibei (Wu, Lung, and Jan 2013) • European urban regions (Schwarz and Manceur 2014)
City configuration and agglomerations	• OLS regression • Correlation	• 50 most populous cities in U.S. (Debbage and Shepherd 2015) • European urban regions (Schwarz and Manceur 2014)
City size, etc.	• OLS regression	• 419 global big cities (Peng et al. 2012) • Top 38 most populated urban areas in U.S. (Imhoff et al. 2010) • 32 cities of China (Zhou et al. 2014) • Yangtze River Delta Urban Agglomeration (Du, Wang, et al. 2016) • St. Lawrence Lowland (Oke 1973) • Huabei Plain (Tan and Li 2015)

Table 1.2-Continued

Sky view factor, building heights, building configuration, etc.	• Multiple linear model • SAR • Spatial error model (SEM) • General spatial model(GSM)	• Szeged (Hungary) (Bottyán and Unger 2003) • Columbus (Chun and Guldmann 2014) • Atlanta, Georgia (Chun and Guhathakurta 2016) • Guangzhou (Guo 2016)
Albedo, building material, etc.	• OLS regression • SAR	• Beijing (Kuang et al. 2014) • 419 global big cities (Peng et al. 2012) • Chicago (Coseo and Larsen 2014) • Columbus (Chun and Guldmann 2014) • Baltimore (Levy 2016)
Anthropogenic factors		
Population density, distribution, income, housing units and structure, etc.	• OLS model • longitudinal OLS • Multiple regression model • Stepwise correlation analysis • Principal component regression analysis • Correlation • Spatial autocorrelation • GWR • Logic GWR	• Shanghai (Buyantuyev and Wu 2009; Chen, Jiang, and Xiang 2015; Zhang et al. 2013) • Brisbane (Australia) (Deilami, Kamruzzaman, and Hayes 2016) • Greater Athens, Greece (Keramitsoglou et al. 2011) • Beijing (Xiao et al. 2008) • Yangtze River Delta Urban Agglomeration (Du, Wang, et al. 2016) • European urban regions (Schwarz and Manceur 2014) • 419 global big cities (Peng et al. 2012) • Phoenix (Li et al. 2016; Buyantuyev and Wu 2009; Harlan et al. 2007) • Gwynns Falls watershed, Baltimore (Huang and Cadenasso 2016) • Hong Kong (Wong et al. 2016)

Table 1.2-Continued

Land use activities, anthropogenic heat release, energy consumption, etc.	• OLS model • Time series analysis • Descriptive summary	• Phoenix (Connors, Galletti, and Chow 2013) • Shanghai (Li et al. 2014; Chen, Jiang, and Xiang 2015; Li et al. 2009) • Beijing (Fu and Weng 2016; Guo et al. 2012) • Nanjing (Wang, Ma, et al. 2016) • Yangtze River Delta Urban Agglomeration (Du, Wang, et al. 2016)
Adjacent heat sources	• Regression • ANOVA	• Chicago (Coseo and Larsen 2014)

Empirical estimation models remain effective tools for quantitatively characterizing SUHI formation (Table 1.2) with less computationally intensity as computational simulation models and relatively easily interpreted output. Further, to overcome autocorrelation, spatial regression models including the Spatial Auto-Regression (lag) model (SAR), spatial error model (SEM), and general spatial model (GSM) have been employed. For instance, Chun et al. (2016, 2014) evaluated OLS, SAR, SEM, and GSM and determined that estimation methods that best represent the SUHI are spatial regressions since they can better capture neighboring effects. In addition, GWR also used to address the spatial varying relationships.

Besides the empirical modeling of LST and related surface characteristics (Table 1.2), thermal remote sensing have advanced our understanding of urban surface energy budgets since LST is closely related to the energy balance within the UCL and modifies the microclimate of the urban area. Voogt and Grimmond (2000) explored the links between LST and surface temperatures and calculations of sensible heat flux using a bulk transfer approach. Also, remote sensing data can be used to estimate surface parameters related to the soil–vegetation system and surface soil moisture, radiative forcing components, and indicators of the surface response to them (i.e., LST) Schmid (1988).

Remote sensing also contributes to explaining AUHI phenomenon in terms of physical modeling and mathematical simulations. It has promoted the development of urban canopy model (UCM) with remotely sensed observations related to surface radiative and thermodynamic properties, including moisture, emissivity, albedo, irradiative input, etc. (Becker and Li 1995; Voogt and Oke 2003). One of the earliest studies, which combined surface energy modeling and remote sensing approaches, was conducted by Carlson et al. (1981). Much of this research is based on landscape matrix or vegetation indices (e.g., the Normalized Difference Vegetation Index; NDVI) derived from satellite images or high resolution land cover data. Remote sensing can also be used to provide boundary condition and land cover condition for numerical computational fluid dynamics (CFD) modeling.

1.2.4 UHI mitigation and urban planning

Many studies have reported widely and successfully applied measures on mitigating UHI effects with promising financial and environmental benefits. For example, Konopacki and Akbari (2002) reported that by mitigating UHI effects in Houston it was possible to achieve savings of USD 82 million with a reduction of 730 MW peak power, together with an annual decrease of 170,000 t of carbon emission. The possible mitigating measures could broadly be categorized as relating to: (1) reducing anthropogenic heat release (Shahmohamadi et al. 2010); (2) better roof design (e.g., green roofs, roof spray cooling, reflective roofs, etc.); and (3) other design factors (e.g., humidification, increased albedo, green canopies, etc.) (Bowler et al. 2010; Rizwan, Dennis, and Chunho 2008).

Without taking spatial heterogeneous characteristics into consideration, mitigation strategies tend to inefficiently respond to higher temperature problems (e.g., one mitigation criteria for the whole city) (Luck and Wu 2002; Wang and Ouyang 2017). Inversely, spatially explicit, intra-urban, and neighborhood-level adaptation contributes to reducing hot spots and mitigate UHI effect. Studies have shown that LST change is correlated to the underlying land cover change (Wang, Ma, et al. 2016; Das Majumdar and Biswas 2016; Fu and Weng 2016). For example, Das Majumdar and Biswas (2016) integrated application of local Moran's I on LST change and TVX space to delineate the regions of acute land transformation. In this sense, identifying the land cover changes behind the changing LST hotspots can be used as a decision-making tool for urban land planning and UHI mitigation.

The socioeconomic conditions at the local and even neighborhood scale are receiving increased attention in UHI vulnerability studies (Wong et al. 2016). Studies have demonstrated that neighborhoods with more ethnic minority residents, residents with lower income and education, and an aging population often experience higher LST than other neighborhoods (Buyantuyev and Wu 2010; Huang et al. 2011). Remote sensing provides data support to this type of neighborhood-level assessment of UHI vulnerability. Human comfort and health concerns are far more serious than the other potential threats in UHI mitigation. A bunch of studies focused on how to reach population who are most vulnerable and at risk to reduce heat-related illness. Exploratory mapping approach for neighborhood-level heat vulnerability assessment have been contacted for Toronto (Rinner et al. 2010). Wong et al. (2016) identified the heat-vulnerable groups and areas of SUHI inequities by integrating methods of remote sensing retrieval, logistic regression modelling, and spatial autocorrelation.

Furthermore, although the importance of urban surface characteristics has been taken into consideration in urban planning and UHI mitigation (e. g., urban greening, higher surface albedo) in some cities worldwide, other cities hesitate in implementing such adaptation strategies (Wang and Ouyang 2017). Without a specific case investigation, it is not easy for urban planners to make selections among various mitigation strategies since UHI formation is related to local climate and geographic location.

2 CONCEPTUAL FRAMEWORK AND RESEARCH QUESTIONS

Due to the complexity of SUHI formation, there is no single approach to provide a comprehensive database for a city, and no feasible principle to describe SUHI mechanisms at each scale. However, it is a phenomenon observed in conjunction with the urbanization process, which is viewed as a heterogeneous human-environment interaction. It is reasonable and necessary to put UHI studies into a boarder urban landscape view and incorporate related geographic and ecological theories into UHI studies. In this chapter, a framework to study UHI is built by incorporating related theories and concepts from a broader area of knowledge. Subsequently, research questions are identified.

2.1 Key Concepts and Principles

1) Landscape ecology, urban ecology, and sustainable urban development

Partly motivated by environmental change issues, landscape ecology is a relatively synthetic discipline with new concepts, theory, and methods to reveal the importance of spatial heterogeneity on ecological process (Gergel and Turner 2006). In this discipline, the spatial approach of geographers and functional approach of ecologists are essentially combined. Urban ecology is the study of understanding the relationship between spatial pattern of urbanization and ecological processes (Wu 2014). Past interactions between biophysical and human processes created the current urban landscape pattern. Also, urban landscaping and management activities may substantially influence the timing, duration, and magnitude of ecological processes.

Different from other land cover types, urban land is inherently affected by human activities. Landscape planning policies and design, dynamics and associated ecological processes across scales need to be emphasized for sustainable urban development (Ahern 2013; Wu 2014).

2) Spatial autocorrelation and heterogeneity, and scale issue

Every place is unique and space is a variable (rather than a parameter) is the essence of geography (Harvey 1969; Curran and Atkinson 1998). In geoscience, it is a fact that spatial phenomena often involve spatial dependence. For example, values (e.g., LST) observed at one place are related to values at adjacent places (e.g., LST in the neighborhood due to the land surface heat fluxes). Opposite from autocorrelation, heterogeneity means the phenomenon is variable within the space. They can be represented and modelled using geostatistical approaches (Redman 1999).

'Scale' is used to refer both to the magnitude of a study (e.g., its geographic extent) and also to the degree of detail (e.g., its level of geographic resolution). It is used in the context of space (geographic scale), time (temporal scale), and many other dimensions of research (Goodchild and Quattrochi 1997).

Landscape ecology emphasizes spatial variation and scale-dependency. The spatial heterogeneity and scale characteristics have been also addressed in UHI studies. For example, the energy budget equation is a function of location and characteristics (Nunez and Oke 1977), which are closely related to UHI formation. Also, as an important scale matching issue, determining how to quantify SUHI magnitude and intensity by pixel-based LST measurement is an challenge in urban thermal remote sensing (Weng 2009). The concept of “local climate zones” (LCZs) has emerged within this decade to address this heterogeneity. It is an up-to-date classification of urban landscapes for the unification of the characterization of the neighborhoods of climate research sites. For urban climate studies, the concept of scale is fundamental to understanding the ways in which elements of the urban 'surface' interact with adjacent atmospheric layers.

2.2 Conceptual Framework

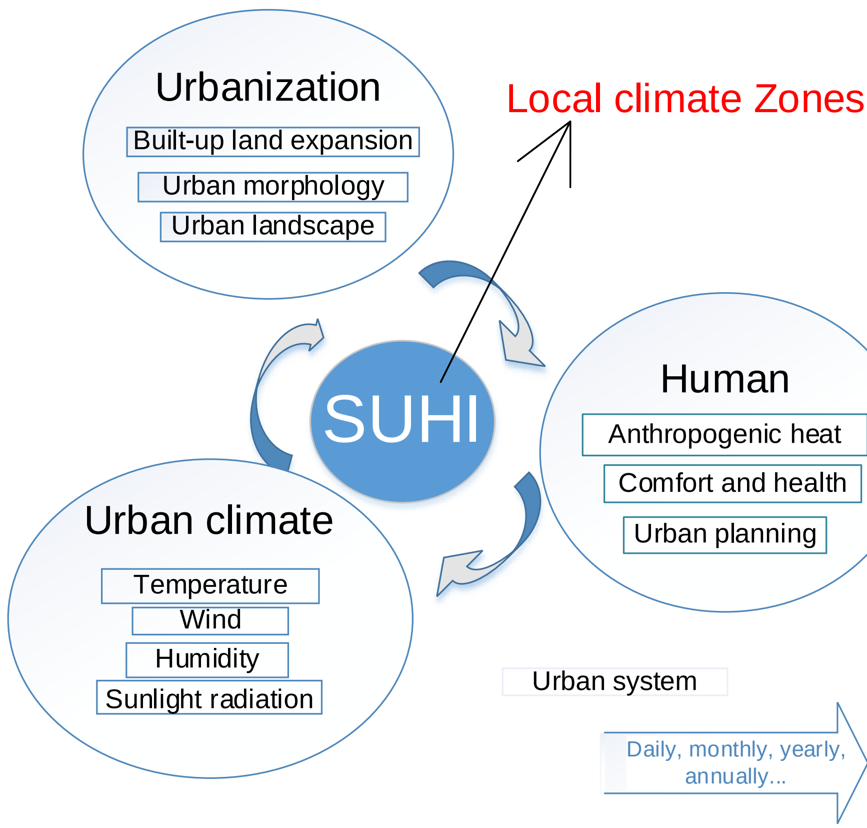

Figure 2.1 Conceptual framework to assess interaction between urbanization and climatic factors on formation of UHI.

The framework for UHI investigation and mitigation is based on the above concepts and theories. First, urbanization is the most dramatic form of land transformation. The increase of built-up land in the urbanization process results in loss of moisture content, increased heat storage, and results in changes in chemical composition, surface structure, and roughness, all of which affect UHI formation (Majumdar and

Biswas 2016; Jiang, Fu, and Weng 2015). For example, vegetation usually has higher evapotranspiration than built-up areas, and thus has lower surface temperatures.

Meanwhile, the roles played by particular factors vary from city to city with respect to differences in geographical location, overall size, etc. (Zhao et al. 2014). Local temperature, precipitation, humidity, wind, sunlight and other climatic parameters affect city design in terms of its general structure, orientation, building forms, materials, etc. All the components and the related relationships are influenced significantly by the urbanization process which is driven by socioeconomic activities. Thus, the UHI phenomenon also changes over time.

The relationships among urbanization process, local geographic background, and human well-being in an urban system are illustrated in the conceptual diagram (Figure 2.1). The connections among the key components and their linkages across spatial (local-landscape–region) and temporal (day-year–decade) scales should be considered for UHI study. All the components and their relationships are influenced profoundly by the speed and spatiotemporal pattern of urbanization that is driven primarily by socioeconomic processes.

Remote sensing provides the main data source for this study. Indicators related to remote sensing used in this study are LST, urban morphology, and underlying biophysical factors.

2.3 Research Objectives

The overall objective of this study is to analyze SUHI with remote sensing techniques for three metropolitan areas of Texas, USA: Dallas-Fort Worth (DFW), Austin, and San Antonio by answering the following questions:

(1) Does the SUHI vary within and among the three major metropolitan areas in Texas and how can LCZ be used to improve the characterization of SUHI?

(2) Can the spatial dynamics of SUHI be explained by the LCZs and underlying factors and if so, are the findings uniform among different areas?

To answer the question, there are three objectives:

1) Build a GIS-based LCZs classification scheme with the aid of airborne Lidar datasets and other freely available GIS data to assess the utility of Lidar to contribute to LCZs classification.
2) Link the Landsat derived LST with LCZs mapping to test if LCZs are able to efficiently analyze the LST variation in the three metropolitan areas; and investigate how LCZs affect the SUHI phenomenon by facilitating comparative analysis.
3) Explore how the underlying landscape properties (e.g., land cover and terrain morphology) are significantly related to the SUHI phenomena, and how the relationship varies within and among different areas.

3 APPLICATION OF AIRBORNE REMOTE SENSING DATA ON MAPPING LOCAL CLIMATE ZONES: CASES OF THREE METROPOLITAN AREAS OF TEXAS, U.S.

3.1 Introduction

Currently, more than half the world's population lives in cities, and this proportion is expected to reach 66 percent by the year 2050 (United Nations 2014). In the urban expansion process, natural landscapes are replaced by built-up land and impervious surfaces. Different from many other land types in the earth system, urban land use and land cover (LULC) is characterized by substantial spatial heterogeneity—due in large part to differences in the configuration and use of these built landscapes. Crucially, variability in urban LULC is linked to heterogeneity in energy absorption, storage and emittance, wind turbulence, and anthropogenic energy release, among other phenomena (Bowler et al. 2010; Mirzaei and Haghighat 2010; Hart and Sailor 2008). One important ecological consequence of urbanization that relates to this observation is urban heat islands (UHIs), which have continuously drawn attention since they were first described in the 1810s (Howard 1818; Oke 1976; Imhoff et al. 2010; Mirzaei 2015). UHIs are generally defined as a city or urban area that is warmer than the surrounding rural area. That being said, despite the ample attention paid to UHIs over the past two decades, it remains difficult for researchers to obtain reliable UHI measurements. Among other reasons, the diversity and spatial arrangement of urban canopy components makes it hard for researchers to set a surface datum for UHI measurements (Weng 2009).

To address this issue, the "local climate zone" (LCZ) classification scheme was designed in 2012 to describe urban landscapes from the aspect of the thermal climate characteristics (Stewart and Oke 2012). LCZs are defined as “regions of uniform land cover, surface structure, construction material, and human activity that span hundreds of meters to several kilometers on a horizontal scale” (Stewart and Oke 2012) (p. 1884). LCZ classification aims to standardize the characteristics of urban morphology for urban places and locate and build weather stations to capture the heterogeneous nature of urban climate processes. Due to this standardized classification, the LCZs concept may be applied across the landscape in different regions of the world for the comparison of urban climate. Additionally, LCZs mapping can significantly broaden our understanding of UHI mechanisms and mitigation by providing a reasonable sampling framework and additional underlying details for surface-energy balance models as well as urban climate models (Alexander, Mills, and Fealy 2015; Bechtel et al. 2015).

The 17 standard LCZ classes (see Table A1) are determined by their surface characteristics, including: composition (building/tree), structure (permeability), fabric (albedo, thermal admittance), and metabolism (e.g., Table 2 on p. 1885 of (Stewart and Oke 2012)). Unique combinations of these properties provide a distinctive thermal regime for each LCZ (Geletič, Lehnert, and Dobrovolný 2016; Stewart and Oke 2012). Researchers have conducted several case studies in cities worldwide to validate the practicability of mapping LCZs with different methods (Bechtel and Daneke 2012; Leconte et al. 2015; Nassar, Blackburn, and Whyatt 2016; Xu, Ren, Cai, Edward, et al. 2017; Zheng et al. 2017; Ng 2015). For example, in an effort to build a worldwide LCZs database for UHI-related studies, the WUDAPT (e.g., World Urban Database and Access Portal Tools) project has conducted several studies with free software and data (Mills et al. 2015; Bechtel et al. 2015; Bechtel et al. 2016; Xu, Ren, Cai, Edward, et al. 2017; Cai et al. 2017).

To date, there is still no standard or optimal method for LCZs mapping. Among all the published case studies by the WUDAPT initiative and other studies, satellite imagery has provided the main data source to derive surface properties suggested in Table A1, Appendix, largely because of the time and accuracy limitations of field measurements of surface characteristics used for LCZs mapping (Ng 2015). Satellite image-based technology has been extensively used for LCZs mapping. Although the WUDAPT method and other straightforward remote sensing classifications provide a fast way to obtain urban morphology information for LCZs mapping (Xu, Ren, Cai, Edward, et al. 2017; Bechtel et al. 2016; Bechtel and Daneke 2012), subjective delineation of training areas in the complex urban settings can result in low-quality LCZ mapping (Geletič and Lehnert 2016). Studies have also indicated non-satisfactory results for high-density cities. For example, Xu, Ren, Cai, and Wang (2017)) evaluated the WUDAPT mapping procedure by Landsat data with a random forest (RF) tree and other remote sensing classification methods (e.g., neural network, support vector machine, maximum likelihood, etc.), and the experimental results showed that the accuracy merely ranged from 59% to 64% in Guangzhou, China.

Some researchers have presented findings using a GIS-based method, whereby a decision-making algorithm delineates LCZs according to thresholds placed on specific geometric and surface cover properties based on the LCZs concept. These studies suggest some advantages of GIS-based methods relative to remote sensing methods, including comprehensiveness of input factors, classification accuracy, standardization, and objectification of the classification procedures (Wang et al. 2017; Zheng et al. 2017; Unger, Lelovics, and Gál 2014; Geletič and Lehnert 2016). Aside from the mapping methods, more accurate delineation of LCZ classes requires supplementary information about building and vegetation structure, considering their indispensable roles in the LCZs definitions (Stewart and Oke 2012). Studies have demonstrated lower-quality LCZs classification results with limited information on urban structure. For example, LCZs mapping in Guangzhou reached around 60% using the WUDAPT method (Xu, Ren, Cai, Edward, et al. 2017) and LCZs mapping of Hong Kong demonstrated lower classification accuracy when comparing results from the WUDPT method and GIS-based method (Wang et al. 2017).

Light detection and ranging (Lidar) data provide a viable source with which to acquire information on structural characteristics of surface features. However, while Lidar data have been employed to detect vegetation structure and digitize urban 3D maps, its application for LCZs mapping has rarely been studied (Koc et al. 2017); and no studies using Lidar for LCZ mapping have been conducted in the U.S. Rather, most current publications are related to cities in European and South Asian regions (Geletič, Lehnert, and Dobrovolný 2016; Zheng et al. 2017; Cai et al. 2017; Xu, Ren, Cai, Edward, et al. 2017; Lehnert et al. 2015; Unger, Lelovics, and Gál 2014). To assess the utility of Lidar to contribute to LCZs classification, this study presents a GIS-based LCZs classification scheme with the aid of airborne Lidar datasets and other freely available GIS data for three major metropolitans in Texas, USA: Dallas-Fort Worth (DFW), Austin, and San Antonio. The LCZs classifications were then mapped and compared in an effort to provide a standardized urban morphology classification for future studies of surface temperature variability and UHI effects.

3.2 Materials and Methods

3.2.1 Study Area

DFW, Austin, and San Antonio were selected for the LCZs mapping because of their hot and humid summers and population concentration (Figure 3.1 and Table 3.1). However, there have been few UHI studies within these metropolitan areas, and comparisons of UHI results are difficult because of variations in mapping units and land cover characteristics. Located in North Texas, Dallas and nearby Fort Worth were developed as a result of the construction of major railroad lines through the area. Rapid industrialization resulted in accelerated socioeconomic growth and land use changes, leading to the consistent rise of the UHI phenomenon (Winguth and Kelp 2013). In addition, Dallas is projected to continue to grow rapidly. Growth projections forecast an approximate increase of 45% in population, 44% in employment, and 55% in vehicle-miles traveled from 2013 to 2035.

Austin, the capital city of Texas, connects the main metropolitan areas (including Houston) of Texas with each other. The low unemployment rate and high quality of life combine to create a rapidly increasing population. The year 2014 alone witnessed a 2.5 % population growth and 5.88 % economic expansion, and Austin is currently ranked among the top 20 fastest-growing cities in the U.S. (America’s 20 Fastest-Growing Cities last accesed March 21th, 2018). Austin is influenced by a humid subtropical climate, with long hot summers and short mild winters.

San Antonio is located in south central Texas; situated between the Edwards Plateau to the northwest and the Gulf Coastal Plains to the southeast. The city is known for its Texas history, culture, and downtown beauty, and it attracts more than one million tourists per year (Bremer 2004). Interstate highways (I-35, I-37, and I-10) connect San Antonio to major Texas population centers and to primary border crossing points into Mexico.

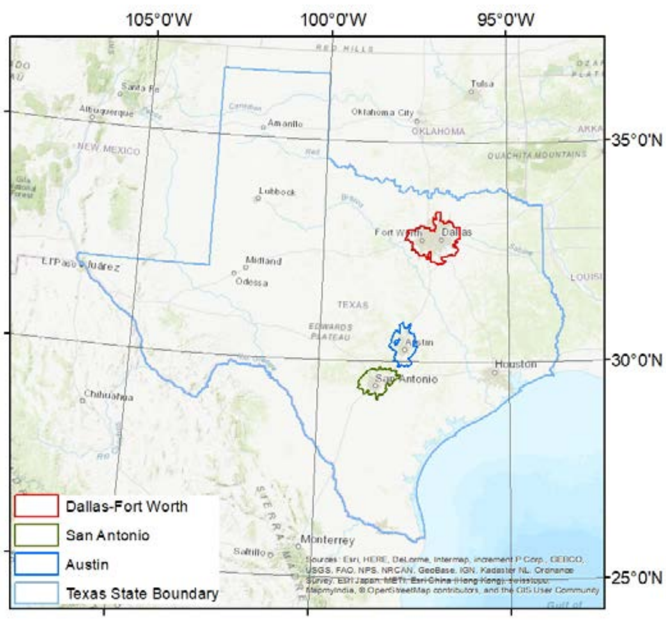

Figure 3.1 Location of the three metropolitan study areas in Texas, USA.

Table 3.1 Population statistics of the study areas from the U.S. Census Bureau.

	Population, Census, April 1, 2010	Land area (square miles), 2010	Estimated population (July 1, 2015)	Housing units (July 1, 2015)	Estimated population change (2010-2015, %)
Texas Total	25,145,561	261,231.71	27,469,114	10,587,752	9.2
San Antonio	1,327,407	460.93	1,469,845	524,246	10.7
Dallas	1,197,816	340.52	1,300,092	516,639	8.5
Austin	790,390	297.90	931,830	354,241	14.8
Fort Worth	741,206	339.82	833,319	291,086	12.2

3.2.2 Data Derivation and Preprocessing for LCZs Mapping

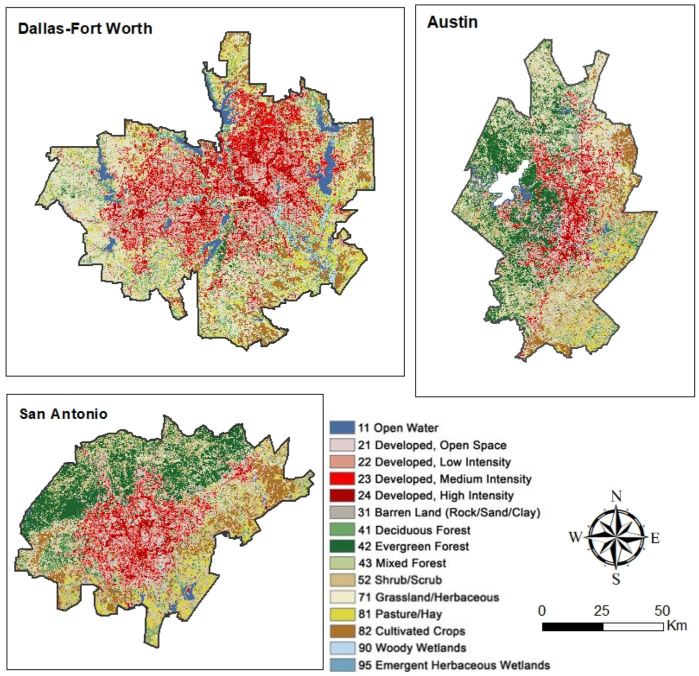

Figure 3.2 Land use and land cover distributions of three metropolitan areas derived from NLCD 2011.

3.2.2.1 LCZs Preliminary Classification by Surface Cover Properties

The development of a GIS-based LCZs classification scheme was based mainly on the LCZs definition and LCZs delineation criteria (Stewart and Oke 2012). Considering that the original proposal of LCZs mapping is to investigate UHI, individual LCZs are supposed to be constant throughout the year compared to the seasonal and even annual variation of the surface and air temperature. LCZs classes can be categorized as two types: built-up cover and natural cover. Hence, a preliminary classification was performed based on the 30*30 m resolution 2011 National Land Cover Database (NLCD), the thematic accuracy of which has been established in the literature (Wickham et al. 2017). First, a customized Arcpy Package was designed by the author to reclassify the surface cover properties from NLCD into LCZs groups or LCZs in the ArcGIS environment. Some land cover classes were directly classified or merged into individual categories of LCZs (C, D, E, F, and G), while others were classified into LCZ groups (LCZs 1-10 built-up type category or LCZ E Bare rock or paved) (Table 3.2).

Table 3.2 The look-up table of Local Climate Zones (LCZs) pre-classification by NLCD classes.

NLCD code	**NLCD class name**	**LCZ code**	**LCZ class name**
11	Open Water	LCZ G	Water
21 22 23 24	Developed, Open Space Developed, Low Intensity Developed, Medium Intensity Developed, High Intensity	LCZs 1-10 LCZ E	Built-up types Bare rock or paved
31	Barren land	LCZ E LCZ F	Bare rock or paved Bare soil or sand
41 42 43	Deciduous Forest Evergreen Forest Mixed Forest	LCZ A LCZ B	Dense trees Scattered trees
52	Shrub/Scrub	LCZ C	Bush, scrub
71 81 82 90 95	Grass/Herbaceous Pasture/Hey Cultivated Crops Woody Wetland Emergent Herbaceous Wetlands	LCZ D	Low plants

3.2.2.2 Lidar Data Acquisition and Processing

Lidar datasets were obtained from the Texas Natural Resources Information System (TNRIS), downloaded manually per tile online, or transferred directly from a hard drive. They were derived from different projects acquired between 2007 and 2013 (Figure 3.3). The point density, horizontal and vertical accuracies, datum and projection information are provided in Table 3.3Table 3.3 Metadata of Lidar projects for the study areas..

Table 3.3 Metadata of Lidar projects for the study areas.

Project Name	Point Space (cm)	Horizontal/ Vertical Accuracy (cm, MSE)	Horizontal/ Vertical Datum	Projection	Units	Point Classes
Dallas-Fort Worth						
StratMap 2013 Ellis, Henderson, Hill, Johnson, Navarro	50	NA/3.43-6.1	NAD83, NSRS2007/NAVD88, GEOID 12A	UTM Zone 14N	Meters	1, 2, 3, 4, 5, 6, 7, 9, 13
StratMap 2012 TCEQ Dam Sites	50	75/25	NAD83/NAVD88, GEOID 09	UTM Zone 14N	Meters	1, 2, 3, 4, 5, 6, 7, 9, 13
FEMA 2011 Parker	100	60/37	NAD83/NAVD88, GEOID 09	UTM Zone 14N	Meters	1, 2, 7, 9, 10, 11
StratMap 2011 Collin, Denton, Kaufman	50	NA/6.03-7.13	NAD83/NAVD88, GEOID 09	UTM Zone 14N	Meters	1, 2, 4, 6, 7, 9, 13
Grand Prairie 2009	70	30-45/9.1	NAD83/NAVD88, GEOID 03	State Plane Texas North Central	Feet	Ground, man-made, vegetation
StratMap 2009 Dallas	100	NA /12-15.9	NAD83/NAVD88	UTM Zone 14N	Meters	1, 2, 6, 7, 9, 12, 13
StratMap 2009 Tarrant	50	100/NA	NAD83/NAVD88, GRS80	UTM Zone 14N	Meters	1, 2, 3, 4, 5, 6, 7, 9
Austin						
CAPCOG 2012 Travis	140	N/A	NAD83/NAVD88	State Plane Texas Central	Feet	1, 2, 3, 4, 5, 6, 7, 9, 11, 15, 17
StratMap 2011 Caldwell, Gonzales	50	75/15	NAD83/NAVD88	UTM Zone 14N	Meters	1, 2, 4, 6, 7, 9, 13
CAPCOG 2008 Bastrop, Fayette, Hays	140	100/18.5-37	NAD83/NAVD88	State Plane Texas South Central	Feet	Ground/unclassified

Table 3.3-Continued

CAPCOG 2007 Caldwell, Travis, Williamson	140	100/18.5	NAD83/NAVD88	State Plane Texas Central	Feet	Ground/unclassified
San Antonio						
FEMA 2011 Comal, Guadalupe	100	60/12.5	NAD83, NSRS2007/NAVD88, GEOID 09	UTM Zone 14N	Meters	1, 2, 7, 9 ,10, 11
StratMap 2010 Bexar	50	100/19	NAD83/NAVD88, GEOID 09	UTM Zone 14N	Meters	1, 2, 6, 7, 9, 12, 13
CAPCOG 2007 Caldwell, Travis, Williamson	--	--	--	--	--	--
CAPCOG 2008 Bastrop, Fayette, Hays	--	--	--	--	--	--

Notes: NAD refers to North American Datum; UTM refers to Universal Transverse Mercator. Point Classes are based on ASPRS classification: Class 1: Unclassified; Class 2: Bare Earth; Class 3: Low Vegetation; Class4: Medium Vegetation; Class5: High Vegetation; Class 6: Buildings; Class 7: Low point/Noise; Class 9: Water; Class10: Rail; Class11: Road Surface; Class 12: Overlap; Class 13: Bridges/Culverts; Class 15: Transmission Tower; Class 17: Bridge Deck. – refers to “Same as Above”

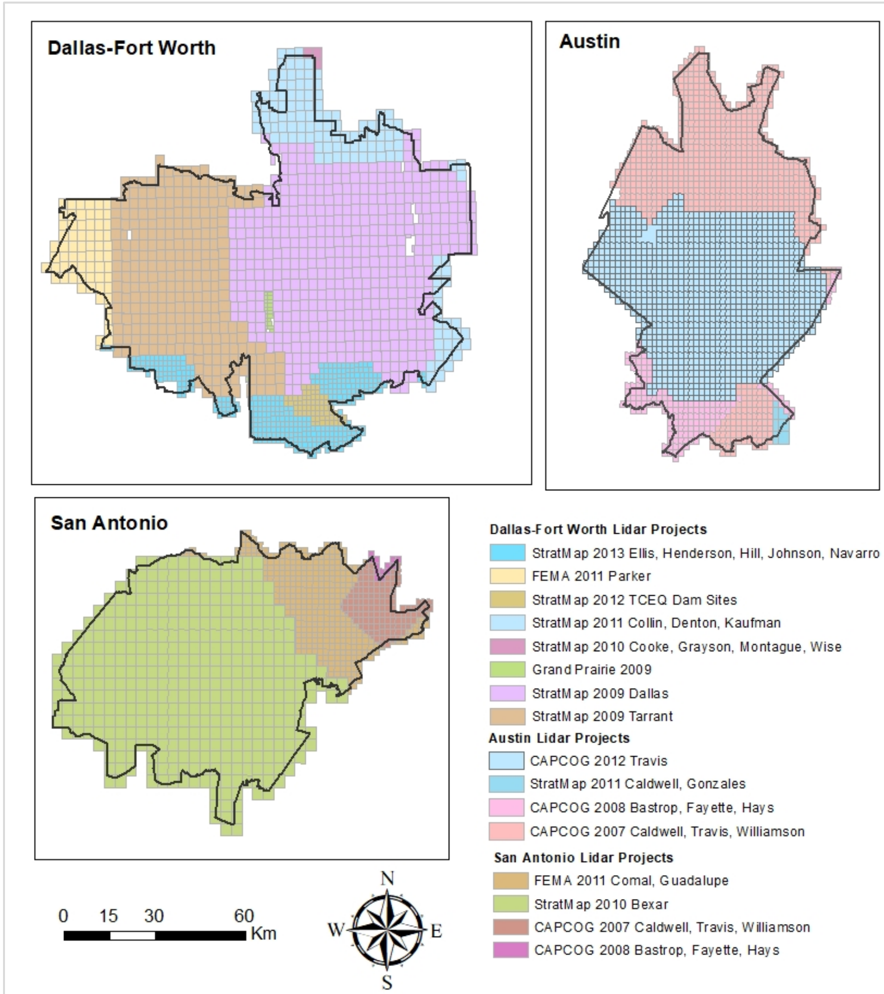

Figure 3.3 Lidar dataset coverages and project names for DEM production and building footprint extraction per metropolitan area.

All Lidar datasets were delivered with ground points classified. Specific metadata regarding acquisition parameters and subsequent project deliverables are provided in Table 3.3. Given the variable nominal point spacing of the different Lidar acquisitions, digital terrain models (DTMs) with 3m*3m and 1m*1m resolution were generated for the three study areas using the "LAS Dataset to Raster" tool in ArcGIS 10.5 Conversion Toolbox and "Average Cell Assignment Type" using ground points only. Similarly, the digital surface models (DSMs) were generated with 3m*3m and 1m*1m resolution and

“Maximum Cell Assignment Type” to represent the surface combined ground, built-up, vegetation, etc. DTMs from different sources were merged together after being re-projected to same spatial reference (NAD UTM Zone 14N) for the three study areas. The same procedures were applied to the DSMs. Then, normalized digital surface models (nDSMs) with 3m*3m and 1m*1m resolutions were built by subtracting the DTMs from the DSMs. Figure 3.4 shows the spatial pattern of nDSMs for the study areas and Figure 3.5 provides a detailed illustration of nDSMs for a selected area in San Antonio.

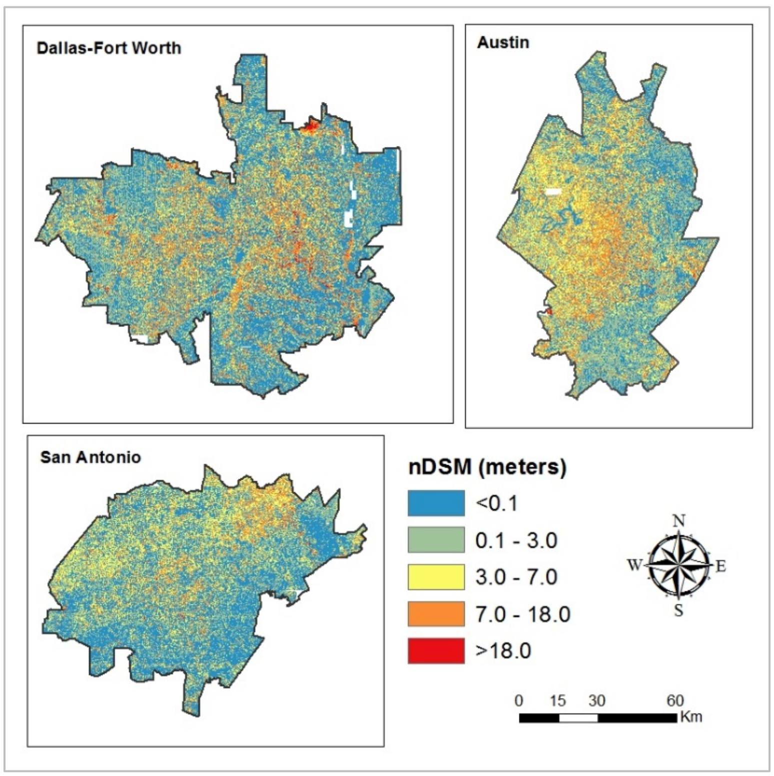

Figure 3.4 Normalized digital surface models (nDSMs, unit: meters) with 3m*3m resolution of three metropolitan areas.

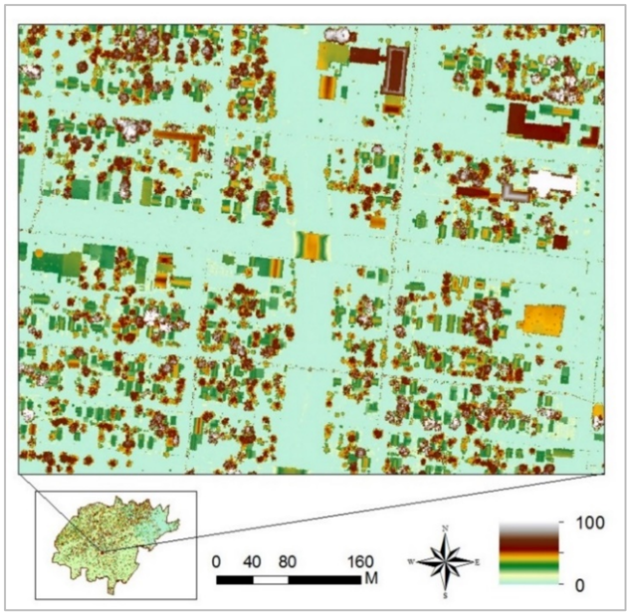

Figure 3.5. Detailed illustration of normalized digital surface models (nDSMs, meters) with 1m*1m resolution for a small area in San Antonio.

Building footprints are very important to distinguish individual LCZs among the LCZs 1-10 built-up category, in terms of the building height (high-rise, mid-rise, or low-rise) and fraction (compact or open). The available datasets from the different sources were first checked. Building footprints of the central and south parts of Austin were created by the City of Austin Enterprise Geospatial Services. They were digitized mainly from 2012/2013 orthoimagery and made available through the official website of the City of Austin, but they did not cover the entire metropolitan area. Similarly, building footprints for the downtown area of Dallas were digitized from 2009 aerial photography and available through “City of Dallas City GIS Services” website (Dallas City GIS Services last accessed March 21th, 2018.), but the coverage extent was very small and not up-to-date.

Here, the buildings footprint for the three metropolitan areas was extracted using the Lidar mass point clouds. For several projects (e.g., CAPCOG 2007”, “CAPCOG 2008”, and “FEMA 2011 Comal, Guadalupe”), buildings had not yet been classified from the mass point clouds (Table 3.3). Also, even though the Lidar point clouds were already pre-classified for buildings in the StratMap 2010 Bexar Lidar dataset in San Antonio, I found that most that the data had a high omission error in this project. Hence, building classification was still necessary for this project. The buildings from point clouds for Austin and San Antonio were first classified with point cloud task tool “Planar Point Filter”, in which the parameters were set after several trial and error runs (Table 3.4). Subsequently, together with the Lidar projects (e.g., projects in DFW) in which buildings had already been classified, the building outlines were extracted as shapefile polygons from Lidar data in LP360, a software for the Lidar data management and post-processing, with the automated point cloud task tool “Point Group Tracing and Squaring” for the developed areas.

Table 3.4 Parameter settings for building classification and extraction in LP360.

Parameters	**Value**	**Unit**
Building Filter: Planar Point Filter		
Minimum and Maximum Building Height	8/6000	Feet
N Threshold	0.40	Feet
Minimum and Maximum Slope	0/45	Degree
Minimum Plane Edge	10	Feet
Maximum Grow Window Area	5000	Square Feet
Plane Fit	0.2	NA
Building Extractor: Point Group Tracing and Squaring		
Max Planar Patch Area	5000	Square Feet
Grow Window Size	5.5	Feet
Trace Window Size	12	Feet
Minimum Area	100	Square Feet
Regularization Angle Degrees	30	Degree

Note: “N Threshold” refers to the distance to consider a point as part of the plane. “Plane Fit” refers to the tightness of the fit of the planar surface.

To assess the building extraction performance, high-resolution 30cm imagery provided by ERSI ArcGIS was chosen as a base map and overlain by the building points. The result showed that numerous trees were misclassified as buildings, especially in northern Austin and northern San Antonio (Figure 3.6). Additionally, the buildings points were not fully classified where the buildings were under trees in some mixed development/vegetated areas. From the LCZs definition, single or scattered buildings in undeveloped areas or highly vegetated areas (e.g., a single family house located in NLCD classes 31-95, and refer to Figure 3.2 for NLCD distribution for the study areas) were excluded from potential classification as LCZs 1-10 (Table 3.2). Therefore, to avoid this classification error due to the limitation of the algorithm in software and insufficient data points due to tree canopy, the buildings located in developed land areas (NLCD 21-24) were only considered and extracted in the subsequent building extraction step.

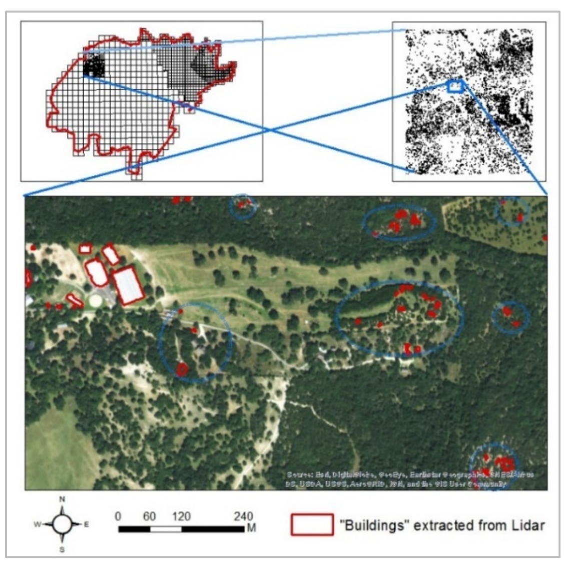

Figure 3.6 Errors of building classification for an area in northern San Antonio. (Note: Red outlines demonstrate algorithm identification of buildings, while blue circle indicates errors of commission.)

To further improve the accuracy of the buildings extraction steps detailed above, I manually interpreted and deleted erroneous building outlines with the aid of high-resolution historical images from Google Earth and base maps in ArcGIS, as well as the above-mentioned building footprints for parts of Dallas and Austin. The algorithm also identified elevated highways and major roads as buildings, and the large extent of the study areas makes it time-intensive to drop them off manually. Considering that the aim of building footprints is to calculate the buildings surface fraction, while the material and shape of these man-made above ground properties makes them meet the general concept of "buildings", I did not delete these small proportion of properties from the building footprints. Figure 3.7 shows examples of the detailed buildings extraction results at selected intensively developed areas.

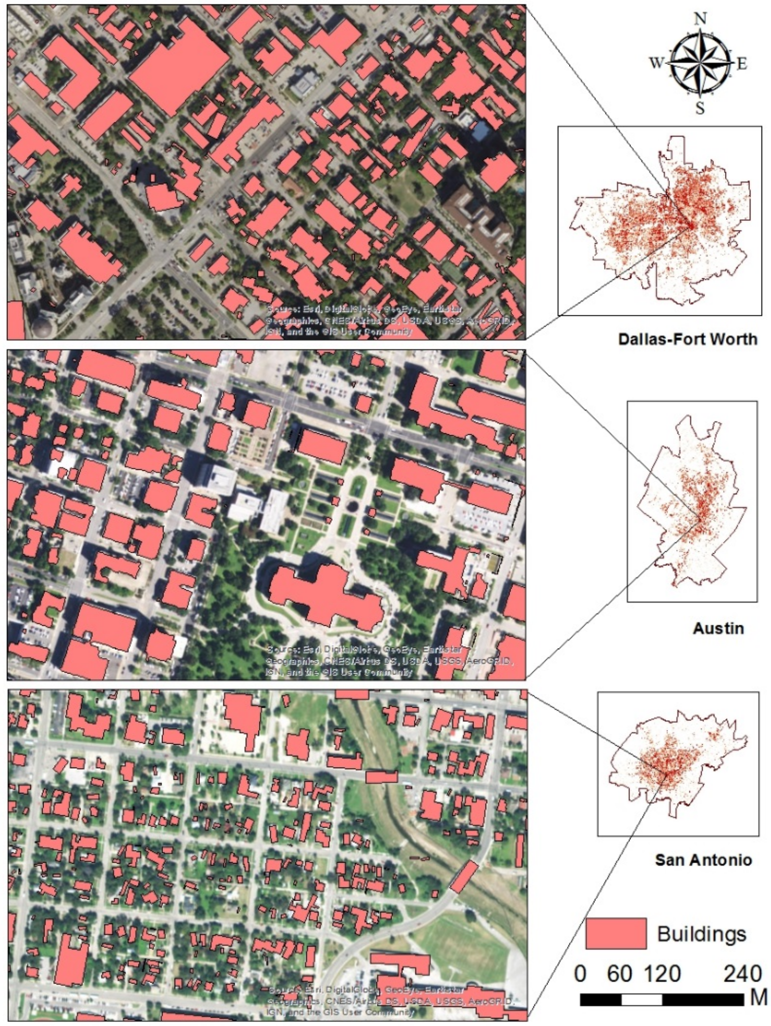

Figure 3.7 Detailed illustrations (left) of building extractions from a selected part (right) of the three study areas.

3.2.3 LCZs mapping Scheme

3.2.3.1 Determination of LCZs Mapping Scale

It was necessary to set a common scale for different properties calculations as well as the further aggregation for LCZs mapping. The NLCD with 30*30 m resolution was the original data source for LCZs preliminary classification. Meanwhile, the definition of LCZs mentioned uniform region spans “hundreds of meters to several kilometers on a horizontal scale” to ensure the homogeneity of the zones. In climatology, this is often referred to as a scale between micro and meso-scales.(Bechtel et al. 2015). This broad range of scale definition allows us to customize the scales for the derivation of properties to map LCZs according to the data sources and urban characteristics. However, it is certain that the smallest unit of LCZs should be a homogenous area in terms of the surface conditions related to the local climate formulation, including building structure, vegetation types, etc.

There is more morphological variation for high density building areas within a certain distance than other areas in the city environment (Zheng et al. 2017). In this study, three sites with the same area of 131.25 square kilometers located at the most intensely developed land cover area were selected to test the spatial dependency characteristics of the building structure to objectively identify the LCZ mapping scale. The best-fit parameters of the variogram models for each sampled dataset were explored using the Geostatistical toolset in ArcGIS 10.5.

3.2.3.2 LCZs properties generation and LCZs mapping

Using the reclassified NLCD and Lidar-derived datasets, seven geometric and surface cover properties (provided in Table A1) were calculated. The ability of the threshold, which was codetermined by seven properties, to identify individual LCZ was first tested for a fraction of the study area using the “knowledge-based classification” tool in ERDAS IMAGINE 2015. It demonstrated that the definition of thresholds of LCZs properties in Table A1 cannot be directly used for LCZs classification and that a straight combination of all the seven thresholds can lead to a situation in which a substantially redundant area will not belong to any LCZ. A similar issue was also identified in other

GIS-based LCZs mapping studies (Zheng et al. 2017; Geletič and Lehnert 2016). Published case studies confirmed that not all features defined in the LCZs concept are equally important for LCZs mapping (Bechtel et al. 2015), and that not all features can be included in a GIS-based LCZs delineation algorithm (Geletič, Lehnert, and Dobrovolný 2016). According to the analysis by Bechtel et al. (Bechtel et al. 2015), the height of roughness is the most important characteristic of the urban structure while the pervious surface fraction (PSF) is important to represent urban fabric and cover. We referred to recent publications and determined three properties which had been most frequently used for LCZs mapping: height of roughness (Wang et al. 2017; Unger, Lelovics, and Gál 2014; Zheng et al. 2017; Geletič and Lehnert 2016; Koc et al. 2017), building surface fraction (Wang et al. 2017; Unger, Lelovics, and Gál 2014; Zheng et al. 2017; Geletič and Lehnert 2016; Koc et al. 2017), and pervious surface fraction (PSF) (Koc et al. 2017; Zheng et al. 2017; Geletič and Lehnert 2016; Unger, Lelovics, and Gál 2014).

The height of roughness elements was considered as the principal properties for LCZs mapping after the pre-classification from NLCD. The height of roughness elements refers to the geometric average of building heights (LCZs 1–10) and tree/plant heights (LCZs A–F). The absolute height of surface objects (e.g., built-up, vegetation, etc.) was calculated based on the nDSMs to extract height of roughness, which was used to subdivide the LCZ 1-10 into three groups (e.g., LCZs high-rise 1 and 4, LCZs mid-rise 2 and 5, as well as LCZs low-rise 3, 6, 7, 8 and LCZ sparsely built) and extract the LCZ D low plant from the group LCZ A, B, and D (Figure 3.8). Building surface fraction refers to the ratio of building plan area to total plan area. The average building surface fraction was calculated as the proportion of building footprints in a 30*30 m^2 pixel area. PSF was calculated as the opposite proportion of Impervious Surface Fraction (ISF), gathered from the 2011 NLCD.

Furthermore, due to the lack of specific information, thermal, radiative, and metabolic properties, which are important to determine a certain class (e.g, LCZ 10 Heavy industry), we checked the City GIS Services websites of the related study areas, and gathered the city land use planning datasets for recent years. The heavy industry areas were extracted and mapped to LCZ 10 Heavy industry. Together with the height of roughness, those variables delineate the grouped LCZs in the last step. Python statements were used for the automated classification of these grids according to the modified values from Table A1. Figure 3.8 shows the overall LCZs decision-mapping scheme by considering different properties and in each step.

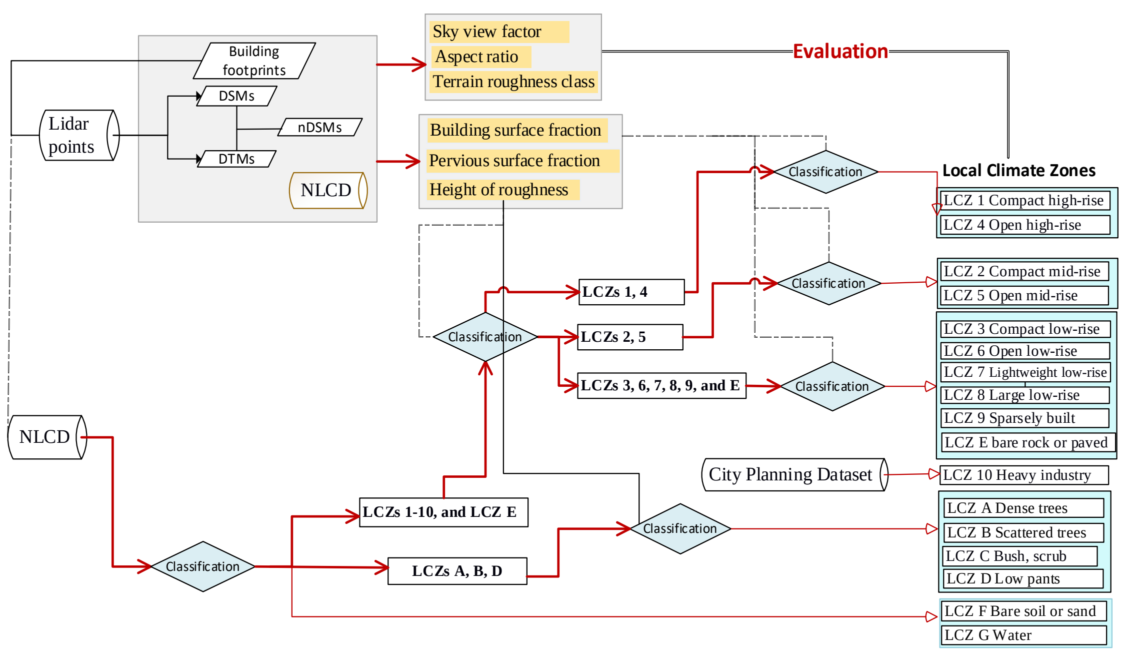

Figure 3.8 Overall Local Climate Zones (LCZs) mapping scheme.

Sky view factor (SVF), Aspect ratio (H/W), and terrain roughness classes are also defined with the specific threshold for LCZs identification (Stewart and Oke 2012). SVF varies with height and spacing of buildings and trees and it affects radiational heating/cooling. For LCZs identification, it refers to the ratio of the amount of sky hemisphere visible from ground level to that of an unobstructed hemisphere (Stewart and Oke 2012). In this study, the nDSMs with 3m*3m resolution was used to calculate SVF using the open source Relief Visualization Toolbox. The 3m*3m resolution was chosen mainly because of the capability of the tool, and the 3m*3m resolution SVF meets the accuracy requirement. Aspect ratio (H/W) refers to the mean height-to-width ratio of street canyons (LCZs 1–7), building spacing (LCZs 8–10), and tree spacing (LCZs A–G). Due to the variation of the city architecture and building geometry, there is no standardized method for calculating aspect ratio, especially for LCZ mapping (Houet and Pigeon 2011; Zheng et al. 2017). For this study, the maximum height in a 30*30 pixel area based on nDSMs was calculated. Areas with height lower than 0.5 meters were assumed to be ground, and the average width of the ground surface in a 30*30 pixel area was calculated based on nDSMs dataset with 3m*3m resolution. Then, the aspect ratio map (maximum height/average width of the ground surface) was calculated as a property for LCZs mapping evaluation according to the LCZs definition. The Davenport roughness classification method has been adopted as the terrain roughness classes for LCZs definition (Stewart and Oke 2012; Davenport et al. 2000). The values of roughness length were grouped into eight classes of roughness. The roughness classes with this method was defined based on the current database of NLCD and nDSM. Due to the complementarity of ISF and PSF from the data sources, PSF was abandoned for LCZs evaluation.

3.3 Results

3.3.1 Scale Selections for GIS-based LCZs Mapping

Considering the role of the height of roughness in LCZs mapping, the major ranges of variograms for building heights were compared (Figure 3.9). By performing an ordinary prediction, the Gaussian process regression was used to fit the experimental variogram to obtain optimized parameters. The variogram shows that the semivariance of the height of buildings increases as the distance of the building increase, especially for San Antonio, and then stays in the sill when the distance reaches to certain extent (e.g., the range of the variogram) (162.87 m, 193.41 m, and 139.18 m for DFW, Austin, and San Antonio, respectively). Hence, the scale of the LCZs mapping should be higher than the maximum of the ranges of the variograms of building heights for the selected areas to ensure homogenous climate zones in terms of the urban morphology.

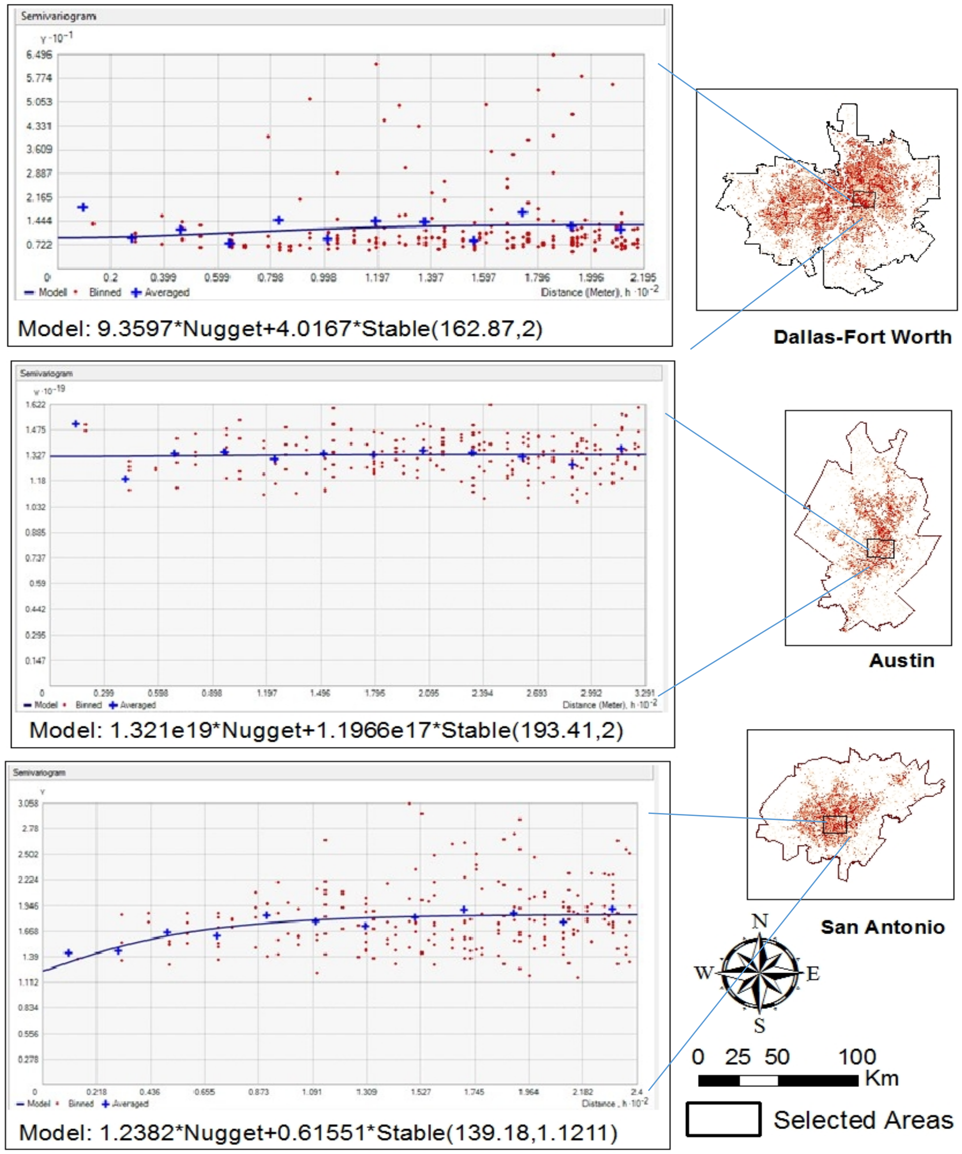

Figure 3.9 Experimental variogram models (left) of building height for selected areas (right).

Additionally, it was also necessary to set a common scale for various parameter calculations to further identify possible LCZs. The maximum resolution of the data sources for LCZs mapping is 30 meters (e.g., NLCD). Here, the spatial resolution of 90 m was considered for LCZs parameters generation. Subsequently, to meet the requirement of the homogenous building morphology condition as explored by the variogram models and to facilitate LCZs mapping conveniently and efficiently, a 3 × 3 cell (270 m × 270 m) moving window around each cell was used for further aggregation. Hence, in accordance with the proposal of LCZs for urban climate study as a uniform of land cover and surface structure, the scale for the LCZs mapping was determined to be 270 × 270 meters.

3.3.2 Spatial Distribution of LCZs Maps

LCZs were identified and tested with the mapping scheme and the threshold defined by Stewart and Oke (2012) (Table A1). Overall, the LCZs maps show a generally similar pattern in all the three metropolitans, with LCZ 1-10 “built-up cover” types generally surrounded by LCZs A-G “natural cover” types (Figure 3.10). The LCZs mapping results were overlaid with the high resolution historical Google Earth imagery to evaluate the mapping accuracy. This spatial distribution corresponds with the underlying land cover shown with high resolution imagery (e.g., Figure 3.11). As illustrated, profiles of some LCZs in Figure 3.11, most of the LCZs were matched correspondingly with the representative examples shown in Table 2 in p. 1885 of Stewart and Oke (2012). In our mapping, I found that the areas with building fraction less than 15% are usually occupied by dense or tall vegetation, leading to the height of roughness elements higher than 15 meters (Figure 3.11). Thus, the height of roughness threshold was adjusted for LCZ Sparsely built identification (Table A1).

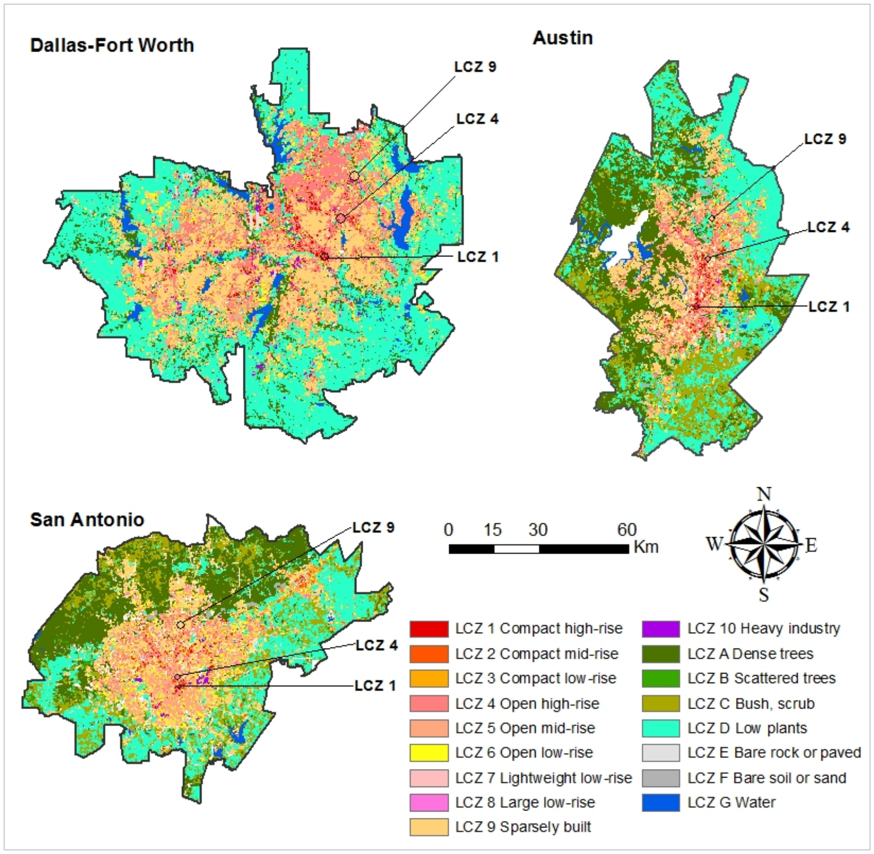

Figure 3.10 Spatial distribution of LCZs for the three metropolitan areas at Texas. (Note: the labels on the map are the locations of the illustrated sites in Figure 3.11 with the detailed examination at Google Earth.)

The LCZs maps capture most of the underlying land cover and urban morphological characteristics, with less than 1% of "holes" which were not assigned to LCZs. I noted that LCZ E Bare rock or paved is mosaicked with LCZ 1-10 "Built-up cover" types by zooming in the LCZs maps, filling in the LCZ 4 Open high-rise in the form of straight lines. The more intensely developed city system in DFW along with transportation construction (car parking lot, wide traffic roads, railway yards, etc.) lead to a higher percentage of LCZ E (e.g., Dallas-Fort Worth airport is distinguishable in Figure 3.10) than the other two metropolitans.

LCZ 1 Compact high-rise LCZ 4 Open high-rise LCZ 9 Sparsely built

Figure 3.11 Examples of the typical LCZs for the three metropolitan areas. (Note: The first line shows the profiles of DFW, the second line shows the profiles of Austin, and the third line shows the profiles of San Antonio.)

For Austin and San Antonio, LCZs 1-10 are compactly distributed in the central urbanized area, and the surrounding rural areas of these two metropolitans shows a large percentage of LCZ A and LCZ B relative to LCZ D. LCZ A Dense trees is the typical LCZ in the eastern part if the cities, while the LCZ B Scattered trees is concentrated in the southern part, and LCZ D Low plants is concentrated in the western part. For the San Antonio area, there is a clear contrast of the northern and southern part, dominated by LCZ A Dense trees and LCZ D Low plants, respectively.

3.3.3 Validation of GIS-based LCZs Mapping

I examined the SVF, aspect ratio, and terrain roughness of the main LCZs of the study areas to evaluate the LCZs mapping result (Figure 3.12). Findings of the differences of the SVF and aspect ratio is in agreement with results from a prior GIS-based LCZs mapping study (Zheng et al. 2017). SVF thresholds of LCZs urban areas (especially LCZs compact) are generally lower than LCZs natural types, with noticeable variation among them. For most of the major LCZs of the three areas, their mean SVF values are within, or close to, the thresholds provided in Table A1, except LCZ 9 Sparsely built, LCZ A Dense trees, and LCZ G Water. (Figure 3.12). This indicates that the SVF is an important factor for LCZs fine delineation. In the SVF calculation, I used a DEM with 3 meters resolution and set the diameter to 90 meters, which may lead to SVF differences. In addition, I consider the effects introduced by buildings, bridges, or vegetation for SVF calculation according to the definition, though some studies exclude the impacts of trees when calculating SVF for LCZs “built-up” types delineation. , considering that the green cover in suburb areas might affect the calculation (Koc et al. 2017).

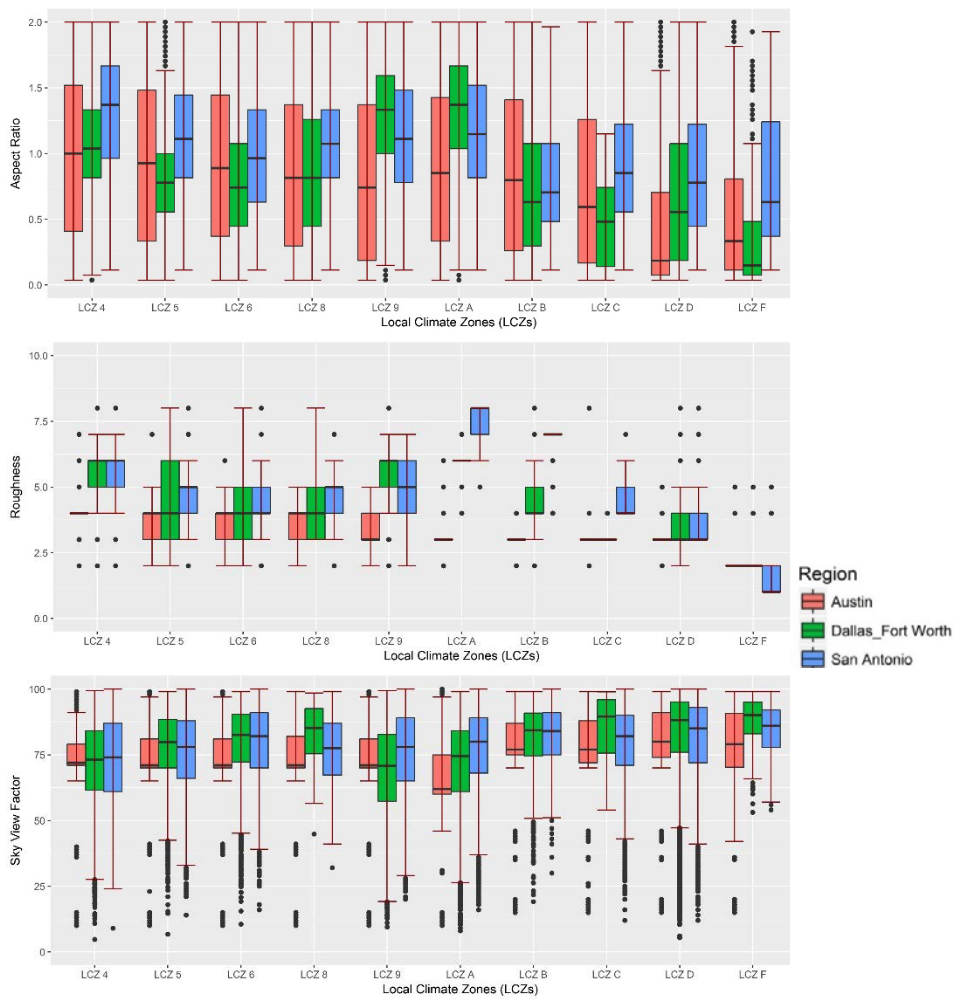

Figure 3.12 Boxplot of LCZ parameters of the main LCZs types of three metropolitan areas.
(Note: Please refer to the name of LCZs from Figure 3.10).

Regarding aspect ratio, LCZ 4 showed higher and wider range of aspect ratio than other LCZs built-up types due to the variation in height of tall buildings, and LCZ A also demonstrate high aspect radio due to tall trees. However, most of LCZs showed considerable variation and departure from the standardized threshold (e.g., LCZ 8 Large low-rise, LCZ 9 Sparsely built, and LCZ A Dense trees, and LCZ G Water). So far, there is no standard method for the aspect ratio calculation, which lead to the differences from thresholds defined by Stewart and Oke (2012). Hence, in future, it is necessary to achieve the consensus in terms of the interpretation of different properties for GIS-based LCZs mapping.

Due to the coarse classification of the terrain roughness classes, its value matches the definition of LCZs.

3.4 Discussion

3.4.1 Advantages of Lidar for GIS-based LCZs Mapping

The integration of Lidar data helped to incorporate detailed urban and vegetation morphology information for LCZs mapping at the scope of whole metropolitans. So far, there has only been one study using Lidar data for LCZs mapping, and it was conducted within a small portion of suburban Sydney, Australia, owing mainly to the time and expense limitations of data acquisition (Koc et al. 2017). With the free availability of Lidar datasets and updated NLCD in the U.S., the study provides evidence that the automated GIS-based LCZs mapping can be replicable to other cities in the U.S. by extracting and incorporating fine-scale 3D urban morphological information from a couple of Lidar-derived products.

Additionally, Lidar datasets provide detailed urban geomorphology to analyze LCZs mapping scale. There are different findings for LCZs mapping scale, indicating that spatial characteristics vary worldwide due to urban forms, urban development history, geographical location, and hydrogeological setting. For example, the scales for LCZs mappings have been assigned with 100 m in a suburb area of Sydney, Australia (Koc et al. 2017), and Seoul, South Korea (Lee and Oh 2017), 120 m in Khartoum, Sudan

(Bechtel et al. 2016), and 500 m in Szeged (Unger, Lelovics, and Gál 2014). In addition, Kotharkar and Bagade (2017) mapped the LCZs of Nagpur, India with different scales (e.g., 250 m, 500 m and 1000 m) to explore the appropriate LCZ zoning unit, and they found that 250 m led to fragmented LCZs maps for the city with scattered distributions of slums (Kotharkar and Bagade 2017). Based on the height of buildings, 270 m was defined as a homogeneous scale in this research, and it is in accordance with the 300 m LCZs mapping scale in Hong Kong, which was based on a more intensive and sophisticated examination of building characteristics (Zheng et al. 2017). However, the compatibility and rationality of the mapping zoning still need more verification in the future UHI study of the areas.

With detailed urban morphology information provided by Lidar data, the decision-making algorithm considers land cover, the height of roughness, building surface fraction, pervious surface fraction, and industrial sites from top to done to get LCZs maps. This GIS-based mapping scheme ensures that only one LCZ can be assigned to a given morphological area without “overlaps” or “holes” caused by parameter combinations of all the LCZs properties (Bechtel et al. 2015). In addition, other geometric and surface cover properties including SVF in the mapped LCZs are basically in accordance with the LCZs definition, which indicates the effectiveness of the LCZs mapping. Since the main propose of LCZs maps are for urban climate studies, a comprehensive examination of LCZs maps would consider the thermal characteristic (e.g., surface or air temperature) in future studies.

3.4.2 Uncertainties of the LCZs mapping Method

For the LCZs mapping itself, the LCZ was defined as an area with uniform land cover, surface structure, constructions material, and human activity (Stewart and Oke 2012). On the one hand, both the urban and natural landscape are heterogeneous, meaning that each LCZs is not an absolute homogenous region and there is no clear boundary between different LCZs. For instance, the LCZ G Water considers different water bodies with the same surface properties in the LCZs definition, given that the LCZs were mainly developed for a city environment. Similarly, the LCZ 9 Sparsely built showed different landscape characteristic for different sites when linking with Google Earth 3D imagery (Figure 3.11). Through they all match the LCZs definitions, their corresponding climate can be different due to the different thermal characteristics. LCZ E includes two types of land surface cover: Bare rock and paved. Nevertheless, linking the LCZs maps with Google Earth showed that most LCZ E in these three metropolitans are from urban transportation (roads, highways, parking places, airports, etc.). These examples indicate that some types of LCZs might need to be further sub-classified in terms of LCZs mapping at the metropolitan level or to fit the characteristics of different cities worldwide. Overall, LCZs mapping is a compromise between the universality and local accuracy.

Additionally, the LCZs definition did not consider the seasonal variation, which might lead to misinterpreted surface property results. Furthermore, the related properties for LCZs mapping were derived from secondary data sources with a time gap. NLCD 2011 data was derived from 2008-2010 Landsat data whereas Lidar projects were conducted by a suite of vendors working for various agencies or clients that all had different accuracy thresholds and acquisition period requirements (Table 3.3). An example of how the combination of various projects may manifest in the results is for areas dominated by broadleaf deciduous trees to produce spatial inconsistencies in the output maps.

In terms of the geometric and surface cover properties for LCZs definitions, not all features can be observed straightforwardly by Earth observation techniques. For example, human activities are still challenging to observe from space. I used the land use planning data for the industrial sites to represent the anthropogenic heat release, which does not take other surface properties into account. Furthermore, the study provided evidence that properties in Table A1 cannot be equally utilized to identify an individual LCZ with GIS decision-mapping method. In addition, the area along the LCZs boundary can be considered as fuzzy areas if the local heterogeneity being considered as mentioned, leading to another uncertainty for LCZs delineation. Future work can include the Fuzzy membership classification method or incorporate other remote sensing classification methods to explore the "cut off" values of LCZs properties.

3.4.3 Comparative Analysis of LCZs Maps for Three Metropolitan areas

In this study, LCZs mapping provides a platform to make a comparative analysis of the urban morphology and vegetation structure of the three metropolitan study areas. Regarding LCZs built-up types, there is a tendency that most of the urbanized area is categorized into open LCZs (e.g., LCZ 4 Open high-rise, LCZ 5 Open mid-rise, LCZ 6 Open low-rise), especially for DFW and San Antonio. Overall, DFW shows more diversity in terms of LCZ "built-up cover" types due to the complex regional character compared to other metropolitan areas. The highest urbanization rate of DFW manifested itself with the highest percentage of LCZ “built-up cover” types.

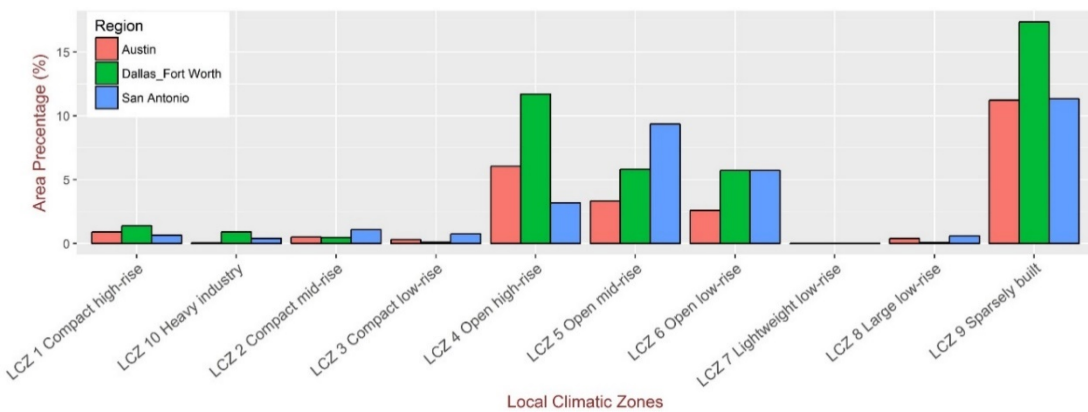

Figure 3.13 Statistical summary of the area proportion of LCZ 1-10 “Built-up cover” types in the respective LCZs maps of three metropolitan areas.

Additionally, the LCZs maps indicate an urban develop trajectory and the related urban form. DFW has the largest absolute amount and proportion of LCZs 1-10 “built-up” types. It corresponds to the fact that DFW is one of the largest inland metropolitan areas in the country and the economic hub of Texas. The relatively high proportion of LCZ 10 Heavy industry for DFW also indicates that the historical railroad construction and rapid industrialization led to the development of the DFW metropolis. The LCZs “built-up types” is concentric along the Highway I-35 across Austin, which corresponds with the function of Austin as the hub of communications to link DFW, Houston, and San Antonio. As a fast-growing and economic center similar to DFW, the Austin-Round Rock metropolitan area also has a considerable amount of LCZ 4 Open high-rise with compacted urban morphological structure concentrated on downtown areas. In contrast, the high buildings in San Antonio are loosely distributed, leading to a larger proportion of LCZ 5 Open mid-rise intersect with LCZ 6 Open low-rise. As the oldest city with landmark events and a slower pace of economic development, San Antonio-New Braunfels metropolitan has maintained this diversely distributed urban form.

The LCZs "natural types" distribution reflects the slightly different natural environment of the natural land of these three metropolitans. Given the geographical location and the climate environment, DFW is also different from the other two metropolitans regarding LCZs "natural types" diversity. Obviously, LCZ D low plants is dominant in the surrounding areas of DFW, which corresponds to the flat topology that more than 90% of the area lies in an elevation ranging from 130 meters to 300 meters (calculated from DTM) and land coverage with grassland and pasture. In addition, LCZ D Low plants and LCZ G Water also play role in intersecting LCZs 1-10 "built-up types" for the entire DFW and separating the area into four major city centers: Dallas, Fort Worth, Arlington, and Irving in the role of metropolitan "corridors". Further investigation of "corridors" at DFW implies that the main rivers, streams (with a length of more than 100 kilometers), and water bodies lead to the formation of the strip of LCZ D Low plants and LCZ G Water (Figure 3.14). Their role of separating LCZs 1-10 "built-up types" in the developed land areas warrants additional investigation, and the role of mitigating surface UHI needs further exploration.

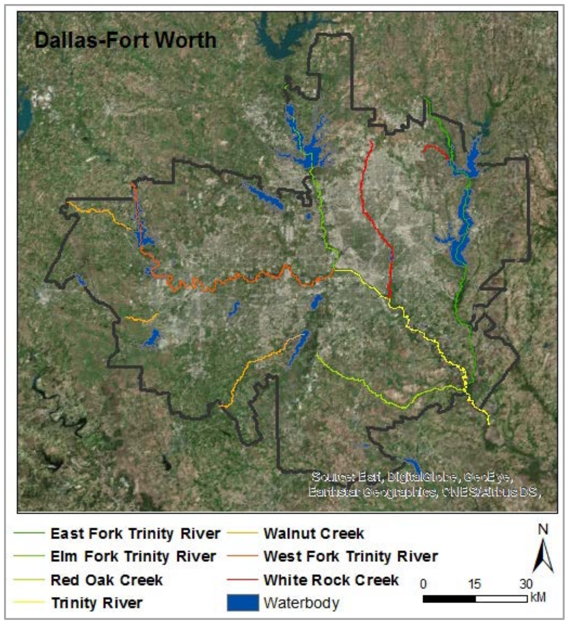

Figure 3.14 Major rivers, streams, and water bodies of DFW metropolitan areas.

LCZ A-G "Natural cover" types were generally more diversely distributed at Austin and San Antonio. With substantial amount grassland, pasture, and cultivated crops distributed along the majority of peripheries, LCZ D is the most typical LCZs types of three metropolitan areas (Figure 3.15). Furthermore, Austin has the highest percentage of LCZ A Dense tree, followed by San Antonio. Austin and San Antonio are also dominated by LCZ C Bush, scrub. In contrast, it is interesting to note the tiny proportion of LCZ C Bush, scrub at DFW, in accordance with the minimal coverage of NLCD class (e.g., 52 Shrub/Scrub). In addition, all metropolitan areas have slightly few LCZ F Bare soil or sand coverage versus other natural cover types, indicating that all of the areas are benefited from the LCZ "natural cover" types with the cooling effect of vegetation and water.

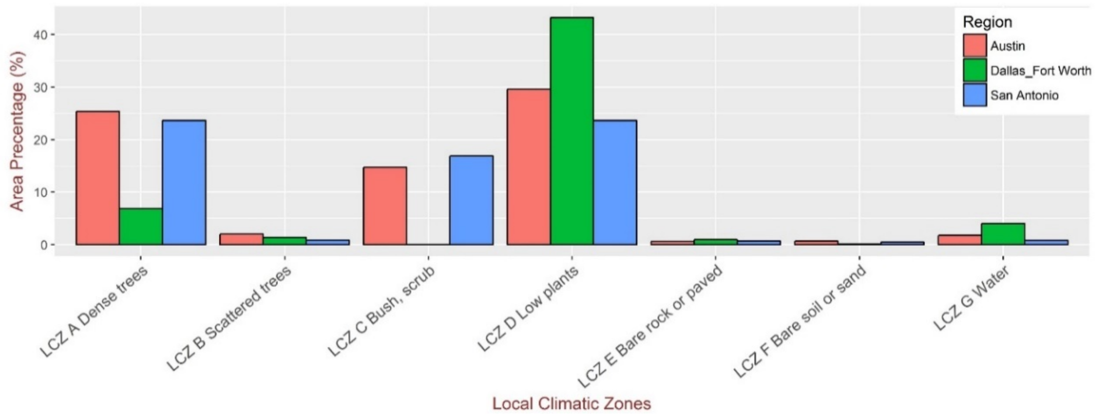

Figure 3.15 Statistical summary of the area proportion of LCZ A-G “Natural cover” types in the respective LCZs maps of three metropolitan areas.

In addition, there is a clear contrast between LCZ A Dense trees and LCZ D low plants at Austin and San Antonio, which apparently corresponds with the coverage by Trees and Grass or pasture. Further investigation indicates that the phenomenon is consistent with the regional geological characteristics. The geological structure of limestone and dolomite combination or limestone and clay combination at the eastern part of Austin and the northern part of San Antonio contribute to the tree growth and thus the distribution of LCZ A Dense trees, while the geological structure with limestone and sand combination or clay and fine-grained mixed clastic type combination lead to the development of grassland or pasture at western Austin or northwestern San Antonio (Figure 3.16).

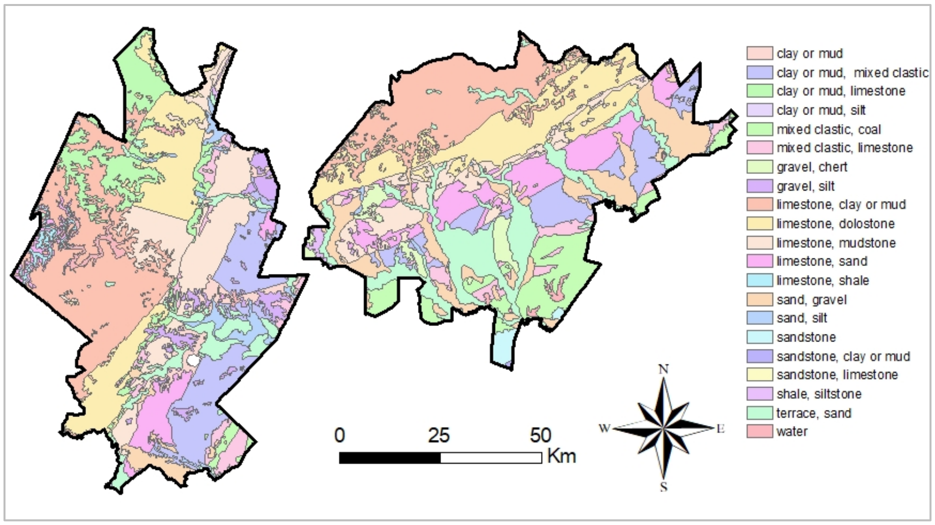

Figure 3.16 The geological structure of Austin and San Antonio metropolitan.
(Data is from U.S Geological Survey)

With a high percentage of LCZ A-D in a natural environment and LCZs Open high-rise and mid-rise in urbanized areas, the LCZs maps contribute to the worldwide LCZs studies in a high-density urbanization scenario. LCZs Compact types have been found in cities or mega-regions which are the economic hub of the region or the country, including Singapore (Ng 2015), Hong Kong (Zheng et al. 2017), the Yangtze River Delta (YRD) (Cai et al. 2017), Wuhan and Guangzhou (Xu, Ren, Cai, Edward, et al. 2017), etc. In contrast, LCZs characteristics of the study areas have relatively low percentages of LCZ compact types but high fragmentation of LCZs open types. There are other LCZs maps similar to the LCZs mapping, including Nagpur city (India) with the considerable LCZ 9 Sparely built (Kotharkar and Bagade 2017), and Szeged (Hungary) with dominant LCZ 6 Open low-rise followed by LCZ 8 Large low-rise (Unger, Lelovics, and Gál 2014). Since each city has own size, and development trajectory, and is exposed to diverse local and synoptic factors, the related urban environmental issues are not comparable without a standard datum. Here, the above LCZs comparisons indicate that LCZs mapping can be a criteria regarding the land cover character and urban morphology to further analyze and comprehensively describe the urban climate with heterogeneous human-environment interactions.

3.5 Conclusions

In this paper, a methodology for LCZs classification was built based on high-resolution airborne remote sensing data, national land cover dataset, and city land use planning data in the three metropolitan areas of Texas, U.S.: DFW, Austin, and San Antonio with different sizes and shape. LCZs mapping scheme is advantageous for the incorporation of detailed urban and vegetation morphology information at the scope of entire metropolitans. The study provided evidence that Lidar-derived products can support automated GIS-based LCZs mapping to identify urban morphological information and standardize the mapping scheme for comparative studies of metropolitan areas in the U.S.

Our LCZs mapping extends the LCZs case studies in the world. The key findings of LCZs of the study areas are that: 1) Most of the urbanized areas are categorized into LCZ open types for all three metropolitans with different proportions and spatial diversity, but that DFW shows more diversity in terms of LCZ “built-up cover” types due to the complex regional character compared to other metropolitans; 2) LCZ D low plants is dominant in the surrounding areas of DFW, and LCZ A Dense trees and LCZ D low plants are dominant in Austin and San Antonio with clear regional contrast; 3) LCZs maps are in accordance with the underlying regional environment and urban develop trajectory of three metropolitans. These findings indicate that the complex urban environment can be comparable by the criteria regarding the land cover character and urban morphology to further analyze and comprehensively describe the urban climate.

Besides the function of the LCZs on measuring UHI effects, it is reasonable and necessary to put LCZs mapping studies into a broader urban landscape view to understand the urban heterogeneity characteristic and the spatial distribution of thermal environment. For example, increasingly confronted with urban heat events, the urban planners are being aware of the need of optimizing urban planning processes with respect to urban thermal comfort and local climate (Scherer et al. 1999). Hence, a further investigation of the thermal behavior characteristic of different LCZs, as the up-to-date classification of urban landscapes, is warranted in the next step. Along with this line, further studies on applying the LCZs mapping results to study UHI formation and evolution are important to fundamentally understand the ways in which elements of the urban 'surface' interact with adjacent atmospheric layers.

4 SURFACE URBAN HEAT ISLAND INVESTIGATION BY LINKING LAND SURFACE TEMPERATURE WITH LOCAL CLIMATE ZONES

4.1 Introduction

In contrast to the direct AUHI measurement, remotely sensed land surface temperature (LST) observation is time-synchronized with pixel values at a considerable areal extent (Nichol 1996). Voogt and Oke (2003) proposed the term SUHI to refer to UHI that is measured with remotely sensed LST data. Compared to traditional air temperature measurement and AUHI study, LST data contributes to a broader understanding of spatial thermal patterns and the influence of surface properties on SUHI formation (Buyantuyev and Wu 2009). Whereas, there was a challenge to apply LST to estimate the SUHI intensity and analyze its spatial variability without a detailed information of the site characteristics. To fill this gap, some urban land cover related properties including LULC, the impervious surface percentage, vegetation intensity indices have been applied as the criteria to analyze the LST spatial variation and thus SUHI intensity. For instance, the LST characteristic of different urban land cover types has been examined (Li et al. 2012; Rinner and Hussain 2011; Zhou et al. 2013; Yue et al. 2007), and the relationships between LST and normalized difference vegetation index (NDVI) have been well researched (Weng, Lu, and Schubring 2004; Yue et al. 2007). Studies have also found that SUHI is strongly related to urban morphology and building characteristics (Chun and Guhathakurta 2016b; Coseo and Larsen 2014). However, these studies made the conclusions regarding the spatial variation of SUHI intensity by using the self-designed criteria for the relevant cases, which hampered the SUHI communication. On the other hand, a comparative analysis of the SUHI intensity is warranted for future urban planning exploration policy initiatives. In terms of comparative studies of the spatial variation of SUHI intensity, there have been limited case studies with the criteria of built-up land intensity (Zhou et al. 2014), or impervious surface area (Imhoff et al. 2010). For instance, the impervious surface area was used to investigate the SUHI amplitude and its relationship to development intensity, size, and ecological setting for 38 metropolises in the continental United States. However, these criteria is just based on one property related to the surface temperature and local climate.

On the other hand, in order to standardize observation protocols, the Local Climate Zones (LCZs) concept was introduced in 2012 to improve the documentation of UHI observations (Stewart and Oke 2012). LCZs are defined as “regions of uniform land cover, surface structure, construction material, and human activity that span hundreds of meters to several kilometers on a horizontal scale” (Stewart and Oke 2012) (p. 1884). The LCZ classification intends to standardize the worldwide exchange of urban temperature observations. The 17 standard LCZ classes (see Table A1) are determined by their surface characteristics, including: composition (building/tree), structure (permeability), fabric (albedo, thermal admittance), and metabolism (e.g., Table 2 on p. 1885 of (Stewart and Oke 2012)). Unique combinations of these properties provide a distinctive thermal regime for each LCZ (Geletič, Lehnert, and Dobrovolný 2016; Stewart and Oke 2012).

Compared to traditional SUHI investigation, the use of LCZs provides a standardized measure, grounded in the zoning practices enacted on urban spaces, by addressing the spatial heterogeneity and 3D characteristics of the urban landscape. With this universally accepted standard, it became possible to make a comperhensively comparative analysis of SUHI. For instance, Geletič et al. (2016) indicated that LCZ classes are distinguishable from each other in terms of surface temperature based on the cases of two central European cities. An LCZs mapping study of the Yangtze River Delta megapolitan region in China further showed LST variation among LCZs (Cai et al. 2017). More recently, Kotharkar and Bagade (2018) assessed the inter-LCZ temperature difference and identified LCZs at Nagpur city with stationary meteorological observation and mobile surveys. A recent study of Wuhan, China explored the climatic effect of the spatial pattern of LCZs by treating the individual LCZ as a homogenous landscape zone, and the result indicated that the spatial pattern of LCZs is an important factor of SUHI (Wang et al. 2017). Still, relative to plentiful studies on LCZs mapping, little research has been done in terms of evaluating and applying LCZs for urban climate studies.

Further investigation of the thermal behavioral characteristics of different LCZs is clearly warranted. This study will incorporate the LCZs concept to study and compare the SUHI effect for three major metropolitan areas, considering their limited scientific SUHI study. These three areas have several similarities including the similar regional climate and relatively flat topography, fast increasing population, top best places to live in U.S., etc. Meanwhile, these three metropolitan areas have their own size, shape, development trajectory, and urban pattern. Here, a comparative analysis of the SUHI intensity related to their LCZs comparison would lead to the communication of the SUHI mitigation strategies. Specifically, I attempt to link the Landsat derived LST with LCZs mapping in order to 1) test if LCZs are able to efficiently analyze the LST variation in the three metropolitan areas; and 2) investigate how LCZs affect the SUHI phenomenon by facilitating comparative analysis based on cases of the three study areas.

4.2 Methodology

4.2.1 Background of study areas

DFW, Austin, and San Antonio are located in the central part of Texas, U.S. (Figure 4.1). The Interstate highway I-35 passes through the metropolitan areas and connects them to other states and to border crossing points into Mexico. They are three of the major population and economic centers of Texas. Each city demonstrates high summer temperatures with humid weather (Table 4.1).

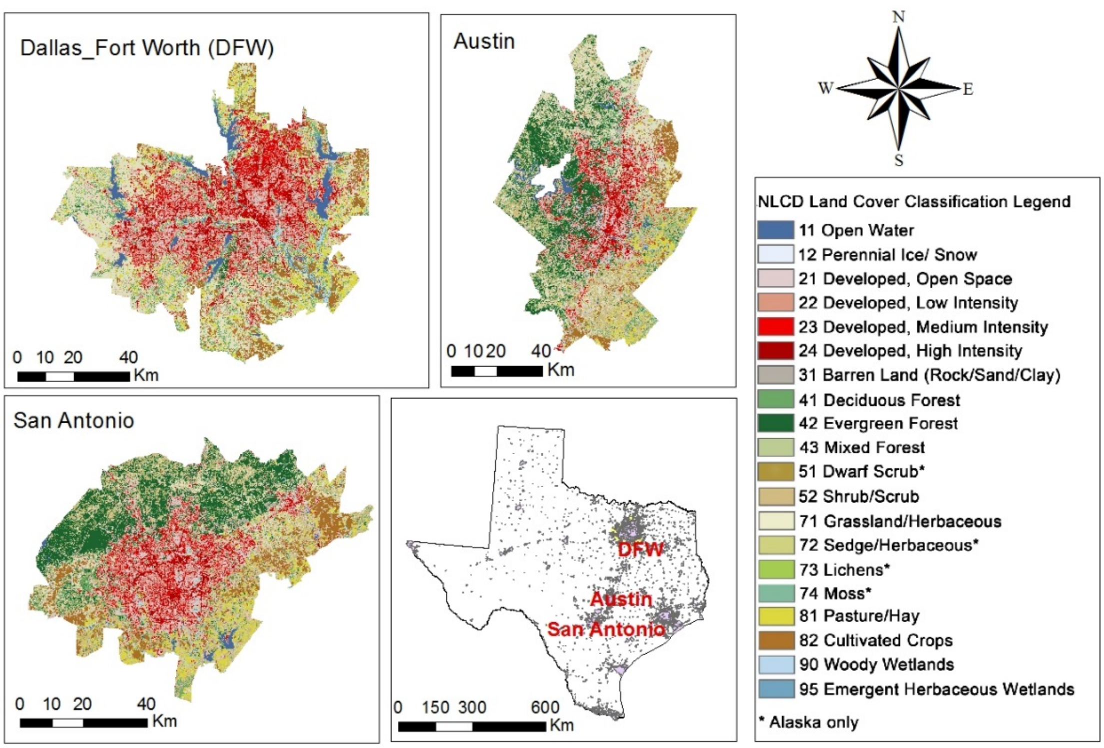

Figure 4.1 Study boundaries and land cover distributions of three metropolitan areas derived from the NLCD 2011.

Table 4.1 Summer monthly air temperature and precipitation summary of the study areas

		June	July	August
Austin	Average high temperature (°C)	33.4	35.3	36.1
	Average low temperature (°C)	22.4	23.6	23.7
	Average precipitation (mm)	110	48	60
Dallas	Average high temperature(°C)	32.9	34.8	35.8
	Average low temperature (°C)	19.6	21.6	21.8
	Average precipitation (mm)	118	71	54
Fort Worth	Average high temperature (°C)	32.7	35.3	36.1
	Average low temperature (°C)	21.3	23.1	23
	Average precipitation (mm)	NA	NA	NA
San Antonio	Average high temperature (°C)	33	34.8	34.8
	Average low temperature (°C)	22	23.3	23.1
	Average precipitation (mm)	109	52	65

Source: U.S climate data website, http://www.usclimatedata.com/

There has been limited scientific research of SUHI within these metropolitan areas, although a study by Darby and Senff (2007) found Dallas was almost 2.2ºC warmer than the surrounding rural area at nighttime when temperatures were averaged over the time period of 2000 to 2006. Their results also indicated that the UHI was more evident in Dallas than in Houston in terms of daytime temperatures (Darby and Senff 2007). The climate of DFW was categorized as humid subtropical, with an annual mean temperature of 18.8°C, and annual precipitation of 839.91mm (Winguth and Kelp 2013). Another study indicated that there was an overall positive trend in the UHI increase of 0.1 °C/decade in DFW from 2001-2011, and urban climate was influenced by the profound inter-annual and decadal variations (North Central Texas Council of Governments 2013). To date, the SUHI effect in Austin and San Antonio has not been well studied. One study reported that the average LST increased by 4.7 °C from 1993 through 2011, and the largest increase occurred for built-up land, barren, and cultivated land cover (Richardson 2015). A more recent study of Austin by Kim et al. (2016) found that larger and better-connected landscape spatial patterns were positively correlated with lower LST at the neighborhood level. Xie et al. (2005) studied the SUHI effect of the San Antonio area using the MODIS/Aqua product from 2002 to 2005, and reported that the downtown San Antonio area was 4-5°C higher compared to the entire region at nighttime and 6-8 °C higher at daytime

4.2.2 Land surface temperature retrieval

Landsat data have become the foremost source for fine scale SUHI studies since 2008 when the entire archive became freely available. Landsat generally meets the basic requirement of a spatial resolution of 50 m or less for SUHI analysis at the district level (Sobrino et al. 2012). This relatively fine spatial resolution and multiple spectral bands make it an ideal data source to study SUHI by linking the spatial thermal characteristics with underlying landscape patterns.

Considering the obvious adverse impact on the human comfort of hot weather for cities in the tropical and subtropical region of the northern hemisphere at summer, we focused on the SUHI phenomenon during the summer months. Thus, three images from Landsat 8 sensors on July 20, 2015, for the three study areas were obtained to calculate LST for SUHI investigation. The TIRS sensor on Landsat 8 has two thermal infrared bands in the atmospheric window between 10 and 12μm. Several algorithms (e.g., Plank function, radiative transfer equation, split-window algorithm, single channel algorithm) can be used to invert LST (Jiménez-Muñoz et al. 2014). A recent study suggested that the Planck function and the single channel algorithm showed the best performance for Landsat 8 TIRS though comparing the different algorithms of LST extraction (Isaya Ndossi and Avdan 2016). In this study, we applied the Planck function for LST calculation and use the normalized LST for SUHI comparison for three study areas. Considering band 11 is associated with higher calibration uncertainty and more sensitive to water vapor continuum absorption (Coll et al. 2012; Yu et al. 2014), LSTs were computed based on band 10 for this study.

First, the Top of Atmosphere (TOA) radiance (e.g., radiance measured by the sensor, $L_{TOA,\lambda}$) was converted to brightness temperature with the following equation.

$$T_{sen} = \frac{K2}{ln\left(\frac{K1}{L_{TOA,\lambda}}+1\right)} \quad (1)$$

where T_{sen} is temperature in Kelvin (K), and K_1 and K_2 are calibration constants specific to the Landsat TIRS sensor, which can be obtained from the metadata of the imagery.

The brightness temperature was further corrected against the land surface emissivity (LSE), which is essential for LST inversion due to the notable thermal variation of different land surface properties at a large spatial extent. The variation of vegetation coverage, surface moisture, surface roughness, and viewing angles leads to different LSEs for different cover types (Yu et al. 2014). The NDVI threshold emissivity estimation algorithm (Sobrino et al. 1990; Sobrino et al. 2004), a common method for LSE estimates was applied in this study. The NDVI values were used to distinguish between soil and vegetated pixels before LSE calculation. The TOA radiance values converted from digital number of band 4 (Red) and band 5 (NIR) from Landsat OLI were used for correspondent NDVI calculation to mitigate the effect from vegetation phenology.

Specifically, a NDVI threshold for rocks/soil ($NDVI_s$) was assigned with a value of 0.2, and the NDVI threshold for vegetation ($NDVI_v$) was assigned a value of 0.5 (Peng et al. 2016; Yu et al. 2014). Thus, for a pixel with NDVI < $NDVI_v$, it was assumed to be bare soil or rock, with ε_λ value of 0.966; and if NDVI > $NDVI_v$, it would be assumed to be covered by full vegetation, with ε_λ value of 0.986 (Yu et al. 2014). If the NDVI is between $NDVI_s$ and$NDVI_v$, then the pixels are considered to be a combination of vegetation and rocks/soil. Equations (2-4) were used to represent the relationship between NDVI and LSE to calculate the LSE for corresponding pixels.

$$\varepsilon_\lambda = \varepsilon_{v\lambda} P_V + \varepsilon_{s\lambda}(1 - P_V) + C_\lambda \qquad (2)$$

where $\varepsilon_{v\lambda}$and $\varepsilon_{s\lambda}$are emissivity of vegetation and soil, respectively. C_λ calibrates the cavity effect due to surface roughness.

$$C_\lambda = (1 - \varepsilon_{s\lambda})\varepsilon_{v\lambda}\, F'(1 - P_V) \qquad (3)$$

F' is a geometrical factor, assigned to 0.55, by assuming different geographical distributions (Sobrino et al. 1990), while P_V is vegetation fraction.

$$P_V = [\frac{NDVI - NDVI_{min}}{NDVI_{max} - NDVI_{min}}]^2 \qquad (4)$$

The Planck's function was used to perform for LSE correction of the substance compared to the blackbody. Thus, the value of brightness temperature was converted to LST (Artis and Carnahan 1982; Isaya Ndossi and Avdan 2016).

$$Ts = \frac{B_T}{1 + \frac{\lambda B_T}{\rho} ln\varepsilon_\lambda} \qquad (5)$$

where Ts is LST in Kelvin (K), and B_T is brightness temperature (e.g., $Tsen$) in this study. λ is the wavelength of emitted radiance (band 10 was used for LST calculation, and λ = 10.895 µm for Landsat 8 TRIS), ρ (e.g., $\frac{h*c}{\sigma}$) =1.438 × 10^{-2} mK. Ts was then converted into Celsius LST (°C).

4.2.3 Applying LCZs for SUHI investigation

To explore the application of LCZ mapping for SUHI analysis, we test the hypothesis that each LCZ demonstrates unique and typical LST characteristics and that LCZs can facilitate intra- and inter-comparisons for SUHI intensity for the three metropolitan areas. To obtain independent observations for statistical tests and exploration, we first examined the autocorrelation characteristics of the LST pixels by using the Geostatistical toolset in ArcGIS 10.5. LST pixels were sampled systematically at a 270 m interval for the subsequent analysis to derive independent LST observations and match the LCZs scales.

Overall, differences in mean LST for each LCZ among all the 17 LCZs were explored in the context of a one-way analysis of variance (ANOVA). After the overall F-test of the ANOVA revealed that mean LST is different for at least one pair of LCZs under investigation, we further identified specific (statistically significant) pairwise differences in mean LST by employing post hoc Tukey's Honest Significant Difference (HSD) test for the three metropolitan areas.

To make intra- and inter-comparisons of SUHI intensities for the three metropolitans by incorporating LCZs mapping results, the "Distribution Index" (DI) method was adopted to explore the relative contribution of individual LCZs to the entire SUHI phenomenon of the metropolitans (Peng et al. 2016). We focused on "high" LST pixels as a direct indicator of the SUHI phenomenon. To quantify "high" LST pixels, the original

LSTs were normalized and recoded into four categories from “cool” to “hot” using Jenks natural breaks classification (Weng et al. 2008).

$$DI_{LCZ_i} = \frac{SHigh_{LCZ_i}/S_{LCZ_i}}{SHigh/S} \quad (6)$$

where *i* means the individual LCZ, ranging from 1 to F, and DI_i refers to distribution frequency of high LST pixels for an LCZ_i. $SHigh_{LCZ_i}/S_{LCZ_i}$ refers to the proportion of the area with high LST ($SHigh_{LCZ_i}$) in the area of a LCZ (S_{LCZ_i}). $SHigh/S$ refers to the proportion of the area with high LST ($SHigh$) in the entire metropolitan area (S). A DI value of 1 represents an average contribution to the overall hot environment of SUHI phenomenon. Therefore, for LCZ 1 to LCZ G, DI_{LCZ_i} larger than 1 means LCZ_i has a heating effect on the SUHI, while DI_{LCZ_i} lower than 1 means the LCZ_i has a cooling effect on the SUHI of the metropolitan area.

4.3 Results

4.3.1 Spatial distributions of LST and LCZs

As meteorological conditions (e.g., synoptic situation) may vary over the three metropolitans at different times, the pixel values of the retrieved LST maps were standardized using the maximum difference normalization method to obtain the normalized temperatures for comparative analysis (**Error! Reference source not found.**). Overall, there was an obvious SUHI phenomenon on July 20, 2015, for all three metropolitans, indicated by the similar characteristics of the LST spatial distributions. The high surface temperatures for each metropolitan area were most apparent both in downtown areas and within isolated urbanized zones (e.g., Plano, DFW; Georgetown, Austin; New Braunfels, San Antonio), while low surface temperatures occurred along the central western side of Austin and northern San Antonio, where the topography was more complex and large forested areas remained intact. As expected, hotspots of LST were primarily located at the downtown areas and were often associated with the distribution of built-up land. The surrounding areas exhibited relatively lower LSTs. The coolest LSTs corresponded to water bodies (e.g., DFW).

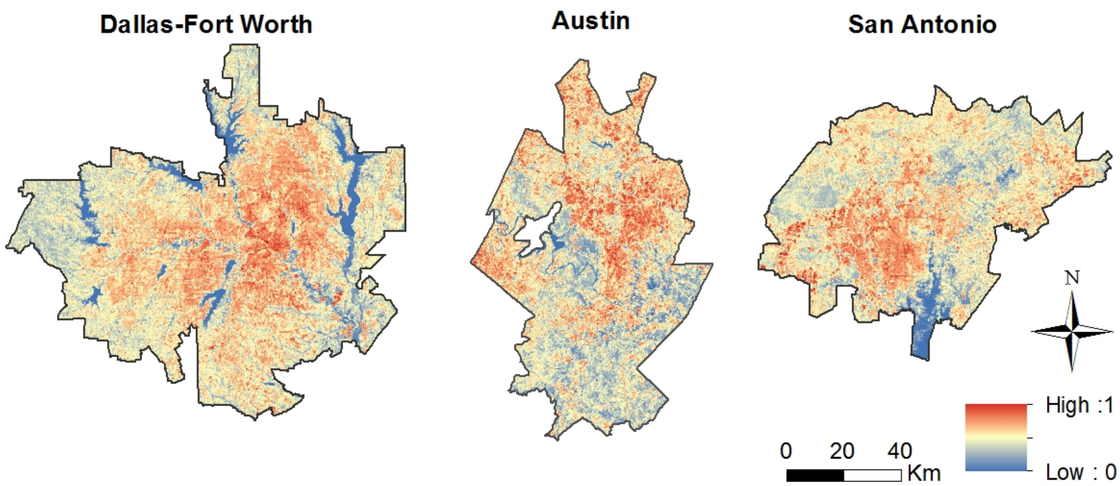

Figure 4.2. Spatial distributions of normalized land surface temperature (LST) for the three metropolitan areas, July 20, 2015.
(Note: The standardized value from 0 to 1, means the LST ranges from low to high.)

Figure *4.3* depicts LCZs classification results. Overall, by linking the spatial distribution of LCZs with Google Earth imagery, LCZs maps were determined to be in accordance with the underlying regional environment and land cover distributions. LCZ D occupied the largest area (e.g., LCZ D of DFW), composed of grassland and pasture (Figure *3.2*). LCZ A (Dense trees) and LCZ B (Scattered trees) were also common LCZs for Austin and San Antonio, located in the eastern and southern part of the area, respectively. There was also a clear contrast between LCZ A (Dense trees) and LCZ D (Low plants) for Austin and San Antonio, respectively.

Regarding LCZs built-up types, there was a tendency that most of the urbanized area was categorized into open LCZs (e.g., LCZ 4 Open high-rise, LCZ 5 Open mid-rise, LCZ 6 Open low-rise), especially for DFW and San Antonio. The most urbanized areas of DFW correspond to spaces with the highest percentage of LCZ “built-up cover” types. DFW showed the highest diversity in terms of LCZ “built-up cover” types due to the region’s complex regional characteristic. San Antonio is markedly different from the other two metropolitan areas in that high buildings are loosely distributed, leading to a larger proportion of LCZ 5 (Open mid-rise) adjacent to LCZ 6 (Open low-rise). As the oldest city of the three under investigation, and with a comparably slow pace of economic development, the San Antonio-New Braunfels metropolitan area has arguably the most diverse morphology of the three study areas.

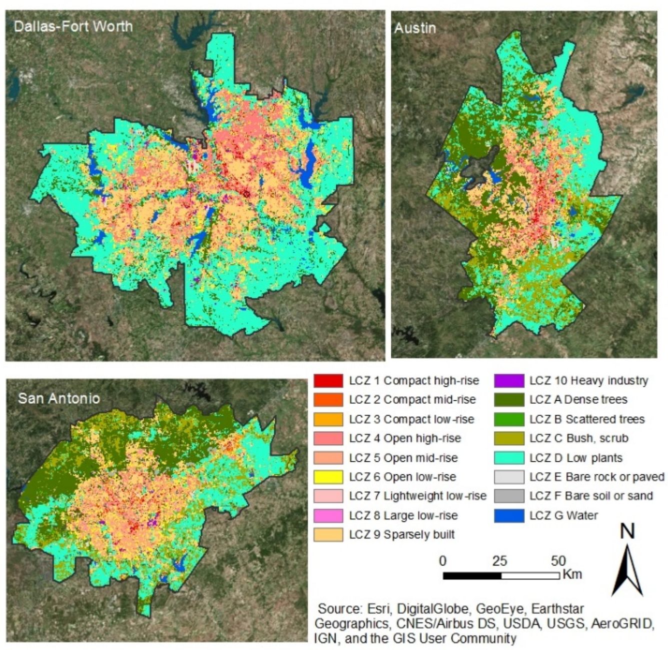

Figure 4.3 Spatial distributions of LCZs for three metropolitan areas in Texas.

4.3.2 Linking LST with LCZs mapping result

The spatial distributions of LCZs and LST indicated that they can be connected to further investigate the SUHI. The statistical summary indicated considerable differences among LCZs in terms of the mean LST (Figure *4.4*). In accordance with the above finding of LST patterns, the LSTs for “built-up cover” types (LCZs 1-10) were generally higher than those in “natural” cover types (LCZs A-G), for all three metropolitan areas. These qualitative LST patterns at LCZs were relatively consistent among the different metropolitan areas, despite their quantitative differences in terms of absolute LST values. On July 20, 2015, LCZ 1 (Compact high-rise) was the warmest LCZ, followed by LCZ 4 (Open high-rise, except Austin), while LCZ G (Water) was the coolest zone among all zones for all three metropolitan areas, followed by LCZ A (Dense tree). We excluded LCZ 7 (Lightweight low-rise) and LCZ 8 (Large low-rise) in the following analysis due to low observed frequencies in the study areas.

We observed LST variation among LCZs with various building densities. For example, LCZs compact types showed higher temperatures than LCZ open types (e.g., LCZ 1 vs LCZ 4; LCZ 2 vs LCZ 5, LCZ 3 vs LCZ 6), especially in DFW and Austin. Additionally, LCZ open types were warmer than LCZ 9 (Sparsely built). LCZs mapping helps to differentiate urban morphology characteristics within unique climate regions. Figure *4.4* demonstrates that the LCZs high-rise exhibited the highest median temperature, followed by LCZs mid-rise (e.g., LCZ 2 vs LCZ 5), and LCZs low-rise then LCZ sparsely built (e.g., LCZ 1> LCZ 2> LCZ 3, LCZ 4> LCZ 5> LCZ 6). Compared to other LCZs “built-up cover” types, LCZ 10 (Heavy industry) took on an entirely different distribution for all three study areas.

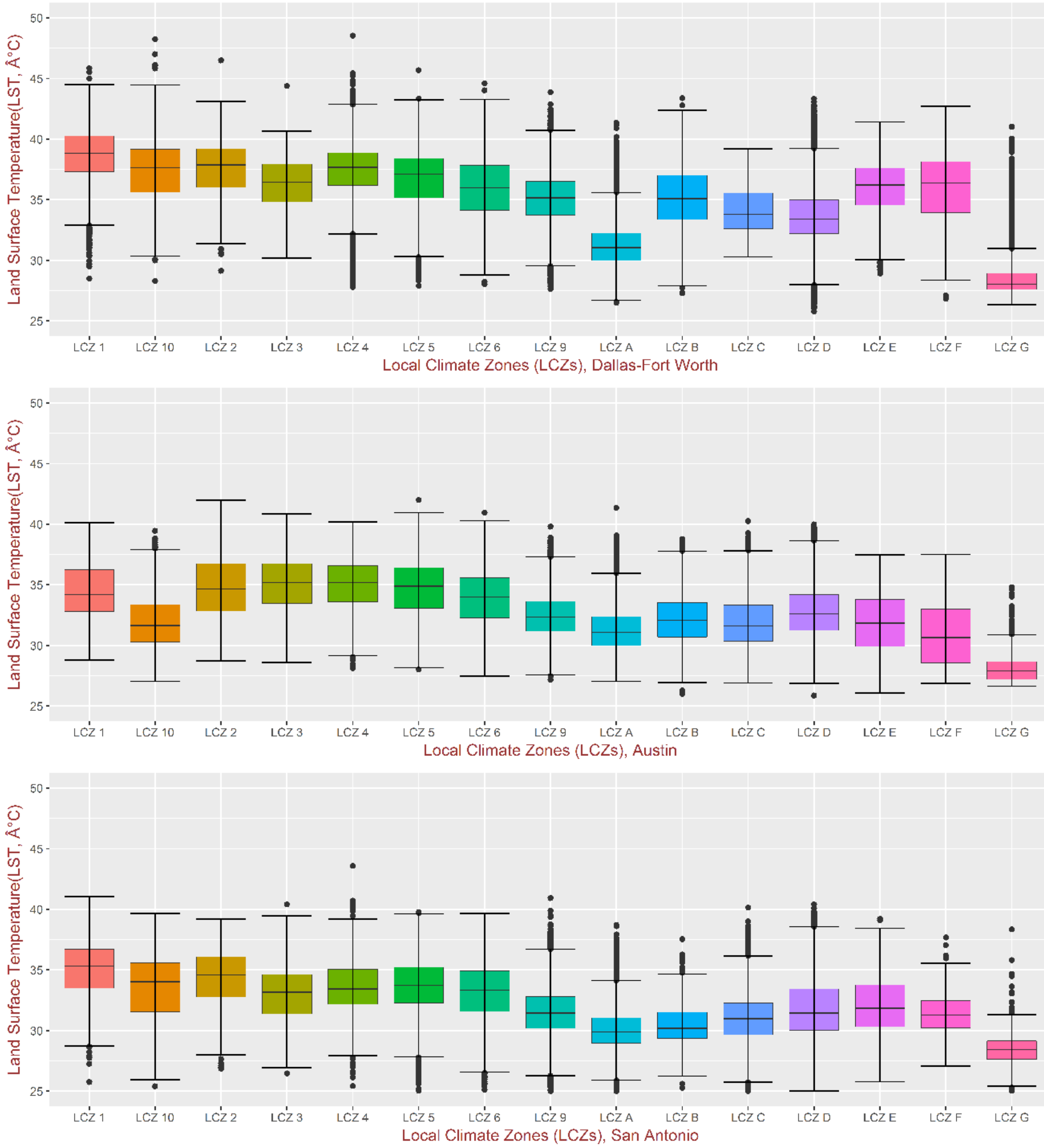

Figure 4.4 Box-plot summaries of LST values for LCZs for the three metropolitans on July 20, 2015.
(Note 1: Please refer to the name of LCZs from Figure 4.3. Note 2: The line within each box represents the median of LST values at the corresponding LCZ, the bottom of the box indicates the first quartile of LST values, and the top indicates the third quartile of LST values.)

LST values were further evaluated on distribution density for each LCZ to ensure the assumption of normality was met for the subsequent ANOVA analysis (Figure *4.5*). Most of the LST distributions were Gaussian except LCZ F Bare soil or sand for Austin and LCZ G Water for all three metropolitans. Along with greater variation and more outliers evident in the box plot summaries, significant departures from the mean LST were also demonstrated for the LCZ G Water. The homogeneity of variance assumption was not satisfied in the ANOVA; however, a nonparametric K-W test and post hoc Conover tests produced results that were qualitatively the same as the ANOVA and Tukey's HSD. Therefore, the latter (parametric) results were presented. The results of the one-way ANOVA F-test demonstrated that the differences among LCZs were significant in terms of the surface temperature (p < 0.001) (Table 4.2).

Table 4.2 Summary of ANOVA for testing the difference of LCZs in terms of the LST for three metropolitan areas, July 20, 2015.

	DF of Model	DF of Residuals	SSM	SSR	F	*p*
Dallas-Fort Worth	14	130219	557472	665913	7787	<2e-16
Austin	14	58586	67197	258722	1087	<2e-16
San Antonio	14	61708	97066	337060	1269	<2e-16

DF: degrees of freedom; SSM: Sum of squares of model; SSR: Sum of squares of Residuals

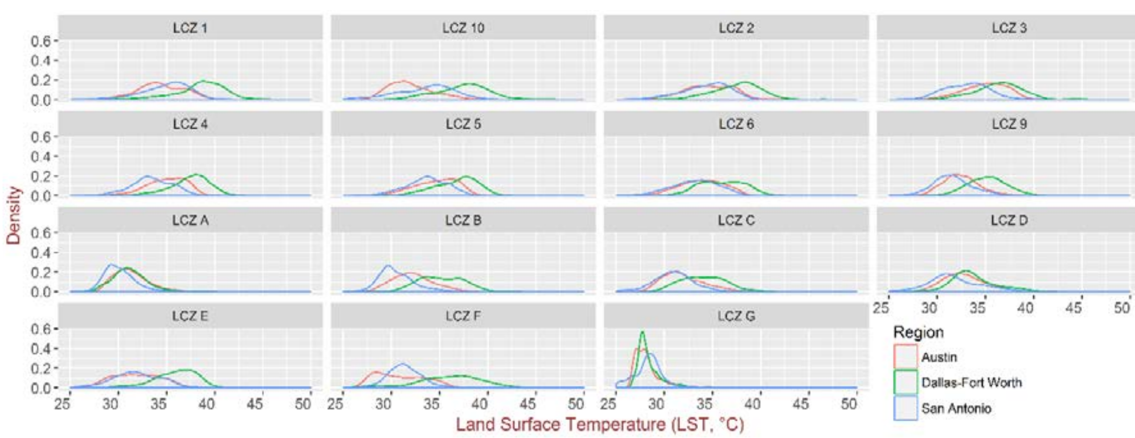

Figure 4.5 Density distributions of land surface temperature (LST) values for LCZs on July 20, 2015, for the three metropolitans.
(Note: Please refer to the name of LCZs from Figure 3.10)

Results from the Tukey HSD tests are provided in Figure 4.6. An empty space for a pair of correspondent LCZs means that they did not show significant differences in terms of the LST. Most pairs of LCZs showed significant differences in mean LSTs on July 20, 2015, with high significance levels. This suggests that LCZs plausibly have utility for identifying distinctive, relatively homogeneous LST zones. Among 91 pairs of LCZs, there are 78, 82, and 81 pairs of LCZs indicating significant LST differences for each of DFW, Austin, and San Antonio, respectively (e.g., 85.71%, 90.11%, and 89.01%).

Combined, the results suggest that for the three metropolitan areas, LCZ 1 (Compact high-rise), LCZ 4 (Open high-rise), LCZ 5 (Open mid-rise), LCZ 6 (Open low-rise), LCZ 10 (Heavy industry), LCZ A (Dense trees), LCZ B (Scattered trees), LCZ D (Low plants), and LCZ G (Water) might have the most discriminatory power for identifying different LST zones. For DFW, LCZ E (Bare rock or paved) and LCZ F (Bare soil or sand) was not distinguished from each other, as well as some LCZs built-up types, in terms of surface temperature. Also, for DFW, LSTs for LCZ 3 (Compact low-rise) could not be distinguished from other LCZ open types. For the zones in Austin, most of the LCZs built-up types were associated with significant pairwise differences in LST, except for LCZ 2 (Compact mid-rise), which was statistically indistinguishable from LCZ 1 (Compact high-rise), LCZ 3 (Compact low-rise), and LCZ 5 Open mid-rise. However, the LCZs “natural cover” types (LCZ A-LCZ G) were all significantly different from each other in terms of LST. For San Antonio, most LCZs showed that LSTs were distinguished very well, especially for the LCZ 9 (Sparsely built) and LCZ 10 (Heavy industry).

	LCZ 1	LCZ 2	LCZ 3	LCZ 4	LCZ 5	LCZ 6	LCZ 9	LCZ 10	LCZ A	LCZ B	LCZ C	LCZ D	LCZ E	LCZ F
LCZ 2	***													
LCZ 3	***	***												
LCZ 4	***		***											
LCZ 5	***	***		***										
LCZ 6	***	***		***	***									
LCZ 9	***	***	*	***	***	***								
LCZ 10	***		**	***	***	***	***							
LCZ A	***	***	***	***	***	***	***	***						
LCZ B	***	***	***	***	***	***		***	***					
LCZ C	***	***	**	***	***	**		***	***					
LCZ D	***	***	***	***	***	***	***	***	***	***				
LCZ E	***	***		***	***		***	***	***	***	***	***		
LCZ F	***	***		***	***		***	***	***	**	**	***		
LCZ G	***	***	***	***	***	***	***	***	***	***	***	***	***	***

Dallas-Fort Worth

	LCZ 1	LCZ 2	LCZ 3	LCZ 4	LCZ 5	LCZ 6	LCZ 9	LCZ 10	LCZ A	LCZ B	LCZ C	LCZ D	LCZ E	LCZ F
LCZ 2														
LCZ 3	**													
LCZ 4	*	*												
LCZ 5			**	***										
LCZ 6	*	***	***	***	***									
LCZ 9	***	***	***	***	***	***								
LCZ 10	***	***	***	***	***	***	***							
LCZ A	***	***	***	***	***	***	***	***						
LCZ B	***	***	***	***	***	***	***	***	***					
LCZ C	***	***	***	***	***	***	***		***	***				
LCZ D	***	***	***	***	***	***	***	***	***	***	***			
LCZ E	***	***	***	***	***	***	***		***	***		***		
LCZ F	***	***	***	***	***	***	***	***	*		***	***	***	
LCZ G	***	***	***	***	***	***	***	***	***	***	***	***	***	***

Austin

	LCZ 1	LCZ 2	LCZ 3	LCZ 4	LCZ 5	LCZ 6	LCZ 9	LCZ 10	LCZ A	LCZ B	LCZ C	LCZ D	LCZ E	LCZ F
LCZ 2	***													
LCZ 3	***	***												
LCZ 4	***	***	*											
LCZ 5	***	***	***											
LCZ 6	***	***		***	***									
LCZ 9	***	***	***	***	***	***								
LCZ 10	***	***					***							
LCZ A	***	***	***	***	***	***	***	***						
LCZ B	***	***	***	***	***	***	***	***	**					
LCZ C	***	***	***	***	***	***	***	***	***					
LCZ D	***	***	***	***	***	***		***	***	***	***			
LCZ E	***	***	***	***	***	***		***	***	***	***	***		
LCZ F	***	***	***	***	***	***		***	***	***	***		***	
LCZ G	***	***	***	***	***	***	***	***	***	***	***	***	***	***

San Antonio

Figure 4.6 Tukey HSD test result for LCZs in terms of the LST differences. (Note: ‘***’: significance at 0.001 level; ‘**’: significance at 0.01; ‘*’: significance at 0.05 level for that pair of LCZs. Empty space implies no significant difference of the corresponding LCZs pairs. Pairs with red color indicates the mean value of the column LCZ is higher than that of the row LCZ, while the green color indicates the mean value of the column LCZ is lower than that of the row LCZ.)

4.3.3 Application of LCZs on SUHI investigation

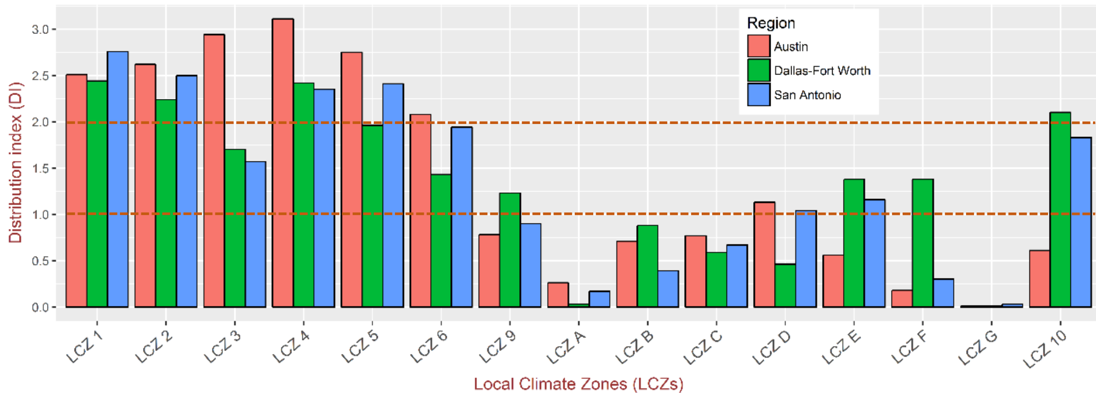

Figure 4.7 Distribution index (DI) of high-temperature centers for LCZs in three metropolitans on July 20, 2015.
(Note: Please refer to the name of LCZs from Figure 4.3. The horizontal lines indicate that DI equals to 2.0 and 1.0, respectively.)

DI values related to “high” LST pixels were calculated to quantify the contributions of “hot” LST pixels from various LCZs within each metropolitan and compared to the relative contributions of the specific LCZs between metropolitans (Figure *4.7*). The DI value further demonstrated the heterogeneity LST by LCZ. Overall, “built-up cover” types (LCZs 1-10) had DI values greater than 1 on July 20, 2015 except for LCZ 10 (Heavy industry) and LCZ 9 (Sparsely built) for Austin and LCZ 9 (Sparsely built) for San Antonio. LCZ 1 (Compact high-rise), LCZ 2 (Compact mid-rise), LCZ 4 (Open high-rise), and LCZ 5 (Open mid-rise) demonstrated high detrimental impacts on the thermal environment with DI ranges at or exceeding DI=2.

In contrast, LCZs “natural cover” types had DI values of lower than 1, except LCZ D (Low plants) (1.13 in Austin and 1.04 in San Antonio), and LCZ E (Bare rock or paved) (1.16 for San Antonio and 1.38 for DFW). In terms of the effect of individual LCZ for the overall SUHI high temperature effect, LCZ G (Water) had DI values near 0, followed by LCZ A (Dense trees). This finding can be interpreted as there were rarely “high” LST pixels in the normalized LST map on July 20, 2015 for these two LCZs types, indicating a clear cooling effect for the corresponding metropolitan areas.

Overall, we observed a similar tendency of the heating/cooling effect of corresponding LCZs for the three metropolitan areas. Nevertheless, some of the inter-metropolitan differences are noteworthy. In particular, LCZs of Austin demonstrated higher DI variation. Compared to DFW and San Antonio, most of the LCZs “built-up cover” types of Austin and some LCZ “natural cover” types (e.g., LCZ A Dense trees, LCZ C Bush, scrub, and LCZ D Low plants) demonstrated relatively higher DI values, indicating higher heating effects than the corresponding LCZs of other the two areas. On the other hand, other types of LCZs had higher cooling effect and could serve to mitigate the SUHI. For example, in Austin, both LCZ 10 (Heavy industry) and LCZ 9 (Sparsely built) had DI values less than 1, and this SUHI cooling effect was not observed in DFW or San Antonio.

4.4 Discussion

4.4.1 Applicability of LCZs for SUHI characterization

With generally consistent findings for the three metropolitan areas, the significant differences of LSTs among LCZs demonstrated that LCZs mapping can facilitate LST variation analysis for SUHI measurement.

First, LST variations were demonstrated among LCZs characterized by different LULC (LCZs “built-up cover” types and individual LCZs “natural cover” types). For example, due to the high thermal heat capacity of water relative to other surface properties, LCZ G Water had the lowest average surface temperature (around 27°C). LCZ

A Dense trees had the next lowest average surface temperature and accounts for a considerable proportion of the landscape in Austin and San Antonio. Similar findings regarding LST variation among LCZs were also observed in the Yangtze River Delta, China (Cai et al. 2017) and Prague, Brno, Czech Republic (Geletič et al. 2016). The variations in thermal behavior by different LULC has been well documented for several areas (Amiri et al. 2009; Bokaie et al. 2016; Lazzarini et al. 2013; Zhou et al. 2013). Together with these findings, the study demonstrates that land cover was the most important factor for the spatial variation of LST.

Aside from LST variation with different land cover, one advantage of evaluating LST based on LCZs was that LCZ mapping considered complex urban morphology as homogenous climate zones, especially for LCZs "Built-up" types. In terms of the effect of the heterogeneous character of the urbanized area on LST spatial variation, previous studies have implied that various urban land uses and urban functional zones, such as commercial/resource/industrial land/parks and recreational land (Rinner and Hussain 2011), or residential/commercial/industrial/institutional land (Li et al. 2014), or residential/industrial/CBD/ commercial/services/transportation areas (Yue et al. 2007) had very different thermal characteristics. The factors for LCZs definition have been studied separately, and they have been all reported to affect the LST spatial variation and SUHI formation, such as SVF (Chun and Guhathakurta 2016a; Unger 2008), albedo (Levy 2016), solar radiations (Chun and Guldmann 2014), etc.

This study departed from previous research in that it addressed the need to examine 3D urban morphological information with alternative parameters to derive a uniform zone in order to accurately report the LST spatial variation and render the results comparable. First, our results show that LCZs Compact types were warmer than LCZs Open types and LCZ 9 Sparsely built. Further, LCZs Open high-rise (e.g., LCZ 1 and LCZ 4) were generally warmer than LCZs mid-rise (e.g., LCZ 2 and LCZ 5) and LCZs low-rise (e.g., LCZ 3, 6, 7, and 8). Of note, the LCZs differentiated by building density (e.g., Compact vs Open vs Sparsely built) demonstrated higher LST variations than those differentiated by the height roughness (High-rise vs mid-rise vs low-rise). Hence, the LST variation among LCZs 1-10 “Built-up” types suggested that building density had a prominent impact on the spatial variation of LST.

Considering that the warm thermal environment in the urbanized area is due to the reduction of evapotranspiration by vegetation cover, the relationship of LST and NDVI has been explored in a number of studies to characterize the thermal behavior of urbanized areas (Bokaie et al. 2016; Li et al. 2011; Weng and Fu 2014; Weng et al. 2004; Yue et al. 2007). We further explored the relationship of LST and NDVI (calculated from the same Landsat 8 imagery) to evaluate the thermal behavior of different LCZs. With sufficient sampling size and strong statistical significance (p<0.001), the results of regression analysis showed a close inverse correlation between mean LST and NDVI for different LCZs (Figure 4.8).

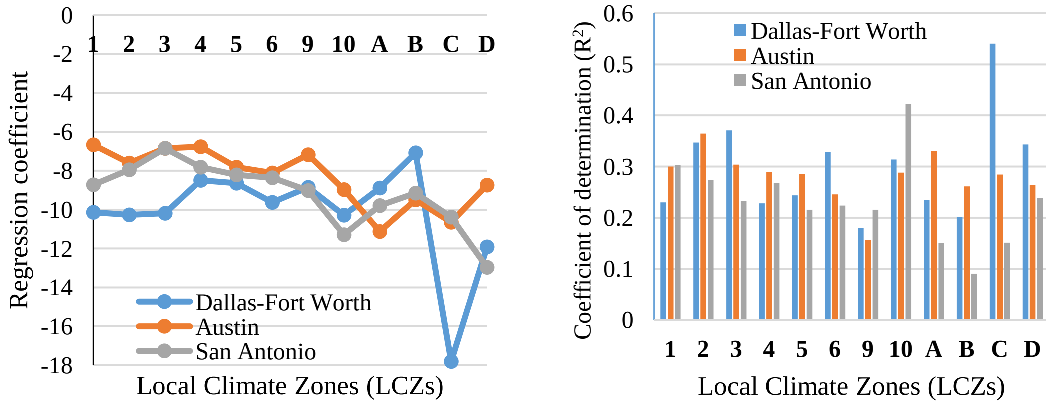

Figure 4.8 Regression coefficients and coefficient of determinations (R2) for the linear regression between LST on July 20, 2015 and NDVI by LCZs.
(Note 1: Please refer to the name of LCZs from Figure 4.3. Note 2: The LCZ E Bare rock, LCZ F Bare soil or sand, and LCZ G Water were excluded due to the low vegetation cover.)

There was an apparent difference in the regression coefficient (-6.67 to -11.8) among LCZs, which showed the same pattern in the three metropolitans. This finding indicated the different thermal environments were formed in different LCZs. Here, LCZ C Bush, scrub of DFW showed a strong correlation with LST, which can explain its strong cooling effect, a contrast to the slight heating effect from LCZ C for the other two cities (Figure 4.8). It is noteworthy that the LCZ C of DFW corresponded to shrub and scrub along the river corridor, which run through the urban areas.

4.4.2 Uncertainties of the LCZs mapping on SUHI analysis

For each specific metropolitan area, there were several LCZs which cannot be well-distinguished in terms of their LSTs, including LCZ 3 (Compact low-rise), LCZ E (Bare rock and paved), and LCZ F (Bare soil or sand). The phenomenon can partly be explained by the LCZs mapping limitation of this study. With relatively small composition, LCZ E and LCZ F showed different normalized main temperature ranges and heating/cooling effects among the three metropolitans. Also, LCZ F had the highest

LST variation. This can be explained by the fact that our GIS-based LCZs mapping emphasized the morphological characteristics rather than the surface materials. For example, LCZ E included two types of land surface cover: Bare rock and paved, and image interpretation in Google Earth showed that some areas of LCZ E belonged to transportation related impervious surfaces (highways, parking places, and airports). Nevertheless, the bare rock or impervious surface may show different thermal behavior of the surface materials during the late morning when Landsat passed over the study areas. It indicates that some other types of LCZs may need to be further classified in terms of LCZs mapping at the metropolitan level or to fit the characteristics of different cities worldwide.

Compared to other LCZs "built-up cover" types, LCZ 10 (Heavy industry) demonstrated different thermal characteristics among the three metropolitan areas. This could be in part because LCZ 10 (Heavy industry) was also sparsely distributed and contiguous with other LCZs throughout DFW (and to some extent for San Antonio). Also, we delineated LCZ 10 based on city planning data, which did not provide sufficient details about the intensity of industrial activities, thus leading to unexpected findings for LSTs.

The uncertainties of LCZs mapping on SUHI investigation is also related to issues of scale. The common characteristic for LCZs with undistinguishable LST is the small area proportion and high fragmentation of those LCZs, which affected their thermal characteristics due to contributions from adjacent land covers. For LCZs mapping, the LCZs were defined as areas with uniform land cover and surface structure, construction material, and human activity, yet 270 m was assigned as the LCZs mapping scale based on the height of buildings in this study. However, each LCZ was not an absolute homogenous region, and there was no clear boundary between them. We used the LST values at pixel level as samples for analysis, which might be located along the LCZ boundary. In addition, some surface properties may show heterogeneous thermal variation at a smaller scale than LCZs. For example, Zhang et al. (2009) reported that smaller patches of vegetated area provided less cooling than larger vegetated patches. In this study, several outliers of LCZ A Dense trees showed high temperatures, but this result was also observed by Geletič et al. (2016). In short, LCZs mapping was a compromise between universality and local accuracy.

4.4.3 The effect of LCZs on SUHI formation

With a uniform LCZ classification scheme, this study provided evidence that LCZ mapping can be replicable for comparative analysis of SUHI phenomenon. DI of high temperature further demonstrated that the LCZs mapping result can efficiently facilitate intra- and inter-comparisons for SUHI intensity. Apparently, the overall SUHI effect was primarily caused by the heating effect of built-up land cover. Furthermore, this study indicates that some LCZs contributed to opposite heating/cooling effects (e.g., LCZ 9 Sparsely built, LCZ D Low plants). Previous research has found that the effect of LCZ on SUHI is related to the geographic location. For instance, the complex and diverse urban morphology of LCZ 9 and the corresponding LSTs were also found in the LCZ mapping in the Yangtze River Delta, China (Cai et al. 2017).

Furthermore, the spatial distributions of LCZs on SUHI intensity need be further studied. The LCZs distributions reflected the varying spatial arrangements of natural and built-up environments which in turn affected the LST spatial variation. It is noteworthy to recognize that the LCZs at DFW showed a lower capability to distinguish the LST variation throughout the region (Figure *4.6*). Specifically, DFW was different from the other two metropolitans regarding LCZs "natural cover" diversity and spatial distribution due to the geographical location and the climatic environment. Especially, LCZ D (Low plants) and LCZ G (Water) intersected with LCZs 1-10 "built-up cover" types with the highest proportion compared to the respective composition at Austin and San Antonio. They separated the urbanized areas of DFW into four major city centers: Dallas, Fort Worth, Arlington, and Irving in the role of metropolitan "corridors". Further examination of the LCZs with Google Earth indicated that the main river and stream basins led to the formation of the strip of LCZ D (Low plants) and LCZ G (Water), neighboring with built-up land (correspondent with LCZ 4, and LCZ 5). This arrangement of LCZs for DFW was in accordance with the LSTs in terms of the low LST outliers in LCZ 4 (Open high-rise), LCZ 5 (Open mid-rise), and LCZ D (Low plants) and high LST outliers in LCZ G (Water). This intersection effect by different LCZs can also help to explain other outliers (e.g., LST in LCZ 9 Sparsely built and LCZ A Dense trees of San Antonio). An recent study of Wuhan, China also indicated that landscape layout of LCZs was an important factor of the SUHI formation (Wang et al. 2017). The spatial heterogeneity and scale characteristics have been also addressed in other SUHI studies (Luo and Peng 2016; Zhou et al. 2011). In this sense, further on the spatial heterogeneity and scale characteristics of the LCZs is needed in the future to lead a comprehensive finding.

Our GIS-based LCZs delineation considered the incorporation of detailed urban and vegetation morphology information at the scope of entire metropolitan areas. Considering that our aims of LCZs mapping are to investigate SUHI, individual LCZs were assumed to be constant throughout the year compared to the seasonal and even annual variation of surface temperature. However, some types of vegetation cover were more responsive to climate and environmental conditions and likely changed over time, leading to different heating/cooling effects for the entire region. Further investigation of the SUHI phenomenon at night time and in different seasons would contribute to a better understanding of the overall relationship between LCZs and LST.

4.5 Conclusions

This study assessed the utility of LCZs for comparative analysis of LST spatial variations and analyzed how the different LCZs affect the SUHI phenomenon. The linkage of LCZs and LST proved that the LCZs mapping can be used to compare and investigate the SUHI. With sufficient 3D urban morphological information, this study provided evidence that LCZs mapping can provide a guideline to synthesize SUHI studies. It considers the temperature differentiation among LCZ classes rather than between the traditional “urban” and “rural” classes. In this study, we delineated the built-up land based mainly on the height of roughness elements, building surface fraction, pervious surface fraction, and city planning study. This study further indicates the heterogeneity character of the built-up land in the urban environment, thus different LCZs “built-up types” also showed different LST character.

The study demonstrated the advantage of LCZs mapping on understanding SUHI. The intra-urban temperature comparison among different LCZ contributed to investigating the influence of heterogeneous urban environment on SUHI phenomenon. Since different heating/cooling effect of LCZs on SUHI phenomenon in the metropolitan areas, the spatial distribution of LCZs can further benefit spatially SUHI migration strategies. Moreover, they can be incorporated into climatic models to understand the UHI formation and dynamics with detailed underlying surface information.

5 A GEOGRAPHICALLY WEIGHTED REGRESSION ANALYSIS OF THE UNDERLYING FACTORS RELATED TO SURFACE URBAN HEAT ISLAND PHENOMENON

5.1 Introduction

Examination of how underlying surface characteristics affect SUHI formation has become one of the major applications of remote sensing for urban climate studies. Supported by remote sensing technology, spectral indices have been used to indicate SUHI formation, including the Normalized Difference Vegetation Index (NDVI) (Weng, Lu, and Schubring 2004), the Normalized Difference Built-up Index (NDBI) (Chen et al. 2006), and the Normalized Difference Water Index (NDWI) (Jiang, Fu, and Weng 2015), among others. Moreover, several studies have reported that green spaces or water bodies mitigate high LSTs (Connors, Galletti, and Chow 2013; Li et al. 2012; Zhou, Huang, and Cadenasso 2011; Peng et al. 2016). On the other hand, built-up or impervious land cover increases LST and exacerbates SUHI effects (Guo et al. 2015; Peng et al. 2016; Xian and Crane 2006). Furthermore, research involving analysis of high-resolution imagery has demonstrated the impacts of spatial components and configurations of detailed LULC on LST (Zhou, Huang, and Cadenasso 2011; Zheng, Myint, and Fan 2014; Li et al. 2012; Peng et al. 2016; Myint et al. 2015). These studies indicate that empirical estimation models are effective tools for quantitatively characterizing SUHI formation with less computational intensity compared to simulation models. In addition, empirical estimation outputs are relatively easily to interpret. Conventional statistics (e.g., ordinary least squares (OLS)) are the primary vehicle for researchers in most studies that investigate the impact of underlying factors on SUHI formation. However, the prominent limitation of conventional statistics in geoscience is spatial non-stationarity, which refers to the spatially varying relationships between dependent and independent variables (Deilami, Kamruzzaman, and Hayes 2016). Moreover, OLS has been shown to be of limited utility when spatial data are coupled with highly correlated independent variables (Fan, Rey, and Myint 2016). An alternative to conventional regression is Geographically Weighted Regression (GWR), which can model spatial variation in relationships between dependent and independent variables. Li et al. (2010) first indicated that GWR provides a better fit and provides more localized information than a global model when exploring the landscape drivers of LST. Additional assessments of GWR have compared to global regression (e.g., OLS) with respect to residual spatial autocorrelation and model goodness-of-fit has also been explored (Ivajnšič, Kaligarič, and Žiberna 2014; Luo and Peng 2016; Li et al. 2017).

Compared to the numerous studies that analyze SUHI for single cities, SUHI research on broader metropolitan areas is far less common. This larger analysis extent warrants further investigation since the underlying factors are likely more complex and variable in space. On that backdrop, the main objectives of this study are to answer the following questions: 1) What underlying landscape properties (e.g., land cover and terrain morphology) are significantly related to the SUHI phenomena for Austin and San Antonio, Texas, and 2) Compared to a global regression approach, does GWR provide improved insight about landscape drivers of LST?

5.2 Methods

5.2.1 Study areas

As two of the four major metropolitan areas of Texas, the Austin–Round Rock (Austin) and the San Antonio–New Braunfels (San Antonio) metropolitan areas are located in the Central South region of Texas, U.S. (Figure *5.1*). The Interstate highway I-35, a major transportation corridor, passes north-south through these two metropolitan areas. Both areas are characterized by relatively flat terrain to the east, grading to more complex topography along the western edge of the Balcones Escarpment. Based on the Köppen climate classification, the region is considered humid subtropical with long and hot summers, short and mild winters, and warm and rainy Spring and Fall seasons (Peel, Finlayson, and McMahon 2007) (Table *5.1*). Both the Austin–Round Rock and San Antonio-New Braunfels metropolitan areas are located in a unique and narrow transitional zone that ranges from semi-arid vegetation cover dominated by trees and shrubs in the west to humid and more densely vegetated prairie/grassland to the east.

Table 5.1 Summary of the geographic, demographic, and climatic characteristics of Austin and San Antonio, Texas.

Areas	Location (the center point) [1]	Land area (square km^2) [1]	Estimated population (July 1, 2015) [2]	Bare earth elevation (approximately, meters) [3]	Average temperature range (°C), July [4]	Average precipitation (mm), July [4]
Austin	30.36°N, 97.78°W	4587.36	931,830	(107, 405) Mean: 235	(23.6, 35.3)	48
San Antonio	32.76°N, 96.97°W	4752.04	1,469,845	(116, 579) Mean: 263	(23.3, 34.8)	52

Sources: 1. Inquired or calculated by the authors in ArcMap based on the projection system "WGS 1984 UTM Zone 14N". 2. U.S. Census Bureau. 3. Derived from 5 m Digital Terrain Models (DTMs), built by the authors from lidar data provided by the Texas Natural Resources Information System (TNRIS). 4. U.S. climate data website (www.usclimatedata.com).

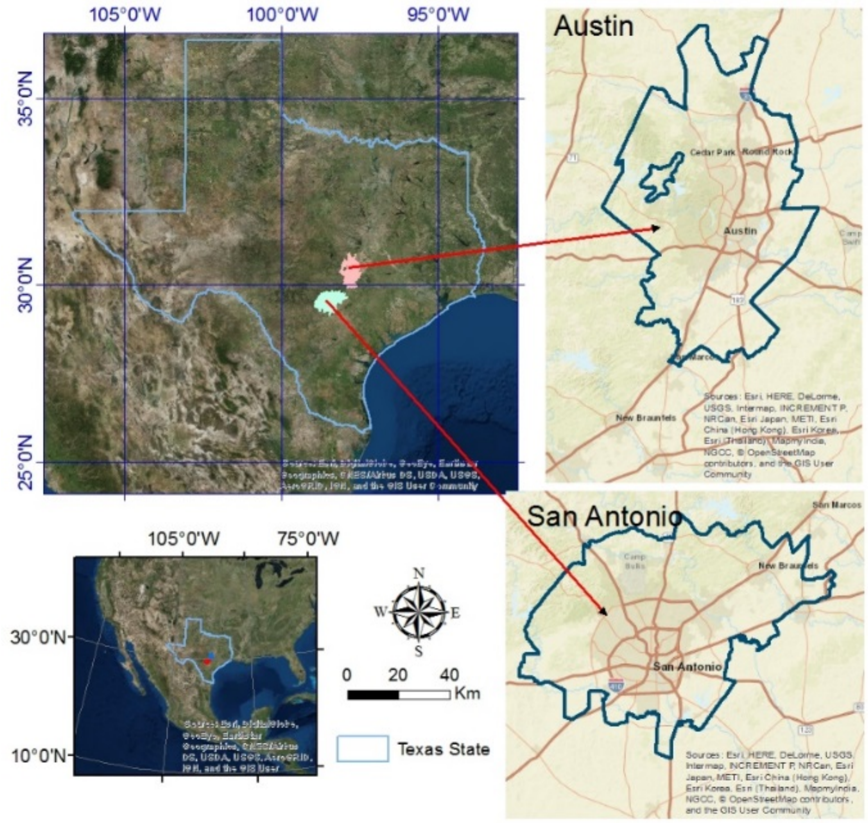

Figure 5.1 The Austin and San Antonio metropolitan areas in Texas, U.S.

5.2.2 OLS and GWR analysis

Unlike a conventional (global) regression model, GWR is able to model spatial variation in relationships between dependent and independent variables. A GWR model takes the following form:

$$y_i = \beta_0(u_i, v_i) + \sum_k \beta_k(u_i, v_i)x_{ik} + \varepsilon_i \qquad (7)$$

where y_i, x_{ik}, and ε_i are the dependent variable, the kth independent variable (subscripted as k) and random error at the point i (subscripted as subscript i), respectively. Location is denoted by the coordinates (u_i, v_i) of a given point i. The coefficients $\beta_k(u_i, v_i)$ are varying weights on the location, and $\beta_0(u_i, v_i)$ is the geographically varying intercept. Thus, the GWR extends the global regression model by adding the geographical location parameter to generate the local coefficients to account for spatial non-stationarity. The estimates of $\beta_0(u_i, v_i)$ and $\beta_k(u_i, v_i)$ are based on the unbiased estimation by of a set of observations, in which the weight matrix is used to weight the observations differently (Guo, Ma, and Zhang 2008). Here, an adaptive Gaussian kernel function was adopted for the analysis, where optimal bandwidth was detected through a golden search algorithm in GWR 4.

Global regression models were also developed to compare to GWR results. The coefficient of determination (R^2), global Moran's I of the residuals, Akaike Information Criterion (AIC), and the corrected AICc were used to compare the performances of global regression models versus the GWR model with respect to goodness-of-fit and residual spatial autocorrelation. In this paper, both GWR and global regression models were built using the open source platform GWR 4 (Nakaya et al. 2014).

5.2.3 Explanatory variables derivation and selection

Based on knowledge from prior SUHI studies (Zhou, Huang, and Cadenasso 2011; Zheng, Myint, and Fan 2014; Li et al. 2012; Peng et al. 2016; Myint et al. 2015; Guo et al. 2015; Xian and Crane 2006), a suite of potential explanatory variables was selected for two models, one each for the metropolitan areas under consideration. Considering the variable type, the explanatory variables were categorized into three groups, as summarized in Table 5.2.

Table 5.2 Potential explanatory variables: derivation sources and statistical summary of the observations.

Variables	Derivation sources		Max.	Min.	Mean	S.D.
Land use/land cover composition variables						
Canopy (tree canopy fraction)	2011 NLCD Tree Canopy dataset	Austin	87.46	1.26	32.89	19.83
		San Antonio	86.48	0.46	32.30	20.00
ISF (impervious surfaces Fraction)	2011 NLCD ISF dataset	Austin	80.83	0.00	9.44	14.25
		San Antonio	86.42	0.00	12.12	17.10
BF (Buildings fraction)	Building footprints	Austin	43.96	0.00	5.07	8.43
		San Antonio	51.25	0.00	5.52	8.72
NDVI (normalized difference vegetation index)	Landsat 8 OLS, July 20, 2015	Austin	0.53	-0.44	0.31	0.10
		San Antonio	0.57	-0.38	0.30	0.10
Landscape pattern metrics variables						
CONTAG (Contagion Index)	NLCD LULC data	Austin	87.34	10.68	40.76	11.08
		San Antonio	97.90	10.18	41.67	11.90
PD (Patch Density)	–	Austin	137.22	4.56	53.83	30.26
		San Antonio	128.74	0.65	53.51	30.88
SHDI (Shannon's Diversity Index)	–	Austin	2.42	0.25	1.54	0.33
		San Antonio	2.34	0.02	1.49	0.36
PR (Patch Richness)	–	Austin	15.00	3.00	8.65	2.12
		San Antonio	15.00	2.00	8.46	2.48
Terrain variables						
Elevation	Aggregated from 5m*5m DTMs	Austin	403.51	113.14	227.66	56.95
		San Antonio	526.87	124.96	255.19	75.88
Northness	Aggregated from 5m*5m Northness dataset	Austin	0.48	-0.66	-0.04	0.13
		San Antonio	0.93	-0.67	-0.06	0.14

Notes: "Max.": Maximum. "Min.": Minimum. "S.D.": Standard Deviation. "NLCD": National Land Cover Database. "DSM": Digital Surface Model. "DTM": Digital Terrain Model. “–”: “Same as above”.

(1) Land use/land cover composition (LULC) variables

Buildings Fraction (BF), ISF, NDVI, and Canopy were considered for SUHI explanatory variables in terms of LULC composition. ISF and Canopy were downloaded as independent layers from National Land Cover Database (NLCD) 2011 (Homer et al. 2015), the thematic accuracy of which has been established in the literature (Wickham et al. 2017). BF was derived using the building footprint features based on the Lidar datasets.

(2) Landscape pattern metrics

Thirty meter NLCD 2011 data was used to compute landscape metrics at the landscape level to quantify the general characteristics of the overall mosaic of LULC patches (Homer et al. 2015). The LULC types of the study area include Open water, Developed land (in four intensity levels), Forest (Deciduous, Evergreen, and Mixed), Shrub/Scrub, Grassland/Herbaceous, pasture/Hay, Cultivated land, and Wetlands (Woody, Herbaceous).

Contagion Index (CONTAG) and Patch Density (PD) were applied to describe aggregation. CONTAG is inversely related to edge density. For instance, when a single class occupies a very large percentage of the landscape (low edge density), contagion is high, and vice versa. It is affected by both the dispersion and interspersion of land types. PD is the number of patches on the landscape and describes the aggregation and subdivision characteristics of the various land covers. Shannon's Diversity Index (SHDI), considers the proportional abundance of each patch type across all patch types and Patch Richness (PR) quantifies the number of different patch types. These metrics were selected to measure the diversity characteristics on the landscape. All landscape metrics were calculated in FRAGSTATS using a radius of 1000 m centered on sampling points distributed throughout the study areas.

(3) Terrain factors: elevation and Northness

Air temperatures are influenced by elevation (Khandelwal et al. 2017) and variation in elevation results in spatial patterns of LST on the landscape (Li et al. 2010). Additionally, landform aspect strongly affects the intensity of solar radiation and has been included in several SUHI studies (Li et al. 2010; Ivajnšič, Kaligarič, and Žiberna 2014). Aspect (the compass direction of a slope) was transformed to Northness to mitigate the circular property of the data using Equation 7:

$$\text{Northness} = \cos(aspect) \qquad (8)$$

All of the explanatory variables were aggregated or resampled to 90 m resolution to match the dependent variable (LST). Furthermore, to mitigate spatial autocorrelation and to ensure that the sampling dataset represented the study area with sufficient information to understand SUHI patterns, a systematic sampling scheme was designed to obtain sampling points for the regression models. We referred the previous SUHI explanatory studies at the megacity level and used 1000 m as the sampling interval for further exploration (Li et al. 2010). The 1000 m*1000 m grids cells were generated and the center points of the cells which were completely within the boundary of the study areas were selected as independent observations. Finally, 3887 and 4113 samples were generated for the Austin and San Antonio metropolitans, respectively.

5.3 Results

5.3.1 Diagnostics of the regression models

Prior to modeling, correlation analyses were conducted among the explanatory variables to assess for multi-collinearity. variance inflation factors higher than 10 were considered highly correlated. Of the total candidate variables, five were used for analysis in the following global and local regression analysis: Shannon's Diversity Index (SHDI), building fraction (BF), NDVI, Northness, and Elevation. For the sake of comparability and interpretation, all the dependent and independent variables for each were transformed to a range of values spanning from 1 to 100 as the input for the global and GWR model.

The global regression models for each of the two study areas estimated statistically significant ($p<0.001$) relationships between LST and all explanatory variables (Table *5.3*). For Austin, the coefficient of determination (R^2) for the global regression model was estimated to be 0.53. Among the explanatory variables, the SHDI, BF, and Elevation were found to vary positively with LST, while NDVI and Northness were negatively correlated with LST. The global model for San Antonio resulted in an R^2 of 0.45 and revealed the same tendencies regarding the explanatory variables and LST with one exception—namely, the relationship between SHDI and LST was not statistically significant in the San Antonio model.

Compared to these global regressions, GWR models seem better suited to investigating the SUHI and the underlying influencing factors for both study areas. Specifically, in the case of the Austin metropolitan area, the higher R^2 (0.85) for the GWR model suggests that the relationships between LST and the modeled underlying physical factors may exhibit spatial non-stationarity. Such circumstances are one reason why the GWR model seems to outperform the global regressions (Table *5.3*). Additionally, a full comparison of other diagnostic measures further suggests improved performance for GWR compared to the global regression model, including AICc (e.g., 25271.62 for GWR vs 29740.25 for global model, Austin), F-tests of GWR model improvement (34.42, Austin), and the Global Moran's I of the residuals (e.g., 0.44 for GWR vs 0.058 for global model, Austin).

Table 5.3 Comparison of global regression and GWR: summary of the coefficients and diagnostics.

	Austin					San Antonio				
	Global regression			GWR		Global regression			GWR	
	β	S.E.	t	Mean β	STD	β	S.E.	t	Mean β	STD
SHDI	0.04***	0.013	3.38	0.04	0.09	0.01	0.007	1.24	-0.01	0.07
BF	0.29***	0.010	29.50	0.28	0.23	0.19***	0.007	27.42	0.13	0.14
NDVI	-0.74***	0.018	-41.08	-0.83	0.46	-0.38***	0.011	33.66	-0.48	0.14
Elevation	0.20***	0.010	20.35	0.18	0.20	0.09***	0.006	14.05	0.09	0.36
Northness	-0.15***	0.016	-9.41	-0.09	0.10	-0.23***	0.013	18.59	-0.07	0.10
Intercept	104.46***	1.935	53.97	109.41	40.04	104.62***	1.154	90.68	109.29	14.87
Diagnostics										
Residual sum of squares	476925.15			137817.06		194028.74			55084.50	
−2 Log likelihood	29726.22			24900.77		27523.09			22344.25	
Classic AIC	29740.22			25254.64		27537.09			22700.98	
AICc	29740.25			25271.62		27537.12			22717.25	
CV	123.72			39.71		47.37			14.70	
R square	0.53			0.86		0.45			0.84	
Adjusted R square	0.53			0.85		0.45			0.84	
Global Moran's I	0.440***			0.058***		0.745***			0.516***	
Bandwidth of GWR				52.00					52.00	
F-tests of improvement	36.42***					39.20***				

Notes: Please refer to the full variable names from Table 5.2. 'β': The coefficients and intercept in equation (7). '***': significant at 0.001 level.

5.3.2 The global and spatial non-stationarity relationship

Ordinary kriging interpolation using the Spatial Analyst Toolbox in ArcGIS 10.5 was applied to interpret the samples using a resolution of 300 m for the sake of visualization. First, both the global and GWR analyses indicated that LULC affected the LST variation on July 20, 2015, as indicated by BF (building fraction) and NDVI (Table *5.3*). GWR further revealed strong spatial heterogeneity of their relationships based on the coefficient values and t statistics. This covariate relationships were similar for Austin and San Antonio, in the same range of estimates of BF coefficients (ranging from 0 to 0.6). Additionally, the t statistics of BF coefficients for both Austin and San Antonio indicated that the relationship between the LST and BF were significant for most of the study areas, especially in the urban area. Nevertheless, the effect of BF was more prevalent for Austin than for San Antonio, as evidenced from the higher estimates of BF coefficients indicated by the global and local models. While the highest values of the local estimates of BF coefficients (displayed in red) were located in the isolated natural areas (Figure *5.2*), the effect of the BF was prevalent and most of the high values were distributed in areas with compact human settlements (displayed in yellow and slight blue).

As expected, an increase in NDVI reduces the SUHI effect, as suggested by the significantly negative relationship between LST and NDVI across the study areas. The estimated coefficient from the global regression was -0.74 for Austin and -0.38 for San Antonio, revealing a stronger relationship for LST and NDVI for Austin than San Antonio (Table *5.3*). This fact was further proved by the GWR analysis, the values of local absolute coefficients were overall higher in Austin (e.g., displayed in red for majority of the region) than San Antonio, indicating a higher capacity to mitigate the SUHI. However, attention should also be paid to the area around the Lake Travis in Austin and nearby the Calaveras Lake in San Antonio, where LST was notably positively related to NDVI, and the relationship was not significant in some part of this area as indicated by t statistics (Figure *5.2*).

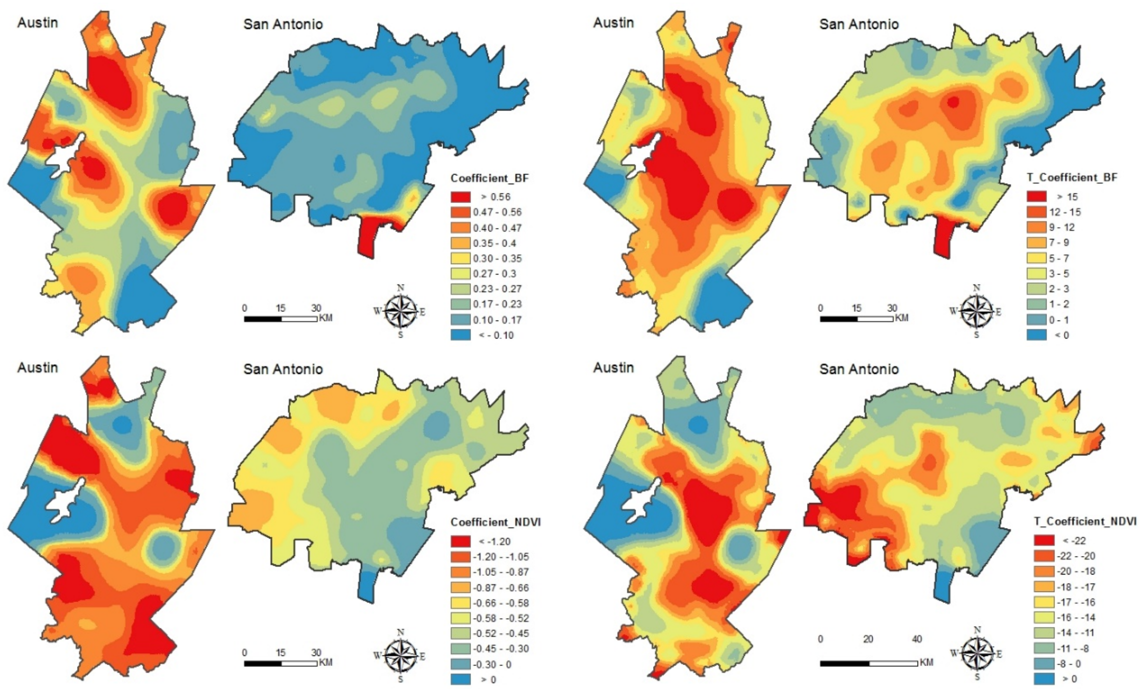

Figure 5.2 Overall spatial variation of the coefficients (left) and the t statistics (right): Building Fraction (BF) and NDVI.

SHDI, as the indicator of the diversity of landscape spatial arrangement, had an overall positive effect on LST intensity, as explained by the global regression for Austin (Table *5.3*). It indicated that the fragmented landscape (e.g., the interaction of different land patches) would lead to the decrease of the capacity to mitigate SUHI. This effect was further proved by the GWR analysis, from which the regression coefficient was positive in most of the area. However, it is notable that the situation was contrary in the area around the Lake Travis in Austin, as indicated by the slightly negative local regression coefficients (Figure *5.3*). Additionally, the global regression revealed a non-relationship between SHDI and LST for San Antonio metropolitan area, and GWR further found that the effects of SHDI on LST variation was not significant for most of the area, as indicted by t statistics (e.g., -1.5 to 1.2, Figure *5.3*). Nevertheless, the GWR analysis did find some exceptions, where the SHDI was a strong predictor for LST variations (e.g., the small area of the southern and northeastern part colored by red, Figure *5.3*). Linking with Google Earth imagery and the NLCD 2011, we found that southern part displayed in red is covered by forest, pasture, and shrub with high complexity. Also, this area demonstrates low DSM as indicated by Figure *5.4*.

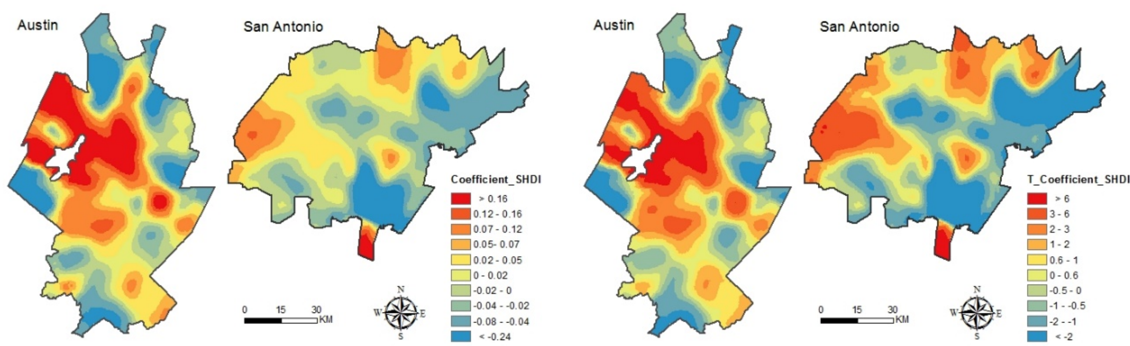

Figure 5.3 Overall spatial variation of the coefficients (left) and the t statistics (right): SHDI.

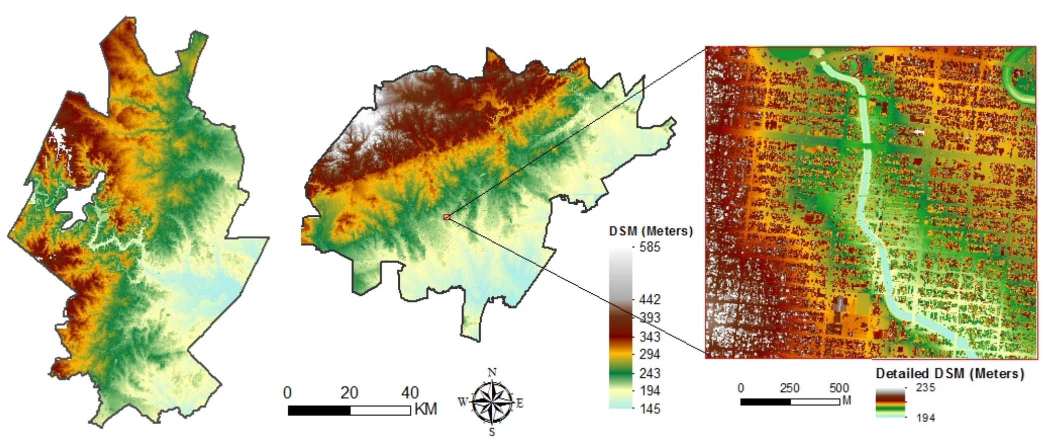

Figure 5.4 Digital surface models (DSMs) with a 5 m resolution for Austin (left), San Antonio (middle), and a detailed illustration of DSMs for a selected area of San Antonio (right).

Terrain factors affected the LST variation on July 20, 2015, as indicated by Elevation and Northness. For both Austin and San Antonio, the Elevation exhibited an overall slight positive effect by the global regression (e.g., 0.20 and 0.09 of coefficients, Table *5.3*). GWR further helped to explore this unexpected finding by indicating that negative coefficients indeed existed in the rural areas for both Austin and San Antonio, especially in the areas with low vegetation cover (e.g., the northeastern part of Austin and eastern San Antonio colored with blue, Figure *5.5*). On the other hand, both the global and local regressions yielded the significantly negative coefficient (average coefficient) of Northness, which indicated that the Northness was a strong predictor for the LST (Table *5.3*). Again, the effect of Northness was spatially varying and it had a stronger effect on San Antonio (-5.34 vs -2.07 indicated by the global regression, Table *5.3*), especially in the northern part (a larger area colored with red indicated by the GWR, Figure *5.5*).

Spatial patterns of the local determination coefficients (R^2) of the GWR model highlighted a marked regional heterogeneity. Overall, GWR outperformed global regression with local R^2 values larger than 0.5 across both study areas. (Figure *5.6*). The GWR modeling was also characterized by higher local R^2 in the city centers (>0.8) while relatively lower values were observed (0.5-0.65) in the surrounding areas. Standardized residuals, indicating the under- or over-prediction of LST, were distributed with significant spatial autocorrelation as tested by the Global Moran's I test in ArcGIS. As shown in Figure *5.6*, the standardized residuals from both global and local regression were distributed in clusters, while the spatial clustering effect resulting from the global regressions was much more apparent than those resulting from the GWR.

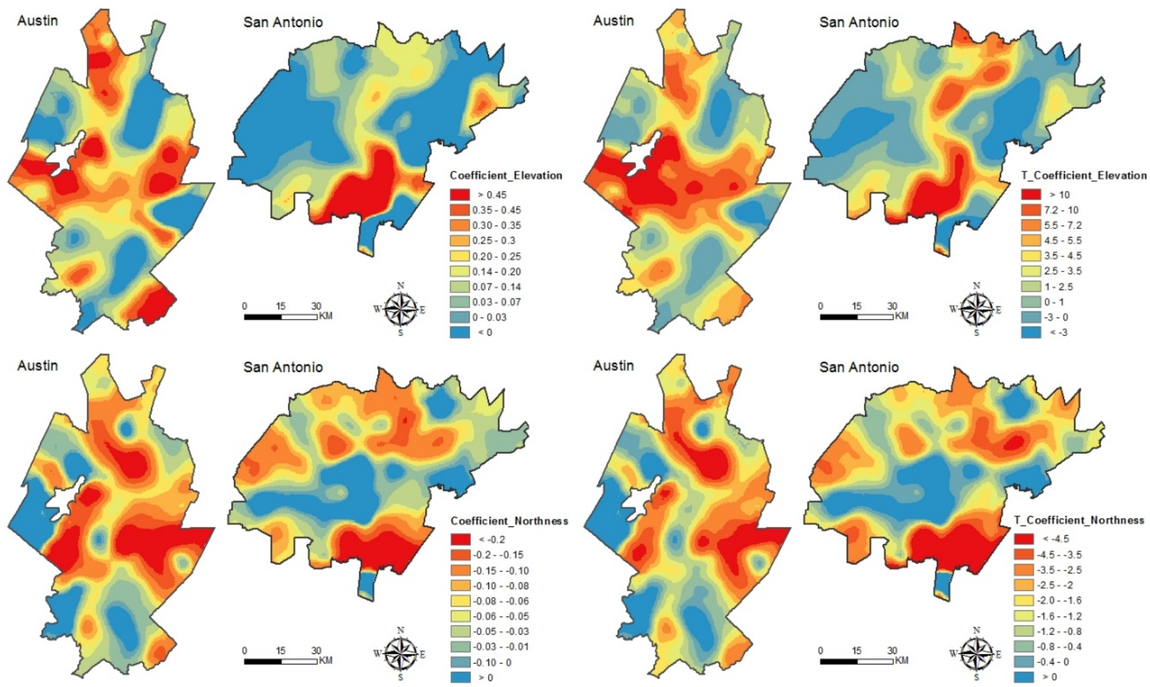

Figure 5.5 Overall spatial variation of the terrain-related coefficients (left) and the t statistics (right): Elevation and Northness.

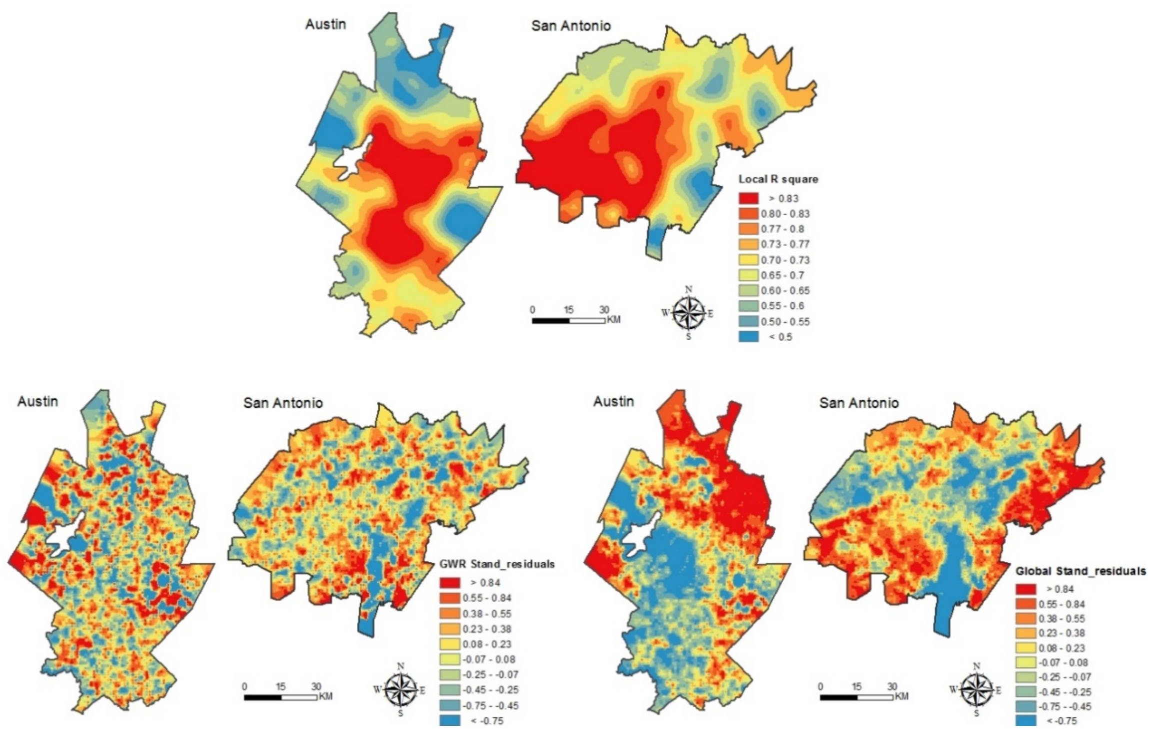

Figure 5.6 Overall spatial distribution of the local R^2 (top), standardized residuals of the GWR (bottom left) and global regression (bottom right) as measures of model goodness of fit.

5.4 Discussion

5.4.1 What underlying properties are significantly related to the SUHI for Austin, in comparison to San Antonio?

Overall, the regression analyses revealed that LULC composition and terrain morphology were closely related to SUHI effects for both metropolitan areas. Similarities in climate and topography for these metropolitan areas facilitates the comparison of their respective SUHIs. First, the composition of land cover was an essential factor influencing the LST pattern for both study areas. Our study confirmed previous findings that an increase of building density (BF) tends to exacerbate the SUHI effect, while the increase of vegetation cover intensity tends to mitigate the SUHI effect (Li et al. 2011; Li et al. 2017; Yue et al. 2007; Estoque, Murayama, and Myint 2017; Guo et al. 2015; Du, Xiong, et al. 2016). Regarding the regional differences, although the effects tended to be similar, building density and vegetation cover intensity were more strongly correlated with the SUHI phenomenon in San Antonio than Austin metropolitan area as indicated by global BF coefficients of 0.29 vs 0.19 and NDVI coefficients of -0.74 vs -0.38, respectively (Table *5.3*). Furthermore, it is notable that the situation was contrary in the area near the water body (e.g., Lake Travis in Austin) as indicated by the slightly negative local regression coefficients. The unique character of water bodies regarding the thermal characteristic was also consistent with previous studies (Weng, Lu, and Schubring 2004; Yue et al. 2007).

Both global and local regressions provided unexpected results for Elevation. Our results show that an increase in elevation was associated with an overall increase of LST. It is different with the fact that temperature decrease with increase in altitude. In fact, it was DTM (e.g., bare earth digital terrain model) that was used as the potential explanatory factor for LST variation, while the actual surface temperature of the property was what being remotely sensed. Thus, in the areas with dense building or forest cover, the effect of Elevation would be not as severe as other factors when incorporating them simultaneously in the modeling. Also, most areas of both Austin and San Antonio exhibit flat terrain, thus the effect of Elevation was not apparent. Furthermore, the Lidar-derived DSM proved to be an effective way to characterize the terrain morphology at the microscale (e.g., 5m*5m) for understanding the relation of Northness and SUHI variation. Consistent with previous studies, this research also indicated that this effect as more apparent for floodplain areas with low and flat terrain for both the Austin and San Antonio metropolitan areas (e.g., Li et al. 2010; Ivajnšič, Kaligarič, and Žiberna 2014).

The effect of landscape configuration on SUHI formulation has drawn attention in recent years by incorporating the landscape matrix at the patch, class, or landscape level (Zhou, Huang, and Cadenasso 2011; Zheng, Myint, and Fan 2014; Li et al. 2012; Peng et al. 2016; Myint et al. 2015; Li et al. 2011). For example, a recent study by Kim et al. (2016a) found that larger and better-connected landscape patches have the effect of mitigating high LST at the neighborhood level, while fragmented and isolated patches have the opposite effect for the city of Austin. Similarly, this study found that the SUHI of Austin on July 20, 2015, was also affected by the spatial pattern of LULC, measured by SHDI, which was not detected for San Antonio metropolitan area.

This inconsistent finding may be explained by the fact that the landscape characteristics of San Antonio were more aggregated and less diverse as indicated by the statistics of potential explanatory variables (Table 5.2). In this study, to balance the spatially detailed characterization of SUHI and the size of samples in the modeling, 1000 m was set as the sampling interval as well as the window size for landscape matrix calculation for both study areas. The fact is that both landscape patterns and LST distributions are scale dependent, and studies have drawn different conclusions on the suitable scale for further investigation of the relationship (e.g., 700 m for Beijing, China (Song et al. 2014); 600 m for Wuhan, China (Wang, Qingming, et al. 2016)). In addition, the appropriate scale also depends on landscape matrix selection. For instance, the SHDI showed the strongest correlation with LST at 700 m scale, which was not the optimal solution if other landscape matrices were taken into account, as indicated by a case study of Wuhan, China (Wang, Zhan, and Ouyang 2017). In this sense, further research to examine the scale sensitivity of their relationships is needed in the future to lead a more comprehensive understanding.

5.4.2 Compared to the conventional regression model, does the GWR provide improved insight of SUHI phenomenon?

As a natural process, SUHI exhibit high spatial heterogeneity, which is difficult to characterize with conventional regression methods. However, most of the previous studies derived the aspatial relationship by focusing on individual cities, especially for cities in Asia (Li et al. 2011; Li et al. 2017; Yue et al. 2007; Estoque, Murayama, and Myint 2017; Guo et al. 2015; Du, Xiong, et al. 2016), and varying heterogeneous impacts have been rarely studied and compared. The results reported in this paper suggest significant spatial non-stationarity in the relationships between the LST and explanatory variables for the two metropolitan areas. Here, the GWR modeling was confirmed as an effective method to detect the non-stationarity underlying mechanism, especially for the urban cores of Austin and San Antonio, as well as western San Antonio, with local R^2 higher than 0.8.

Furthermore, the locally detailed differentiation regarding the underlying mechanism of SUHI provided by non-stationarity GWR modeling is conductive for partitioned regional landscape planning. With the implementation of GWR, studies have suggested site-specific policies designed for effective SUHI mitigation, including land use planning considering the distance to roads to alleviate the high LST effect (Li et al. 2010), the location and configuration of green spaces in urban areas (Ivajnšič, Kaligarič, and Žiberna 2014), etc. Considering natural and socioeconomic factors, Li et al. (2017) mapped the potential heat sources and sinks of the megacity and performed GWR analysis based on the heat source and sink regions, where the partitioned policies were provided.

Whereas a classic regression method would provide an estimate of the mean value for an entire region regardless of spatial pattern, GWR infers a more dynamic approach to parameter estimates by using neighborhoods of data to determine model parameters. In the case of identifying whether the SUHI phenomenon was influenced by local underlying physical factors, this dynamic model approach is desirable, as a “one size fits all” approach may not accurately identify the LST variation across a heterogeneous metropolitan landscape. In short, compared to conventional regression, GWR has the inherent potential to enable a better understanding of SUHI phenomenon and associated physical factors across the metropolitan.

5.5 Conclusions

Urbanized area is characterized by a high density of buildings as well as impervious surfaces fraction (ISF), and low percentage of vegetation cover. These characteristics lead directly to SUHI formation. In this study, we used Landsat imagery for July 20, 2015, Lidar dataset and derived products, NLCD 2011 land cover and associated fractional cover products the main data sources to investigate SUHI spatial distribution for the Austin and San Antonio metropolitan areas. This study further explored how the underlying surface characteristics affect SUHI phenomenon by using global regression and GWR analysis.

In summary, our results indicate that the GWR was in overall agreement with the global regression and both helped to address the contributions a set of specific underlying physical factors related to SUHI phenomenon. The composition of land cover was an essential factor influencing the LST pattern for both study areas. Furthermore, the Lidar-derived DSM was proved to be an effective way to characterize the terrain morphology at the microscale (e.g., 5m*5m) for understanding the relation of Northness and SUHI variation. This study also found that the SUHI of Austin on July 20, 2015, was also affected by the spatial pattern of LULC, measured by SHDI, which was not detected at San Antonio metropolitan area. Overall, this study contributes to an improved understanding of SUHI phenomenon.

By accommodating spatial non-stationarity and allowing the model parameters to vary in space, GWR illustrated the spatial heterogeneity of the relationship of different land surface properties and the LST. Particularly, our GWR analysis revealed considerably stronger relationships in some areas, e.g., some particular LCZs, the areas mapped by urban climatic characteristic. Thus, together with the mapping result, the GWR analytical method of SUHI phenomenon can provide unique information for site-specific land planning and policies implementation for SUHI mitigation.

6 CONCLUSION

This chapter provides a summary of the major findings from this dissertation. It also discusses key limitations encountered in the study and makes recommendations for future research.

6.1 Summary

The goal of this dissertation was to investigate the SUHI phenomenon for three metropolitan areas of Texas, USA with remote sensing techniques, which was addressed by posing the following two main questions. These questions and their associated answers are summarized as follows.

(1) Does the SUHI vary within and among the three major metropolitan areas in Texas and how can LCZs be used to improve the characterization of SUHI?

Prior to answering this question, Chapter 3 developed a GIS-based Local Climate Zones (LCZs) classification scheme with the aid of airborne Lidar datasets and other freely available GIS data, to map and compare the LCZs for the three metropolitan areas: Dallas-Fort Worth (DFW), Austin, and San Antonio. Based on an analysis of the land cover and urban morphology, variables including land cover, height of roughness elements, building surface fraction, pervious surface fraction (PSF), and land use planning codes were generated and selected as LCZs classification properties. A decision-making algorithm was built for LCZs mapping, and LCZs datasets were established. The key findings of LCZs of the study areas are that: 1) Most of the urbanized area are categorized into LCZ open types (characterized by building surface fraction of 15-40% and pervious surface fraction of 30-60%) for all three metropolitan areas with different proportions and spatial diversity; 2) LCZ low plants class is dominant in the areas surrounding DFW, while LCZ A Dense trees and LCZ D low plants are dominant in Austin and San Antonio with clear regional contrast; and 3) LCZs maps are in accordance with the underlying regional environment of the areas. Chapter 3 provided evidence that Lidar-derived products can support LCZs mapping to identify urban morphological information and standardize the mapping scheme for further comparative studies of metropolitan areas, although to extend the study beyond this region, Lidar data may not be necessary as high-resolution imagery could provide an alternative dataset to extract urban morphology with less financial and processing costs.

Subsequently, the question was able to be answered by linking remotely sensed land surface temperature (LST) with LCZs. Chapter 4 investigated the ability of LCZs for studying SUHI phenomenon and analyzes how different LCZs affect the SUHI in three major metropolitan areas. Landsat 8 image data was acquired for July 20, 2015 and used to calculate LST as SUHI measurement. Pairwise comparisons were employed to measure the association between LCZs and LST. Results indicated that large LST variations were first demonstrated among LCZs characterized by different land cover, and then urban morphological information (building density, and the height of roughness). The close association between LCZs and LST demonstrated that the LCZs mapping was useful for comparing and investigating the SUHI.

(2) Can the spatial dynamics of SUHI be explained by the LCZs and underlying factors and if so, are the findings uniform among different areas?

Chapter 4 examined the thermal contribution of LCZs in terms of the relative proportion of high temperature centers. Results found that there was a similar heating/cooling effect for most of the LCZs in three metropolitans, whereas some LCZs in the different metropolitan areas can contribute to the opposite heating/cooling effect, due to the spatial arrangements and geographic locations of LCZs. So basically, the spatial distribution of LCZs can further benefit spatial SUHI mitigation strategies. Chapter 5 investigated how the underlying surface characteristics affect characterization of the SUHI phenomenon by assessing different regression methods: global regression and geographically weighted regression (GWR). The spatial distribution of LST was sought to be estimated based on lidar-derived terrain factors, land cover composition, and landscape pattern metrics developed using the NLCD 2011. Result indicated that 1) land cover composition and terrain morphology were closely related to SUHI effects for both metropolitan areas; 2) the SUHI of Austin on July 20, 2015 was affected by the spatial pattern of LULC, which was not detected for San Antonio; and 3) compared to global regression, GWR more efficiently and accurately explained the underlying factors that contributed to the SUHI based on spatial variation and thus demonstrates improved utility for characterizing SUHI compared to global regression.

6.2 Limitations and Recommendations

It is important to recognize the multi-scale characteristic of the overall UHI phenomenon (including SUHI), varying from small scale anthropogenic heat release to meso-scale atmospheric interactions. In this study, the UHI was investigated at the surface layer with the indicators of LST, and the term SUHI was used to address this unique aspect. Spatial patterns of UHI and SUHI and general characteristics of urban-to-rural temperature differences have been extensively studied. However, the spatial heterogeneity characteristics of the urban environment need to be addressed for both UHI and SUHI studies. This dissertation indicates that the measurement of SUHI with remote sensing techniques advanced our understanding of spatial thermal patterns and their relationship to surface characteristics.

1) Besides the multiple measurement of UHI at different boundaries in terms of atmospheric UHI and SUHI, the urban environment is heterogeneous. In this study, the use of LCZs, which incorporate the urban and vegetation morphology and underlying biophysical factors simultaneously with different measurement techniques, was incorporated to investigate the SUHI phenomenon. Basically, the LCZ concept was used to delineate the heterogeneous urban environment into uniform zone in terms of the local climate in the chapter 3. In reality, the scale of individual LCZs varies within the individual metropolitan area and between different metropolitan areas. Also, the scale of LCZs can vary worldwide due to specific urban forms, urban development history, and geographical location. Both the urban and natural landscape are heterogeneous and spatially auto-correlated, meaning that each LCZs is not an absolute homogenous region and there is no clear boundary between different LCZs.

   For comparative analysis, it is necessary to set a common scale to consider various parameters to identify possible LCZs. Overall, LCZs mapping is a compromise between the universality and local accuracy. The 270 m scale was defined as a homogeneous scale in this research based on the semi-variance analysis of the property of buildings height and the literature review of previous studies. On the other hand, the scale on which the variation of urban and vegetation morphology and underlying biophysical factors affects the surface or air temperature is not necessarily in accordance with the heterogeneous characteristics of the buildings. Moreover, linking LST with LCZs indicated that the surface temperature of some of the LCZs built-up types were not significantly different with others. Hence, the LCZs mapping scale still need more verification in the future case studies to fit the characteristics of different cities worldwide.

2) As indicated by the research framework, the SUHI is a spatiotemporal process with the interaction among the urbanization, local climate, and human component in the urban system. It is important to reflect the temporal variation characteristic of SUHI. In the Chapter 4, the LCZs were considered to be temporally invariant and representative of the urban environment. LCZs were built based on several properties generated by NLCD 2011 and Lidar projects at different periods. NLCD 2011 data was derived from 2008-2010 Landsat data whereas Lidar projects were conducted by a suite of vendors working for various agencies or clients that all had different acquisition requirements. Nonetheless, the SUHI is indicated by the spatial pattern of LST on July 20, 2015. However, both the AUHI and SUHI phenomenon depend on weather conditions and it is generally more intense during dry seasons when leafless canopies and the dry and bright soil increase the albedo. Thus, due to the urban development and urban expansion, the urban environment (e.g., LCZs) may change dramatically by the time of SUHI investigation in this study. Furthermore, the LCZs were built at different season, which could not be reflected by SUHI phenomenon at one time. Further investigation of the SUHI phenomenon at night time and in different seasons would contribute to a better understanding of the SUHI phenomenon.

3) As a spatial process, the analysis of SUHI needs to emphasis the scale issue. For instance, Chapter 5 investigated how the underlying surface characteristics affect characterization of the SUHI phenomenon for individual sites using a 1000-meter sampling interval. For different underlying factors, the influences of lakes and greenspaces as cooling elements can extend far beyond their boundaries, while the effects of building density may also be beyond the extent for the individual sites. Chapter 4 indicated that the significant difference of the thermal behavior within LCZs and it's noted that the influence of some LCZ natural types (e.g., LCZ A Dense trees) as cooling elements can extend in the order of hundreds of meters beyond their boundaries. The spatial composition and configuration of LCZs affect the SUHI phenomenon at a larger scale.
4) In this study, LCZs mapping provides a platform to make a comparative analysis of the urban morphology and vegetation structure of the three metropolitan study areas. Also, with a uniform LCZ classification scheme, this study provided evidence that LCZ mapping can be replicable for comparative analysis of SUHI phenomenon. DI of high temperature further demonstrated that the LCZs mapping result can efficiently facilitate intra- and inter-comparisons for SUHI intensity. The comparison among the three metropolitan areas indicated that the different heating/cooling effect of LCZs on SUHI phenomenon can be further investigated. The urban planning and city policy of one metropolitan can as reference to others in terms of the effect of the vegetation character in the individual LCZ, and the spatial distribution of LCZs on SUHI intensity to benefit spatially SUHI migration strategies. Moreover, the uniform LCZs maps can be incorporated into

climatic models to understand the UHI formation and dynamics with detailed underlying surface information.

APPENDIX SECTION

Table A1. Local climate zones (LCZs) concepts and the related values of geometric and surface cover properties.

Code	Local climate zone (LCZ)	Sky view factor (SVF)	Aspect ratio (H/W)	Building surface fraction	Impervious surface fraction (ISF)	Pervious surface fraction (PSF)	Height of roughness elements	Terrain roughness class
LCZ 1	Compact high-rise	0.2–0.4	> 2	40–60	40–60	< 10	> 25	8
LCZ 2	Compact mid-rise	0.3–0.6	0.75–2	40–70	30–50	< 20	10–25	6–7
LCZ 3	Compact low-rise	0.2–0.6	0.75–1.5	40–70	20-50	< 30	3–10	6
LCZ 4	Open high-rise	0.5–0.7	0.75–1.25	20-40	30-40	30-40	> 25	7-8
LCZ 5	Open mid-rise	0.5–0.8	0.3– 0.75	20-40	30–50	20-40	10–25	5-6
LCZ 6	Open low-rise	0.6–0.9	0.3– 0.75	15-25	20-50	30–60	3–10	5-6
LCZ 7	Lightweight low-rise	0.2–0.5	1–2	60–90	< 20	< 30	2–4	4-5
LCZ 8	Large low-rise	> 0.7	0.2–0.4	30–50	40–50	< 20	3–30	5
LCZ 9	Sparsely built	> 0.8	0.2–0.4	5–15	< 20	60–80	3–10	5-6
LCZ 10	Heavy industry	0.6–0.9	0.2–0.5	20–30	20-40	40–50	5–15	5-6
LCZ A	Dense trees	< 0 .4	> 1	< 10	< 10	> 90	3–30	8
LCZ B	Scattered trees	0.5–0.8	0.25–0.75	< 10	< 10	> 90	3–15	5-6
LCZ C	Bush, scrub	0.7–0.9	0.25–1.0	< 10	< 10	> 90	< 2	4-5
LCZ D	Low plants	> 0.9	< 0.1	< 10	< 10	> 90	< 1	3-4
LCZ E	Bare rock or paved	> 0.9	< 0.1	< 10	> 90	< 10	< 2.5	1-2
LCZ F	Bare soil or sand	> 0.9	< 0.1	< 10	< 10	> 90	< 2.5	1-2
LCZ G	Water	> 0.9	< 0.1	< 10	< 10	> 90	–	1

REFERENCES

Ahern, Jack. 2013. 'Urban landscape sustainability and resilience: the promise and challenges of integrating ecology with urban planning and design', *Landscape Ecology*, 28: 1203-12.

Alexander, Paul John, Gerald Mills, and Rowan Fealy. 2015. 'Using LCZ data to run an urban energy balance model', *Urban Climate*, 13: 14-37.

America's 20 Fastest-Growing Cities. last accesed March 21th, 2018. *Forbes Business*, *https://www.forbes.com/sites/morganbrennan/2013/01/23/americas-fastest-growing-cities/#6b5ed9a6244f*.

American FactFinder. last accessed March 21th, 2018. 'American FactFinder', *https://factfinder.census.gov/faces/nav/jsf/pages/index.xhtml*.

Amiri, Reza, Qihao Weng, Abbas Alimohammadi, and Seyed Kazem Alavipanah. 2009. 'Spatial–temporal dynamics of land surface temperature in relation to fractional vegetation cover and land use/cover in the Tabriz urban area, Iran', *Remote sensing of environment*, 113: 2606-17.

Anniballe, Roberta, Stefania Bonafoni, and Manuele Pichierri. 2014. 'Spatial and temporal trends of the surface and air heat island over Milan using MODIS data', *Remote sensing of Environment*, 150: 163-71.

Barlow, Janet F. 2014. 'Progress in observing and modelling the urban boundary layer', *Urban Climate*, 10, Part 2: 216-40.

Bechtel, Benjamin. 2012. 'Robustness of annual cycle parameters to characterize the urban thermal landscapes', *IEEE Geoscience and Remote Sensing Letters*, 9: 876-80.

Bechtel, Benjamin, Paul Alexander, Jürgen Böhner, Jason Ching, Olaf Conrad, Johannes Feddema, Gerald Mills, Linda See, and Iain Stewart. 2015. 'Mapping Local Climate Zones for a Worldwide Database of the Form and Function of Cities', *ISPRS International Journal of Geo-Information*, 4: 199-219.

Bechtel, Benjamin, and Christian Daneke. 2012. 'Classification of Local Climate Zones Based on Multiple Earth Observation Data', *IEEE Journal of Selected Topics in Applied Earth Observations and Remote Sensing*, 5: 1191-202.

Bechtel, Benjamin, Linda See, Gerald Mills, and Mícheál Foley. 2016. 'Classification of Local Climate Zones Using SAR and Multispectral Data in an Arid Environment', *IEEE Journal of Selected Topics in Applied Earth Observations and Remote Sensing*, 9: 3097-105.

Becker, François, and Zhao-Liang Li. 1995. 'Surface temperature and emissivity at various scales: Definition, measurement and related problems', *Remote Sensing Reviews*, 12: 225-53.

Bottyán, Zsolt, and János Unger. 2003. 'A multiple linear statistical model for estimating the mean maximum urban heat island', *Theoretical and Applied Climatology*, 75: 233-43.

Bowler, Diana E., Lisette Buyung-Ali, Teri M. Knight, and Andrew S. Pullin. 2010. 'Urban greening to cool towns and cities: A systematic review of the empirical evidence', *Landscape and Urban Planning*, 97: 147-55.

Bremer, Thomas S. 2004. *Blessed with tourists: The borderlands of religion and tourism in San Antonio* (Univ of North Carolina Press).

Buyantuyev, Alexander, and Jianguo Wu. 2009. 'Urban heat islands and landscape heterogeneity: linking spatiotemporal variations in surface temperatures to land-cover and socioeconomic patterns', *Landscape Ecology*, 25: 17-33.

Cai, Meng, Chao Ren, Yong Xu, Kevin Ka-Lun Lau, and Ran Wang. 2017. 'Investigating the relationship between local climate zone and land surface temperature using an improved WUDAPT methodology – A case study of Yangtze River Delta, China', *Urban Climate*.

Chen, Liang, Rong Jiang, and Wei-Ning Xiang. 2015. 'Surface Heat Island in Shanghai and Its Relationship with Urban Development from 1989 to 2013', *Advances in Meteorology*, 2016.

Chen, Xiao-Ling, Hong-Mei Zhao, Ping-Xiang Li, and Zhi-Yong Yin. 2006. 'Remote sensing image-based analysis of the relationship between urban heat island and land use/cover changes', *Remote sensing of Environment*, 104: 133-46.

Chun, B., and J. M. Guldmann. 2014. 'Spatial statistical analysis and simulation of the urban heat island in high-density central cities', *Landscape and Urban Planning*, 125: 76-88.

Chun, Bumseok, and Subhrajit Guhathakurta. 2016. 'The Impacts of Three-Dimensional Surface Characteristics on Urban Heat Islands over the Diurnal Cycle', *The Professional Geographer*: 1-12.

Connors, John Patrick, Christopher S Galletti, and Winston TL Chow. 2013. 'Landscape configuration and urban heat island effects: assessing the relationship between landscape characteristics and land surface temperature in Phoenix, Arizona', *Landscape Ecology*, 28: 271-83.

Coseo, Paul, and Larissa Larsen. 2014. 'How factors of land use/land cover, building configuration, and adjacent heat sources and sinks explain Urban Heat Islands in Chicago', *Landscape and Urban Planning*, 125: 117-29.

Curran, Paul J, and Peter M Atkinson. 1998. 'Geostatistics and remote sensing', *Progress in Physical Geography*, 22: 61-78.

Dallas City GIS Services. last accessed March 21th, 2018. 'Dallas City GIS Services', http://gis.dallascityhall.com/homepage/shapezip.htm.

Das Majumdar, Dipanjan, and Atrayee Biswas. 2016. 'Quantifying land surface temperature change from LISA clusters: An alternative approach to identifying urban land use transformation', *Landscape and Urban Planning*, 153: 51-65.

Davenport, Alan G, C Sue B Grimmond, Tim R Oke, and Jon Wieringa. 2000. "Estimating the roughness of cities and sheltered country." In *Proceedings 12th Conference on Applied Climatology, Asheville, NC, American Meteorological Society, Boston*, 96-99.

Debbage, Neil, and J Marshall Shepherd. 2015. 'The urban heat island effect and city contiguity', *Computers, Environment and Urban Systems*, 54: 181-94.

Deilami, Kaveh, Md Kamruzzaman, and John Hayes. 2016. 'Correlation or Causality between Land Cover Patterns and the Urban Heat Island Effect? Evidence from Brisbane, Australia', *Remote Sensing*, 8: 716.

Deng, Chengbin, and Changshan Wu. 2013. 'Examining the impacts of urban biophysical compositions on surface urban heat island: A spectral unmixing and thermal mixing approach', *Remote sensing of Environment*, 131: 262-74.

Du, H., D. Wang, Y. Wang, X. Zhao, F. Qin, H. Jiang, and Y. Cai. 2016. 'Influences of land cover types, meteorological conditions, anthropogenic heat and urban area on surface urban heat island in the Yangtze River Delta Urban Agglomeration', *Sci Total Environ*, 571: 461-70.

Du, Shihong, Ziqian Xiong, Yi-Chen Wang, and Luo Guo. 2016. 'Quantifying the multilevel effects of landscape composition and configuration on land surface temperature', *Remote sensing of Environment*, 178: 84-92.

Estoque, R. C., Y. Murayama, and S. W. Myint. 2017. 'Effects of landscape composition and pattern on land surface temperature: An urban heat island study in the megacities of Southeast Asia', *Sci Total Environ*, 577: 349-59.

Fabrizi, Roberto, Stefania Bonafoni, and Riccardo Biondi. 2010. 'Satellite and ground-based sensors for the urban heat island analysis in the city of Rome', *Remote Sensing*, 2: 1400-15.

Fan, Chao, Sergio J. Rey, and Soe W. Myint. 2016. 'Spatially filtered ridge regression (SFRR): A regression framework to understanding impacts of land cover patterns on urban climate', *Transactions in GIS*.

Fu, Peng, and Qihao Weng. 2016. 'A time series analysis of urbanization induced land use and land cover change and its impact on land surface temperature with Landsat imagery', *Remote sensing of Environment*, 175: 205-14.

Gao, Feng, Jeff Masek, Matt Schwaller, and Forrest Hall. 2006. 'On the blending of the Landsat and MODIS surface reflectance: Predicting daily Landsat surface reflectance', *IEEE Transactions on Geoscience and Remote Sensing*, 44: 2207-18.

Geletič, Jan, and Michal Lehnert. 2016. 'GIS-based delineation of local climate zones: The case of medium-sized Central European cities', *Moravian Geographical Reports*, 24.

Geletič, Jan, Michal Lehnert, and Petr Dobrovolný. 2016. 'Land Surface Temperature Differences within Local Climate Zones, Based on Two Central European Cities', *Remote Sensing*, 8: 788.

Gergel, Sarah E, and Monica G Turner. 2006. *Learning landscape ecology: a practical guide to concepts and techniques* (Springer Science & Business Media).

Goodchild, Michael F, and Dale A Quattrochi. 1997. 'Scale, multiscaling, remote sensing, and GIS'.

Guo, Guanhua, Zhifeng Wu, Rongbo Xiao, Yingbiao Chen, Xiaonan Liu, and Xiaoshi Zhang. 2015. 'Impacts of urban biophysical composition on land surface temperature in urban heat island clusters', *Landscape and Urban Planning*, 135: 1-10.

Guo, Liu Jian, and J McM Moore. 1998. 'Pixel block intensity modulation: adding spatial detail to TM band 6 thermal imagery', *International Journal of Remote Sensing*, 19: 2477-91.

Guo, Luo, Zhihai Ma, and Lianjun Zhang. 2008. 'Comparison of bandwidth selection in application of geographically weighted regression: a case study', *Canadian Journal of Forest Research*, 38: 2526-34.

Guo, Z, SD Wang, MM Cheng, and Y Shu. 2012. 'Assess the effect of different degrees of urbanization on land surface temperature using remote sensing images', *Procedia Environmental Sciences*, 13: 935-42.

Hansen, Matthew C, David P Roy, Erik Lindquist, Bernard Adusei, Christopher O Justice, and Alice Altstatt. 2008. 'A method for integrating MODIS and Landsat data for systematic monitoring of forest cover and change in the Congo Basin', *Remote sensing of Environment*, 112: 2495-513.

Harlan, Sharon L, Anthony J Brazel, G Darrel Jenerette, Nancy S Jones, Larissa Larsen, Lela Prashad, and William L Stefanov. 2007. 'In the shade of affluence: the inequitable distribution of the urban heat island', *Research in social problems and public policy*, 15: 173-202.

Hart, Melissa A., and David J. Sailor. 2008. 'Quantifying the influence of land-use and surface characteristics on spatial variability in the urban heat island', *Theoretical and Applied Climatology*, 95: 397-406.

Harvey, David. 1969. 'Explanation in Geography. London: Edward Arnold., 1972." Revolutionary and counter revolutionary theory in geography and the problem of ghetto formation,"', *Antipode*, 4: 1-13.

Hilker, Thomas, Michael A Wulder, Nicholas C Coops, Julia Linke, Greg McDermid, Jeffrey G Masek, Feng Gao, and Joanne C White. 2009. 'A new data fusion model for high spatial-and temporal-resolution mapping of forest disturbance based on Landsat and MODIS', *Remote sensing of Environment*, 113: 1613-27.

Hilker, Thomas, Michael A Wulder, Nicholas C Coops, Nicole Seitz, Joanne C White, Feng Gao, Jeffrey G Masek, and Gordon Stenhouse. 2009. 'Generation of dense time series synthetic Landsat data through data blending with MODIS using a spatial and temporal adaptive reflectance fusion model', *Remote sensing of Environment*, 113: 1988-99.

Homer, Collin, Jon Dewitz, Limin Yang, Suming Jin, Patrick Danielson, George Xian, John Coulston, Nathaniel Herold, James Wickham, and Kevin Megown. 2015. 'Completion of the 2011 National Land Cover Database for the conterminous United States–representing a decade of land cover change information', *Photogrammetric Engineering & Remote Sensing*, 81: 345-54.

Houet, Thomas, and Grégoire Pigeon. 2011. 'Mapping urban climate zones and quantifying climate behaviors – An application on Toulouse urban area (France)', *Environmental Pollution*, 159: 2180-92.

Howard, Luke. 1818. *The Climate of London: deduced from Meteorological observations, made at different places in the neighbourhood of the metropolis* (W. Phillips, sold also by J. and A. Arch).

Hu, Leiqiu, and Nathaniel A. Brunsell. 2015. 'A new perspective to assess the urban heat island through remotely sensed atmospheric profiles', *Remote sensing of Environment*, 158: 393-406.

Huang, Bo, Juan Wang, Huihui Song, Dongjie Fu, and KwanKit Wong. 2013. 'Generating high spatiotemporal resolution land surface temperature for urban heat island monitoring', *IEEE Geoscience and Remote Sensing Letters*, 10: 1011-15.

Huang, Ganlin, and M. L. Cadenasso. 2016. 'People, landscape, and urban heat island: dynamics among neighborhood social conditions, land cover and surface temperatures', *Landscape Ecology*.

Huang, Qunfang, and Yuqi Lu. 2015. 'The Effect of Urban Heat Island on Climate Warming in the Yangtze River Delta Urban Agglomeration in China', *International journal of environmental research and public health*, 12: 8773-89.

Imhoff, Marc L., Ping Zhang, Robert E. Wolfe, and Lahouari Bounoua. 2010. 'Remote sensing of the urban heat island effect across biomes in the continental USA', *Remote sensing of Environment*, 114: 504-13.

Ivajnšič, Danijel, Mitja Kaligarič, and Igor Žiberna. 2014. 'Geographically weighted regression of the urban heat island of a small city', *Applied Geography*, 53: 341-53.

Jiang, Yitong, Peng Fu, and Qihao Weng. 2015. 'Assessing the impacts of urbanization-associated land use/cover change on land surface temperature and surface moisture: A case study in the midwestern United States', *Remote Sensing*, 7: 4880-98.

Keramitsoglou, Iphigenia, Chris T Kiranoudis, Giulio Ceriola, Qihao Weng, and Umamaheshwaran Rajasekar. 2011. 'Identification and analysis of urban surface temperature patterns in Greater Athens, Greece, using MODIS imagery', *Remote sensing of Environment*, 115: 3080-90.

Khandelwal, Sumit, Rohit Goyal, Nivedita Kaul, and Aneesh Mathew. 2017. 'Assessment of land surface temperature variation due to change in elevation of area surrounding Jaipur, India', *The Egyptian Journal of Remote Sensing and Space Science*.

Kim, J. H., D. Gu, W. Sohn, S. H. Kil, H. Kim, and D. K. Lee. 2016a. 'Neighborhood Landscape Spatial Patterns and Land Surface Temperature: An Empirical Study on Single-Family Residential Areas in Austin, Texas', *Int J Environ Res Public Health*, 13.

Kim, Jun-Hyun, Donghwan Gu, Wonmin Sohn, Sung-Ho Kil, Hwanyong Kim, and Dong-Kun Lee. 2016b. 'Neighborhood Landscape Spatial Patterns and Land Surface Temperature: An Empirical Study on Single-Family Residential Areas in Austin, Texas', *International journal of environmental research and public health*, 13: 880.

Koc, C Bartesaghi, P Osmond, A Peters, and M Irger. 2017. "Mapping Local Climate Zones for urban morphology classification based on airborne remote sensing data." In *Urban Remote Sensing Event (JURSE), 2017 Joint*, 1-4. IEEE.

Kotharkar, Rajashree, and Anurag Bagade. 2017. 'Local Climate Zone classification for Indian cities: A case study of Nagpur', *Urban Climate*.

Kuang, Wenhui, Yue Liu, Yinyin Dou, Wenfeng Chi, Guangsheng Chen, Chengfeng Gao, Tianrong Yang, Jiyuan Liu, and Renhua Zhang. 2014. 'What are hot and what are not in an urban landscape: quantifying and explaining the land surface temperature pattern in Beijing, China', *Landscape Ecology*, 30: 357-73.

Leconte, Francois, Julien Bouyer, Rémy Claverie, and Mathieu Pétrissans. 2015. 'Using Local Climate Zone scheme for UHI assessment: Evaluation of the method using mobile measurements', *Building and Environment*, 83: 39-49.

Lee, Dongwoo, and Kyushik Oh. 2017. 'Classifying urban climate zones (UCZs) based on statistical analyses', *Urban Climate*.

Lehnert, Michal, Jan Geletič, Jan Husák, and Miroslav Vysoudil. 2015. 'Urban field classification by "local climate zones" in a medium-sized Central European city: the case of Olomouc (Czech Republic)', *Theoretical and Applied Climatology*, 122: 531-41.

Levy, Sara H. 2016. 'Detecting spatio-temporal changes in Baltimore, Maryland's heat island with remote sensing imagery', Towson University.

Li, Juan-juan, Xiang-rong Wang, Xin-jun Wang, Wei-chun Ma, and Hao Zhang. 2009. 'Remote sensing evaluation of urban heat island and its spatial pattern of the Shanghai metropolitan area, China', *Ecological Complexity*, 6: 413-20.

Li, Junxiang, Conghe Song, Lu Cao, Feige Zhu, Xianlei Meng, and Jianguo Wu. 2011. 'Impacts of landscape structure on surface urban heat islands: A case study of Shanghai, China', *Remote sensing of Environment*, 115: 3249-63.

Li, Shuangcheng, Zhiqiang Zhao, Xie Miaomiao, and Yanglin Wang. 2010. 'Investigating spatial non-stationary and scale-dependent relationships between urban surface temperature and environmental factors using geographically weighted regression', *Environmental Modelling & Software*, 25: 1789-800.

Li, W., Q. Cao, K. Lang, and J. Wu. 2017. 'Linking potential heat source and sink to urban heat island: Heterogeneous effects of landscape pattern on land surface temperature', *Sci Total Environ*, 586: 457-65.

Li, Weifeng, Yang Bai, Qiuwen Chen, Kate He, Xiaohua Ji, and Chunmeng Han. 2014. 'Discrepant impacts of land use and land cover on urban heat islands: A case study of Shanghai, China', *Ecological Indicators*, 47: 171-78.

Li, Xiaoma, Weiqi Zhou, Zhiyun Ouyang, Weihua Xu, and Hua Zheng. 2012. 'Spatial pattern of greenspace affects land surface temperature: evidence from the heavily urbanized Beijing metropolitan area, China', *Landscape Ecology*, 27: 887-98.

Li, Xiaoxiao, Wenwen Li, A. Middel, S. L. Harlan, A. J. Brazel, and B. L. Turner. 2016. 'Remote sensing of the surface urban heat island and land architecture in Phoenix, Arizona: Combined effects of land composition and configuration and cadastral–demographic–economic factors', *Remote sensing of Environment*, 174: 233-43.

Li, Ying-ying, Hao Zhang, and Wolfgang Kainz. 2012. 'Monitoring patterns of urban heat islands of the fast-growing Shanghai metropolis, China: Using time-series of Landsat TM/ETM+ data', *International Journal of Applied Earth Observation and Geoinformation*, 19: 127-38.

Liu, Hua, and Qihao Weng. 2012. 'Enhancing temporal resolution of satellite imagery for public health studies: A case study of West Nile Virus outbreak in Los Angeles in 2007', *Remote sensing of Environment*, 117: 57-71.

Liu, Kai, Hongbo Su, Xueke Li, Weimin Wang, Lijun Yang, and Hong Liang. 2016. 'Quantifying Spatial–Temporal Pattern of Urban Heat Island in Beijing: An Improved Assessment Using Land Surface Temperature (LST) Time Series Observations From LANDSAT, MODIS, and Chinese New Satellite GaoFen-1', *IEEE Journal of Selected Topics in Applied Earth Observations and Remote Sensing*, 9: 2028-42.

Lu, Dengsheng, and Qihao Weng. 2006. 'Spectral mixture analysis of ASTER images for examining the relationship between urban thermal features and biophysical descriptors in Indianapolis, Indiana, USA', *Remote sensing of Environment*, 104: 157-67.

Luck, Matthew, and Jianguo Wu. 2002. 'A gradient analysis of urban landscape pattern: a case study from the Phoenix metropolitan region, Arizona, USA', *Landscape ecology*, 17: 327-39.

Luo, Xiaobo, and Yidong Peng. 2016. 'Scale Effects of the Relationships between Urban Heat Islands and Impact Factors Based on a Geographically-Weighted Regression Model', *Remote Sensing*, 8: 760.

Majumdar, Dipanjan Das, and Atrayee Biswas. 2016. 'Quantifying land surface temperature change from LISA clusters: An alternative approach to identifying urban land use transformation', *Landscape and Urban Planning*, 153: 51-65.

Mills, Gerald, J Ching, L See, B Bechtel, and M Foley. 2015. "An Introduction to the WUDAPT project." In *9th International Conference on Urban Climate, Toulouse*.

Mirzaei, Parham A. 2015. 'Recent challenges in modeling of urban heat island', *Sustainable Cities and Society*, 19: 200-06.

Mirzaei, Parham A., and Fariborz Haghighat. 2010. 'Approaches to study Urban Heat Island – Abilities and limitations', *Building and Environment*, 45: 2192-201.

Myint, Soe W., Elizabeth A. Wentz, Anthony J. Brazel, and Dale A. Quattrochi. 2013. 'The impact of distinct anthropogenic and vegetation features on urban warming', *Landscape Ecology*, 28: 959-78.

Myint, Soe Win, Baojuan Zheng, Emily Talen, Chao Fan, Shai Kaplan, Ariane Middel, Martin Smith, Huei-Ping Huang, and Anthony Brazel. 2015. 'Does the spatial arrangement of urban landscape matter? Examples of urban warming and cooling in Phoenix and Las Vegas', *Ecosystem Health and Sustainability*, 1: 1-15.

Nakaya, T, M Charlton, S Fotheringham, and C Brundson. 2014. 'GWR4 version 4.0. 80. Application for geographically weighted regression modelling', *National Centre for Geocomputation, National University of Ireland Maynooth and Department of Geography, Ritsumeikan University, Japan*.

Nassar, Ahmed K., G. Alan Blackburn, and J. Duncan Whyatt. 2016. 'Dynamics and controls of urban heat sink and island phenomena in a desert city: Development of a local climate zone scheme using remotely-sensed inputs', *International Journal of Applied Earth Observation and Geoinformation*, 51: 76-90.

Ng, Yvonne XY. 2015. 'A Study of Urban Heat Island using "Local Climate Zones"–The Case of Singapore'.

Nichol, Janet E. 1996. 'High-resolution surface temperature patterns related to urban morphology in a tropical city: a satellite-based study', *Journal of Applied Meteorology*, 35: 135-46.

North Central Texas Council of Governments. last accessed March 12, 2018. 'Mobility 2035 – 2013 Update', http://www.nctcog.org/trans/mtp/2035/OperationalEfficiency.pdf.

Nunez, Manuel, and Timothy R Oke. 1977. 'The energy balance of an urban canyon', *Journal of Applied Meteorology*, 16: 11-19.

Oke, T. R. 1973. 'City size and the urban heat island', *Atmospheric Environment (1967)*, 7: 769-79.

———. 1976. 'The distinction between canopy and boundary-layer urban heat islands', *Atmosphere*, 14: 268-77.

Oke, TR. 1995. 'The heat island of the urban boundary layer: characteristics, causes and effects.' in, *Wind climate in cities* (Springer).

Peel, M. C., B. L. Finlayson, and T. A. McMahon. 2007. 'Updated world map of the Köppen-Geiger climate classification', *Hydrol. Earth Syst. Sci.*, 11: 1633-44.

Peng, Jian, Pan Xie, Yanxu Liu, and Jing Ma. 2016. 'Urban thermal environment dynamics and associated landscape pattern factors: A case study in the Beijing metropolitan region', *Remote sensing of Environment*, 173: 145-55.

Peng, S., S. Piao, P. Ciais, P. Friedlingstein, C. Ottle, F. M. Breon, H. Nan, L. Zhou, and R. B. Myneni. 2012. 'Surface urban heat island across 419 global big cities', *Environ Sci Technol*, 46: 696-703.

Quan, Jinling, Yunhao Chen, Wenfeng Zhan, Jinfei Wang, James Voogt, and Mengjie Wang. 2014. 'Multi-temporal trajectory of the urban heat island centroid in Beijing, China based on a Gaussian volume model', *Remote sensing of Environment*, 149: 33-46.

Rajasekar, Umamaheshwaran, and Qihao Weng. 2009a. 'Spatio-temporal modelling and analysis of urban heat islands by using Landsat TM and ETM+ imagery', *International Journal of Remote Sensing*, 30: 3531-48.

———. 2009b. 'Urban heat island monitoring and analysis using a non-parametric model: A case study of Indianapolis', *ISPRS Journal of Photogrammetry and Remote Sensing*, 64: 86-96.

Rinner, Claus, and Mushtaq Hussain. 2011. 'Toronto's Urban Heat Island—Exploring the Relationship between Land Use and Surface Temperature', *Remote Sensing*, 3: 1251-65.

Rinner, Claus, Dianne Patychuk, Kate Bassil, Shiraz Nasr, Stephanie Gower, and Monica Campbell. 2010. 'The Role of Maps in Neighborhood-level Heat Vulnerability Assessment for the City of Toronto', *Cartography and Geographic Information Science*, 37: 31-44.

Rizwan, Ahmed Memon, Leung YC Dennis, and LIU Chunho. 2008. 'A review on the generation, determination and mitigation of Urban Heat Island', *Journal of Environmental Sciences*, 20: 120-28.

Sarrat, C., A. Lemonsu, V. Masson, and D. Guedalia. 2006. 'Impact of urban heat island on regional atmospheric pollution', *Atmospheric Environment*, 40: 1743-58.

Scherer, D., U. Fehrenbach, H. D. Beha, and E. Parlow. 1999. 'Improved concepts and methods in analysis and evaluation of the urban climate for optimizing urban planning processes', *Atmospheric Environment*, 33: 4185-93.

Schmid, Hans Peter Emil. 1988. 'Spatial Scales of Sensible Heat Flux Variability: Representativeness of Flux Measurements and Surface Layer Structure Over Suburban Terrain', *Ph. D. Thesis*, 1: 170.

Schwarz, N., and A. Manceur. 2014. 'Analyzing the Influence of Urban Forms on Surface Urban Heat Islands in Europe', *Journal of Urban Planning and Development*, 141: A4014003.

Shahmohamadi, P, AI Che-Ani, A Ramly, Khairul Nizam Abdul Maulud, and MFI Mohd-Nor. 2010. 'Reducing urban heat island effects: A systematic review to achieve energy consumption balance', *International Journal of Physical Sciences*, 5: 626-36.

Shen, Huanfeng, Liwen Huang, Liangpei Zhang, Penghai Wu, and Chao Zeng. 2016. 'Long-term and fine-scale satellite monitoring of the urban heat island effect by the fusion of multi-temporal and multi-sensor remote sensed data: A 26-year case study of the city of Wuhan in China', *Remote sensing of Environment*, 172: 109-25.

Sobrino, J. A., R. Oltra-Carrió, G. Sòria, R. Bianchi, and M. Paganini. 2012. 'Impact of spatial resolution and satellite overpass time on evaluation of the surface urban heat island effects', *Remote sensing of Environment*, 117: 50-56.

Song, Juer, Shihong Du, Xin Feng, and Luo Guo. 2014. 'The relationships between landscape compositions and land surface temperature: Quantifying their resolution sensitivity with spatial regression models', *Landscape and Urban Planning*, 123: 145-57.

Stathopoulou, Marina, and Constantinos Cartalis. 2009. 'Downscaling AVHRR land surface temperatures for improved surface urban heat island intensity estimation', *Remote sensing of Environment*, 113: 2592-605.

Stewart, I. D. 2011. 'A systematic review and scientific critique of methodology in modern urban heat island literature', *International Journal of Climatology*, 31: 200-17.

Stewart, Ian D, and Tim R Oke. 2012. 'Local climate zones for urban temperature studies', *Bulletin of the American Meteorological Society*, 93: 1879-900.

Streutker, D. 2003. 'Satellite-measured growth of the urban heat island of Houston, Texas', *Remote sensing of Environment*, 85: 282-89.

Taha, Haider. 1997. 'Urban climates and heat islands: albedo, evapotranspiration, and anthropogenic heat', *Energy and Buildings*, 25: 99-103.

Tan, Minghong, and Xiubin Li. 2015. 'Quantifying the effects of settlement size on urban heat islands in fairly uniform geographic areas', *Habitat International*, 49: 100-06.

Tang, Fei, and Hanqiu Xu. 2016. "A study on the quantitative relationship between impervious surface and land surface temperature based on remote sensing technology." In *Earth Observation and Remote Sensing Applications (EORSA), 2016 4th International Workshop on*, 368-72. IEEE.

Tran, Hung, Daisuke Uchihama, Shiro Ochi, and Yoshifumi Yasuoka. 2006. 'Assessment with satellite data of the urban heat island effects in Asian mega cities', *International Journal of Applied Earth Observation and Geoinformation*, 8: 34-48.

Unger, János, Enikő Lelovics, and Tamás Gál. 2014. 'Local Climate Zone mapping using GIS methods in Szeged', *Hungarian Geographical Bulletin*, 63: 29-41.

United Nations. 2014. *World Urbanization Prospects: The 2014 Revision* (New York: United Nations Department of Economics and Social Affairs, Population Division).

Voogt, James A, and Tim R Oke. 2003. 'Thermal remote sensing of urban climates', *Remote sensing of Environment*, 86: 370-84.

Wang, J., and W. Ouyang. 2017. 'Attenuating the surface Urban Heat Island within the Local Thermal Zones through land surface modification', *J Environ Manage*, 187: 239-52.

Wang, Jiong, Zhan Qingming, Huagui Guo, and Zhicheng Jin. 2016. 'Characterizing the spatial dynamics of land surface temperature–impervious surface fraction relationship', *International Journal of Applied Earth Observation and Geoinformation*, 45: 55-65.

Wang, Jiong, Qingming Zhan, and Huagui Guo. 2015. 'The Morphology, Dynamics and Potential Hotspots of Land Surface Temperature at a Local Scale in Urban Areas', *Remote Sensing*, 8: 18.

Wang, Ran, Chao Ren, Yong Xu, Kevin Ka-Lun Lau, and Yuan Shi. 2017. 'Mapping the local climate zones of urban areas by GIS-based and WUDAPT methods: A case study of Hong Kong', *Urban Climate*.

Wang, Shenmin, Qifang Ma, Haiyong Ding, and Hanwei Liang. 2016. 'Detection of urban expansion and land surface temperature change using multi-temporal landsat images', *Resources, Conservation and Recycling*.

Wang, Yasha, Qingming Zhan, and Wanlu Ouyang. 2017. 'Impact of Urban Climate Landscape Patterns on Land Surface Temperature in Wuhan, China', *Sustainability*, 9.

Weng, Qihao. 2009. 'Thermal infrared remote sensing for urban climate and environmental studies: Methods, applications, and trends', *ISPRS Journal of Photogrammetry and Remote Sensing*, 64: 335-44.

Weng, Qihao, Peng Fu, and Feng Gao. 2014. 'Generating daily land surface temperature at Landsat resolution by fusing Landsat and MODIS data', *Remote sensing of Environment*, 145: 55-67.

Weng, Qihao, Dengsheng Lu, and Jacquelyn Schubring. 2004. 'Estimation of land surface temperature–vegetation abundance relationship for urban heat island studies', *Remote sensing of Environment*, 89: 467-83.

Wickham, James, Stephen V. Stehman, Leila Gass, Jon A. Dewitz, Daniel G. Sorenson, Brian J. Granneman, Richard V. Poss, and Lori A. Baer. 2017. 'Thematic accuracy assessment of the 2011 National Land Cover Database (NLCD)', *Remote sensing of Environment*, 191: 328-41.

Winguth, A. M. E., and B. Kelp. 2013. 'The Urban Heat Island of the North-Central Texas Region and Its Relation to the 2011 Severe Texas Drought', *Journal of Applied Meteorology and Climatology*, 52: 2418-33.

Wong, M. S., F. Peng, B. Zou, W. Z. Shi, and G. J. Wilson. 2016. 'Spatially Analyzing the Inequity of the Hong Kong Urban Heat Island by Socio-Demographic Characteristics', *Int J Environ Res Public Health*, 13.

Wu, Chih-Da, Shih-Chun Candice Lung, and Jihn-Fa Jan. 2013. 'Development of a 3-D urbanization index using digital terrain models for surface urban heat island effects', *ISPRS Journal of Photogrammetry and Remote Sensing*, 81: 1-11.

Wu, Hao, Lu-Ping Ye, Wen-Zhong Shi, and Keith C. Clarke. 2014. 'Assessing the effects of land use spatial structure on urban heat islands using HJ-1B remote sensing imagery in Wuhan, China', *International Journal of Applied Earth Observation and Geoinformation*, 32: 67-78.

Wu, Jianguo. 2014. 'Urban ecology and sustainability: The state-of-the-science and future directions', *Landscape and Urban Planning*, 125: 209-21.

Xian, George, and Mike Crane. 2006. 'An analysis of urban thermal characteristics and associated land cover in Tampa Bay and Las Vegas using Landsat satellite data', *Remote sensing of Environment*, 104: 147-56.

Xiao, Rongbo, Qihao Weng, Zhiyun Ouyang, Weifeng Li, Erich W Schienke, and Zhaoming Zhang. 2008. 'Land surface temperature variation and major factors in Beijing, China', *Photogrammetric Engineering & Remote Sensing*, 74: 451-61.

Xie, Miaomiao, Meichen Fu, and Yanglin Wang. 2011. "Changing trajectory of urban heat islands in Shenzhen, China." In *Remote Sensing, Environment and Transportation Engineering (RSETE), 2011 International Conference on*, 164-67. IEEE.

Xu, Yong, Chao Ren, Meng Cai, Ng Yan Yung Edward, and Tianjun Wu. 2017. 'Classification of Local Climate Zones Using ASTER and Landsat Data for High-Density Cities', *IEEE Journal of Selected Topics in Applied Earth Observations and Remote Sensing*.

Xu, Yong, Chao Ren, Meng Cai, and Ran Wang. 2017. "Issues and challenges of remote sensing-based local climate zone mapping for high-density cities." In *Urban Remote Sensing Event (JURSE), 2017 Joint*, 1-4. IEEE.

Yue, W., J. Xu, W. Tan, and L. Xu. 2007. 'The relationship between land surface temperature and NDVI with remote sensing: application to Shanghai Landsat 7 ETM+ data', *International Journal of Remote Sensing*, 28: 3205-26.

Zhang, Hao, Zhi-fang Qi, Xin-yue Ye, Yuan-bin Cai, Wei-chun Ma, and Ming-nan Chen. 2013. 'Analysis of land use/land cover change, population shift, and their effects on spatiotemporal patterns of urban heat islands in metropolitan Shanghai, China', *Applied Geography*, 44: 121-33.

Zhang, Jinqu, and Yunpeng Wang. 2008. 'Study of the Relationships between the Spatial Extent of Surface Urban Heat Islands and Urban Characteristic Factors Based on Landsat ETM+ Data', *Sensors*, 8: 7453-68.

Zhang, Ping, Marc L. Imhoff, Robert E. Wolfe, and Lahouari Bounoua. 2010. 'Characterizing urban heat islands of global settlements using MODIS and nighttime lights products', *Canadian Journal of Remote Sensing*, 36: 185-96.

Zhao, L., X. Lee, R. B. Smith, and K. Oleson. 2014. 'Strong contributions of local background climate to urban heat islands', *Nature*, 511: 216-9.

Zheng, Baojuan, Soe W. Myint, and Chao Fan. 2014. 'Spatial configuration of anthropogenic land cover impacts on urban warming', *Landscape and Urban Planning*, 130: 104-11.

Zheng, Yingsheng, Chao Ren, Yong Xu, Ran Wang, Justin Ho, Kevin Lau, and Edward Ng. 2017. 'GIS-based mapping of Local Climate Zone in the high-density city of Hong Kong', *Urban Climate*.

Zhou, D., L. Zhang, L. Hao, G. Sun, Y. Liu, and C. Zhu. 2016. 'Spatiotemporal trends of urban heat island effect along the urban development intensity gradient in China', *Sci Total Environ*, 544: 617-26.

Zhou, Decheng, Shuqing Zhao, Shuguang Liu, Liangxia Zhang, and Chao Zhu. 2014. 'Surface urban heat island in China's 32 major cities: Spatial patterns and drivers', *Remote sensing of Environment*, 152: 51-61.

Zhou, Decheng, Shuqing Zhao, Liangxia Zhang, and Shuguang Liu. 2016. 'Remotely sensed assessment of urbanization effects on vegetation phenology in China's 32 major cities', *Remote sensing of Environment*, 176: 272-81.

Zhou, Ji, Yunhao Chen, Jinfei Wang, and Wenfeng Zhan. 2011. 'Maximum nighttime urban heat island (UHI) intensity simulation by integrating remotely sensed data and meteorological observations', *IEEE Journal of Selected Topics in Applied Earth Observations and Remote Sensing*, 4: 138-46.

Zhou, Weiqi, Ganlin Huang, and Mary L. Cadenasso. 2011. 'Does spatial configuration matter? Understanding the effects of land cover pattern on land surface temperature in urban landscapes', *Landscape and Urban Planning*, 102: 54-63.

Zhou, Weiqi, Yuguo Qian, Xiaoma Li, Weifeng Li, and Lijian Han. 2013. 'Relationships between land cover and the surface urban heat island: seasonal variability and effects of spatial and thematic resolution of land cover data on predicting land surface temperatures', *Landscape Ecology*, 29: 153-67.

Zhu, Shanyou, Huade Guan, Andrew C. Millington, and Guixin Zhang. 2013. 'Disaggregation of land surface temperature over a heterogeneous urban and surrounding suburban area: a case study in Shanghai, China', *International Journal of Remote Sensing*, 34: 1707-23.